Block Copolymer Solutions: Transport and Dynamics, Targeted Cargo Delivery, and Molecular Partitioning and Exchange

Xiuli Li

Dissertation submitted to the faculty of the Virginia Polytechnic Institute and State University in partial fulfillment of the requirements for the degree of

Doctor of Philosophy

In

Chemistry

Louis A. Madsen, Chair

Sam R. Turner

Alan R. Esker

John B. Matson

December 16th, 2019

Blacksburg, VA

Keywords: Block Copolymer Micelles (BCMs), Free Unimer Chains, Exchange Kinetics, NMR Diffusometry, Molecular Structure and Interaction, Drug Loading

Block Copolymer Solutions: Transport and Dynamics, Targeted Cargo Delivery, and Molecular Partitioning and Exchange

Xiuli Li

Abstract

Block copolymers have been extensively applied in diverse fields including packaging, electrolytes, delivery devices, and biosensors. Multiple investigations have been carried out on polymeric materials for cargo delivery purpose to understand how they behave over time. Block copolymer micelles (BCMs) have demonstrated superiority to deliver cargo, especially in drug delivery due to their encapsulation of hydrophobic agents. This dissertation will mainly study BCMs for potential applications in cargo delivery.

Methods to study BCMs, including NMR spectroscopy, relaxometry and diffusometry, can provide valuable molecular information, such as chemical structure, translational motion, inter- or intramolecular interaction, dynamics, and exchange kinetics. Therefore, this dissertation describes applications of versatile NMR methods to reveal the fundamental behaviors of block copolymer self-assemblies, such as their dynamic stability, cargo partitioning, polymer chain exchange, and chain distribution in solution.

We have investigated two BCM systems. Poly(ethylene oxide)-b-(ε-caprolactone) (PEO-PCL) is a model system to study BCM dynamic stability. PEO-PCL can self-assemble into spherical micelles at 1% w/v in D_2O-THF-d_8 mixed solvents. We used NMR diffusometry to quantify diffusion coefficients and populations of micelles and unimers (i.e. free polymer chains in solution) over a range of temperature (21 – 50 ℃) and solvent composition (10 – 100 vol % THF-d_8). By mapping the micelle-unimer coexistence phase diagrams, we are able to enhance our ability to understand and design micelle structure and dynamics. Moreover, we can also probe the

chain exchange kinetics between micelles using a new technique we developed – time-resolved NMR spin-lattice relaxation (T_1) or TR-NMR. This technique is an analog to time-resolved small-angle neutron scattering (TR-SANS), which can monitor specific signal intensity changes caused after mixing of isotope-labeled micelle solutions.

A second system, Pluronic® F127 ($PEO_{99}PPO_{69}PEO_{99}$) is a test system to study BCM structure and dynamic changes upon drug uptake. Pluronic® F127 is a commercial copolymer that can solubilize different hydrophobic drugs in micelles. We successfully encapsulated three model drugs into Pluronic® F127 BCMs and investigated the effects of polymer concentration and drug composition on drug partitioning fractions. Also, we proposed to design and synthesize a series of block copolymers with varied glass transition temperatures in core-forming blocks. Using NMR diffusometry, we have measured the existing unimer concentrations in micellar solutions and correlated these results with chain mobility and internal chemical composition.

Lastly, we have extended our expertise in NMR and polymers into the study of ion-containing polymer systems (polyelectrolytes). A critical problem in polymer science is the inability to reliably measure the molecular weight of polyelectrolytes. We are developing methods to solve this problem by using NMR diffusometry, rheology, scattering, and scaling theories to accomplish general molecular weight measurements for polyelectrolytes.

In short, this dissertation describes studies to provide more perspectives on structural and dynamic properties at various time and length scales for polymeric materials. NMR measurements, in combination with many other advanced techniques, have given us a better picture of soft matter behaviors and provided guidance for synthesis and processing efforts, especially in block copolymer micelles for delivery purposes.

Block Copolymer Solutions: Transport and Dynamics, Targeted Cargo Delivery, and Molecular Partitioning and Exchange

Xiuli Li

General Audience Abstract

Block copolymers have been extensively applied in diverse fields in packaging, electrolytes and nano-scale drug delivery carriers. In the area of cancer treatment, only a limited number of drug nanocarriers have been approved for clinical applications. Therefore, it is very important to understand the principles behind drug delivery for targeted purposes. There have been many studies on polymeric delivery carriers but their behaviors have not been completely understood. Therefore, we have tremendous interest in unraveling the mysteries in those polymeric systems.

Among a multitude of techniques to study block copolymer materials, the NMR method serves as a potent tool for its non-destructive, chemical-specific and isotope-selective merits. NMR can provide basic information about block copolymer self-assembly and other polymeric properties, such as chemical structure, molecular interactions and diffusion coefficients of species of interests.

Chapters 3, 4, 5, 6, and 7 have investigated different classes of polymeric materials, mainly block copolymer micelles, for their structure and stability, exchange kinetics of polymer chains or cargo, and translational properties. Greater understanding about the fundamental properties of these polymeric systems, is essential for enabling new applications and new research areas.

Acknowledgements

First and foremost, I would like to thank my PhD advisor, Prof. Louis A. Madsen, for his continued guidance and support for the past five years. Prof. Madsen has a strong passion for both research and life, which encourages me to grow into a more mature scientist and more importantly, a better person. I appreciate the opportunities in his group to learn valuable skillsets and complete various challenging projects. Prof. Madsen's mentorship, professionalism, and respect have been essential to guide me through my PhD.

I also sincerely appreciate my committee members – Prof. S. Richard Turner, Prof. Alan R. Esker, and Prof. John B. Matson. Thank you all for your valuable suggestions and discussions that have helped me to gain insights and solve problems in my research. I have learned more in polymer chemistry and physics from your professional perspectives.

Moreover, I would like to express my appreciations to my nationwide collaborators: Prof. Megan L. Robertson and Tyler J. Cooksey from University of Houston, Prof. Ralph H. Colby and Aijie Han from Pennsylvania State University, Prof. John B. Matson and Ryan J. Carrazzone, and Prof. Timothy E. Long and Dr. Mingtao Chen from Virginia Tech. It is their help and dedication that have made my work possible.

I am fortunate to work with every member in the Madsen group. They are hard-working and brilliant colleagues and are all I can ever ask for. Whenever I have problems in lab or other aspects, they are happy to listen, encourage and help. Thanks to my past and present group members: Dr. Jianbo Hou, Dr. Zhiyang Zhang, Dr. Ying Chen, Dr. Xiaoling Wang, Dr. Bryce Kidd, Dr. Ying Wang, Andrew Kovovich, Curt Zanelotti, Rui Zhang, Deyang Yu, Shravan Uppala, Nicolas Pietra, and Lexi McCarthy. I also would like to appreciate my friends out of my group and department: Xiaoyang Liu, Juntao Wang, and Sumin Shen. Many thanks for the joyful memories

that we shared in the past years at Virginia Tech. Having friends like you guys is a true blessing for me and I wish you all the best in your future journeys. I am so grateful for all the experiences in graduate school, and that I have the opportunities to learn from people with different backgrounds. They are important to build my learning process and have shaped who I am today.

The past years at Virginia Tech are invaluable assets for me and I specially thank my family members in Blacksburg. My boyfriend Chengzhe Gao is a talented young man who is humorous, caring and supportive. He is the one who always supports and accompanies me when I am lost and down. My dog Toby always comforts me with a lovely smile and teaches me more about love and responsibility.

Finally, I sincerely appreciate my family. No words can describe my deepest appreciation and love to my parents, who have provided endless support, understanding, and encouragement to me through my growth. Finishing a PhD is not an endpoint but a marker along my way. I am proud to glance back to what I have gained during this great journey, and my eyes are on the future.

Attribution

Prof. Louis A. Madsen (Research Advisor)

Professor at Department of Chemistry and Macromolecule Innovation Institution, Virginia Tech

Prof. Megan L. Robertson

Professor at Department of Chemical and Biological Engineering, University of Houston and collaborator on Chapters 3-5

Tyler J. Cooksey

Graduate Student at Department of Chemical and Biological Engineering, University of Houston and collaborator on Chapters 3-5

Dr. Bryce E. Kidd

Former Graduate Student in the Madsen group and collaborator on Chapters 3 and 4

Veera Venkata Shravan Uppala

Graduate Student in the Madsen group and collaborator on Chapters 4 and 5

Prof. John. B. Matson

Professor at Department of Chemistry and Macromolecule Innovation Institution, Virginia Tech and collaborator on Chapter 6

Ryan J. Carrazzone

Graduate Student at Department of Chemistry and Macromolecule Innovation Institution, Virginia Tech and collaborator on Chapter 6

Prof. Timothy E. Long

Professor at Department of Chemistry and Macromolecule Innovation Institution, Virginia Tech and collaborator on Chapter 7

Dr. Mingtao Chen

Former Graduate Student at Department of Chemistry and Macromolecule Innovation Institution, Virginia Tech and collaborator on Chapter 7

Prof. Ralph H. Colby

Professor at Department of Materials Science and Engineering, Pennsylvania State University and collaborator on Chapter 7

Aijie Han

Graduate Student at Department of Materials Science and Engineering, Pennsylvania State University and collaborator on Chapter 7

Table of Contents

Chapter 1: Block Copolymer Nanocarriers: Functionalized Design, Targeted Cargo Delivery and Chain Dynamics

Motivation, Strategy and Research Goals

This thesis will focus on nanoscale molecular cargo carriers (block copolymer micelles, BCMs), which can enable, for example, targeted delivery and controlled release of hydrophobic drugs. These nanocarriers have played a vital role in multiple applications, such as less harmful chemotherapy drug delivery and tailored nanoreactors. Especially in cancer therapeutics, only a few targeted nanocarriers have been approved for limited clinical translation. Therefore, it is crucial to understand the principles behind cargo delivery and develop successful strategies. This dissertation will focus on block copolymer micelles as nanocarriers for potential cargo delivery or advanced self-assembly design. In order to provide more perspectives, Chapter 1 will review the principle design and performance studies of various nanocarriers that are applied in targeted cargo delivery and cover the dynamic and kinetic processes in BCMs.

The objective of this dissertation is to study the chemical structure, dynamics and chain exchange kinetics as well as cargo partitioning in block copolymer micelles by various techniques to enhance our current understandings of such systems for potential drug delivery. Chapter 1 will summarize a detailed understanding of BCMs and other nanomaterials for their development as novel delivery carriers. Chapter 2 will focus on the theory and methods of NMR as applied to soft matter. Chapters 3 – 6 will present new results for BCMs using NMR and Chapter 7 will discuss how we can combine NMR with other techniques as a potent tool to understand ion-containing polymer systems.

1.1 Block Copolymers in Nanoscale Cargo Delivery Carriers

The development of effective cancer treatments has been a main concern during the past few decades. The efficiency of traditional chemotherapy is hindered by its nonspecific distribution *in vivo*, rapid clearance, significant toxicity and drug resistance for tumors.[1] Consequently, there has been an increasing demand for more effective therapies for the cancer treatments, which has prompted investigations of novel nanomedicines with tumor-specific targeting and multifunctional properties. Current drug delivery nanocarriers include polymeric micelles,[2] gels,[3] silica and gold nanoparticles,[4-5] liposomes,[6] graphene nanosheets,[7] and prodrugs.[8]

Development of material science and polymer chemistry has enabled the narrow size distribution, controlled structures and wide multifunctionalities of nanoscale drug delivery carriers. Amphiphilic block copolymers that self-assemble in selective solvents can lead to a range of morphologies: spheres, cylinders, lamelles or vesicles.[9] These aggregates formed by block copolymers have been widely investigated for their potential for drug delivery. More importantly, they are able to encapsulate hydrophobic anti-cancer drugs to increase their solubility and release drugs upon external stimuli. Stimuli that have been applied for triggered release include pH,[10] light,[5] enzymes,[11] magnetic field,[12] and ultrasound.[13] Therefore, these nanoscale delivery carriers offer new opportunities to enhance therapeutic effects and controlled release of delivered drugs.

In Chapters 2 – 7, this dissertation covers the solubilization, partitioning and exchange process in two major classes of block copolymer micelles. Chapter 1 focuses on overviewing the development and characterization of micellar drug delivery systems, with introduction of other systems for comparison and general understanding.

1.1.1 Micelles

Micelles are self-assemblies formed of surfactants or amphiphilic polymers. In the year 1913, McBain first introduced the term "*micelle*" to represent the association of surfactants in aqueous solution.[14] In a solvent which is more selective for one of the constitutive groups or blocks, amphiphilic surfactants or polymers have the tendency to aggregate into nanostructures spontaneously.[15] In this thesis, we describe the aggregates of block copolymer micelles (BCMs).

For BCMs, when the polymer concentration increases to a critical value, the self-assembly process will occur.[16-17] This critical concentration that results in the formation of micelles is called the *critical micelle concentration* (CMC). Below the CMC, polymers exist as single polymer chains (i.e. unimers) in solution. Above the CMC, BCMs tend to adopt a low energy configuration and a certain amount of solvent can be observed inside the core of the micelles.[16, 18] Amphiphilic copolymers usually have a CMC on the order of 10^{-6} to 10^{-7} M, which is commonly lower than surfactants with low molecular weights which have CMCs on the order of 10^{-3} to 10^{-4} M.[19] For instance, Liaw et al.[20] have measured a CMC of 10^{-9} M for a poly(ethylene oxide)-poly (beta-benzyl L-aspartate)-pyrene (PEO_{270}-$PBLA_{15}$-Pyrene) BCM.

Theoretically, any sudden changes of physical properties (such as osmotic pressure, conductivity, and interfacial tension) over a range of amphiphile concentrations will indicate the CMC.[21] Fluorescent methods, light scattering, nuclear magnetic resonance and gel permeation chromatography are also developed to determine the CMC for block copolymer micelles.[22-23] Due to the low CMC, BCMs are usually stable in aqueous environments and less likely to dissociate upon dilution *in vivo*. Therefore, their circulation time is enhanced compared to surfactant micelles. This dissertation studies BCMs with low CMCs for applications in targeted cargo delivery and controlled release. Measurements of the free polymer chain content in micellar solutions typically

have limitations using conventional techniques, and Chapter 3 will address our new NMR methods for free polymer chain concentration in solution, which can be applied in CMC determinations.

The micellization of polymers yields commonly studied aggregates with multiple morphologies, including spheres, cylinders, lamellae and vesicles.[9, 24] Also, there are many other macromolecular structures which we investigated, such as planar sheets,[25] bicontinuous rods, short hollow tubes,[26] and reverse micelles.[27] Israelachvili developed thermodynamic equations of self-assembly,[28] describing a packing parameter (p) that indicates the morphology of the self-assembled aggregates depends on relative volume of hydrophobic and hydrophilic proportions as follows:

$$p = \frac{v}{al} \tag{1.1}$$

where v is hydrophobic volume, a is interfacial area of the hydrophilic block at the interface, and l is hydrophobic chain length normal to the interface.[29] The maximum packing parameters for spherical and cylindrical micelles and vesicles are 1/3, 1/2 and 1, respectively, which is shown in **Figure 1.1**.

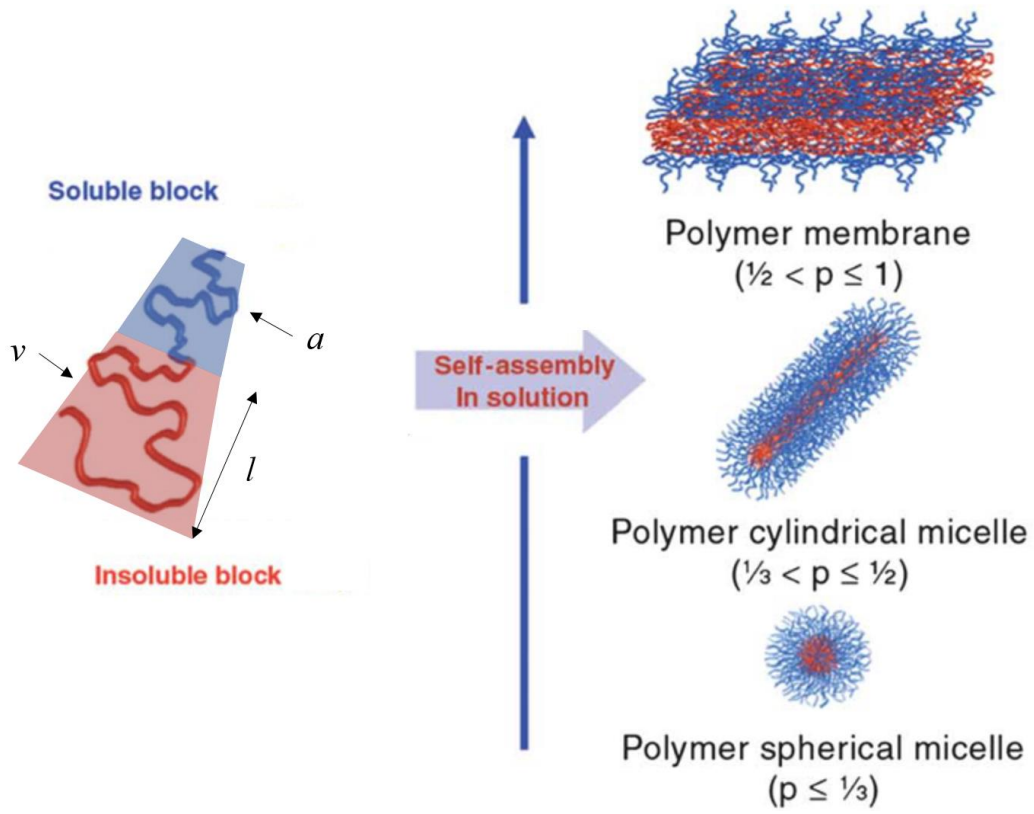

Figure 1.1. Self-assembly of spherical micelle, cylindrical micelle and vesicles. The morphology of the self-assembled aggregates depends on the interfacial area of the hydrophilic block (*a*), hydrophobic volume (*v*) and hydrophobic chain length (*l*). When ½ < p ≤ 1, vesicles are formed; 1/3 < p ≤ 1/2, cylindrical micelles are formed; p ≤ 1/3, spherical micelles are formed. Remade from Reference 29.

The morphology of polymeric micelles not only relies on polymer properties such as the polymer chain length, the relative proportions of hydrophilic and hydrophobic chains, but also solution properties such as solvent composition or presence of additives,[27, 30] Those BCMs with desired morphologies have controllable functionalities, low CMC, capability to solubilize, prolonged circulation time, enhanced bioavailability and *in vivo* degradability,[31] thus they demonstrate enormous potential in targeted drug delivery and other applications.

1.1.2 PEO-based Delivery Systems

Polyethylene oxide (PEO) and its conjugates are often applied to form drug delivery carriers owing to their low toxicity, biocompatibility and biodegradability. PEO is a water soluble polymer which exhibits rapid clearance from the body.[32] Moreover, moieties (e.g. hydrophobic molecules) bonded covalently to PEO can have increased water solubility.[33] Meanwhile, PEO coupled to biological molecules can have enhanced biological activity, such as resistance to cell and protein absorption.[34] Such properties have prepared PEG-based BCMs as excellent candidates in drug delivery systems. The drug release is controlled not only by the preparation method, but also by the molecular weight of the PEO chains and drug solubility.[35] **Table 1.1** lists a few PEG-based micellar drug formulations approved for clinical trials for cancer treatment.[17, 31]

Table 1.1. Block copolymer micelles approved for clinical trials as anti-drug carriers. PEG is poly (ethylene glycol); PLA is poly (lactic acid); Pasp is poly (asparate); PAPB is poly (aminopropyl biguanide); PGlu is poly (L-glutamic acid); PPO is poly (propylene oxide); DOX is doxorubicin and PTX is paclitaxel, both of which are chemotherapy drugs.

Name	Carrier	Drug	Indications
Gnenexol-PM	PEG-PLA	PTX	breast, lung cancer
NK911	PEG-Pasp-DOX conjugate	DOX	pancreatic cancer
NK105	PEG-PAPB	PTX	stomach cancer
NC 6004	PEG-PGlu	Cisplatin	solid tumors
Pluronic®	PEO-PPO-PEO	Haloperidol	psychotic disorders

The goal of improved development of PEO is to utilize it in the multifunctional design of polymeric nano-carriers in drug delivery. For instance, Guo et al.[36] developed a BCM from the

thermoresponsive Pluronic F127-poly(D, L-lactic acid) (FP) with a lower critical solution temperature of 39.2 ℃ and decorated it with the folate acid (FA) for active targeting. FP micelles exhibited a decrease of size in DLS and the increase of absorbance in UV-vis when the temperature was raised from 25 – 55 ℃. The shrinkage of the FP micelles was caused by opposing thermal effects between the two polymers. FP micelles released DOX rapidly above 40 ℃ attributed to polymer shrinkage. FA-decorated FP micelles also demonstrated excellent cytocompatibility and high cellular uptake. Thus, thermo-responsive nanocarriers have great potential as a drug delivery vehicle in cancer therapy.

Cui et al.[12] combined a receptor-binding peptide (T7) with a PEG–poly (lactic acid-co-glycolic acid) to encapsulate both hydrophobic magnetic nanoparticles and anti-cancer drugs. This dual-targeting delivery yielded synergistic effects to inhibit tumor growth, i.e. > 10-fold increase in cellular uptake and > 5-fold enhancement in brain delivery, compared to the non-targeting nanoparticles. Belhadj et al.[6] designed a Y-shape liposome, which could achieve tumor-targeted drug delivery. *In vivo* fluorescence imaging proved DOX-loaded c(RGDyk)-pHA-PEG-DSPG liposome had the better anti-tumor effect and longer survival time compared to DOX-loaded plain or single-ligand-modified liposomes, which implies excellence in anti-cancer therapy. PEG-modified liposomes exhibit long circulation times in the blood and accumulate in tumor via passive targeting, and therefore are widely used in drug delivery systems.

Shen et al.[8] conjugated a strongly hydrophobic anticancer drug: camptothecin (CPT) to a hydrophilic short oligomer chain: ethylene glycol (OEG), forming an amphiphilic phospholipid-mimicking prodrug (**Figure 1.2**). The OEG-CPT has a CPT loading content as high as 40 to 58 wt %. The OEG-DiCPT also showed both high *in vitro* and *in vivo* antitumor activity to release CPT.

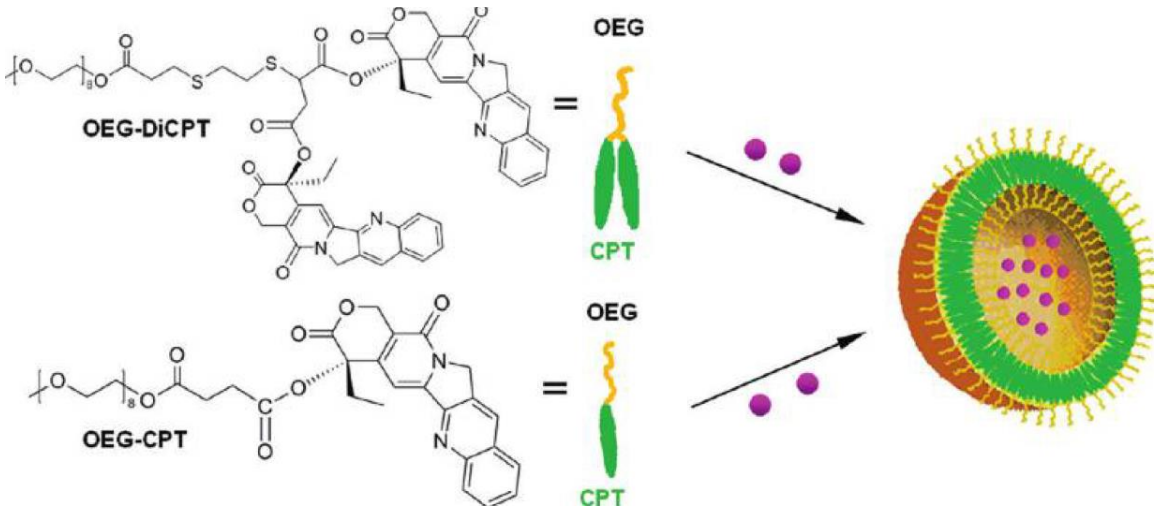

Figure 1.2. A schematic illustration OEG-CPT and OEG-DiCPT drug-polymer conjugates. Poly (ethylene glycol) is conjuaged to increase overall water solubility. Reproduced from Reference 8.

Next we briefly introduce two polymer systems, poly(ethylene oxide)-b-polycaprolactone (PEO-PCL) and poly(ethylene oxide)-b-poly(propyleneoxide)-b-poly(ethylene oxide) (PEO-PPO-PEO, Pluronic®), which form the basis of the micelle investigations in this dissertation. Due to their controllable sizes, rigidity and permeability, enhanced circulation time, *in vivo* degradability and higher stability compared to surfactant micelle,[37] they have exhibited ideal controlled delivery of poorly water-soluble drugs, e.g. paclitaxel (PTX) and doxorubicin (DOX).

Polycaprolactone (PCL) is both biocompatible and biodegradable due to its breakdown of ester bonds upon enzymatic and/or pH treatments. PEO-PCL BCMs have been reported to be internalized by cells and mainly distributed to the cytoplasm. Furthermore, they can realize a slow and steady release of hydrophobic cargo over a monthly timeframe.[38] The Pluronic® system exists as liquid form at lower temperature and transits to gel at higher temperatures. The Pluronic® BCM systems have found many applications in drug delivery, For example, Basak et al.[2] prepared drug-loaded BCMs with a commercial triblock copolymer Pluronic® F127 and investigated effects of

drug hydrophobicity, temperature and pH on drug loading in Pluronic® BCMs. They concluded that hydrodynamic radii and polydispersity of BCMs increase with the decrease of temperature and in the presence of drug molecules.

Moreover, Han et al.[39] investigated the structural changes of Pluronic® L62 BCMs in the absence and presence of three nucleoside analogue antimetabolites (i.e. 5-fluorouracil, floxuridine and gemcitabine). Pluronic® L62 polymers formed micelles at the concentration of 30 % with an oblate shape at 20 – 40 ℃, then transited to lamellae at 50 ℃. The three antimetabolites with similarities in chemical structure but differences in molecular size and water solubility, have resulted in a slight decrease in micellar size, aggregation number and shape anisotropy. More introduction and studies on PEO-PCL and Pluronic® BCM systems will be covered through Chapters 3 – 5. PEO-PCL BCM system has temperature and solvent dependence in structure and dynamic control. Pluronic® BCM system is a test system that is easy to load various drug in micelle formulations.

1.1.3 Other Forms of Nanocarriers

Other delivery systems such as hydrogels, nanoparticles, liposomes or drug-polymer conjugates, have also been applied to targeted cargo delivery for years, due to their extended circulation times, reduced toxicity and side effects, and transport of bioactive moieties (e.g. anti-cancer drugs or proteins).[3] Gels are prepared by physical crosslinking through non-covalent binding (including electrostatic, hydrophobic or hydrogen-bonding forces) or permanent chemical crosslinking. Those crosslinked hydrogels have stable networks that allow controlled cargo release by diffusion or gel dissociation under physiological conditions.[40] Theoretically, hydrogels loaded with model cargos can exhibit desired release by modifying the networks via lyophilization /

rehydration.[3] This strategy provides us with simplified control over the cargo release by a versatile design of gel drug delivery systems.

Nanoparticles (NPs) have been applied as drug delivery platform with high loading efficiency and controlled release, among which mesoporous silica nanoparticles (MSNs) have been commonly used due to their biocompatibility, mesoporous structure, large surface area and tunable volume.[4] Yavuz et al.[5] have displayed a near-infrared-responsive platform of gold nanocages modified with poly(N-isopropylacrylamide)(PNIPAAm)-based polymers. The rising of temperature has caused polymer chain collapse and thereby release of the pre-loaded drug. The release dosage could also be controlled by the power density and irradiation time. Moreover, NPs provide advantages such as strong absorption with designed hollow or porous walls and multifunctionalities with targeting ligands, thereby shedding light on the novel design of cargo delivery systems, such as introducing functional groups into BCMs to realize desired purposes.

Liposomes are closed spherical vesicles with a lipid bilayer that constitutes an aqueous phase that encapsulate hydrophilic cargos.[41] By controlling the lipid–drug interaction, the size, charge and surface hydration in liposomes can be tuned. Potential new treatments for diseases are possible by using novel liposomes, for example, there have been clinical trials such as vasoactive intestinal peptide (VIP)[42] to treat hypertension and amphotericin B (Ambisome®)[43] to treat fungal or parasitic infections. The insights gained from clinical use of liposome delivery systems can also be extended to design BCMs targeted to tissues and cells.[44]

Multifunctional drug-conjugates have offered a class of potent nanocarriers to deliver therapeutic agents. They serve as an ideal platform for safe and efficient drug delivery in cancer therapy. By chemically conjugating the therapeutic drug and delivery polymers, they have combined the merits of both species and enhanced resistance of peptide drugs to proteolysis,

disassembled at reductive conditions in the tumor microenvironment and inhibited cancer cell growth *in vitro* and *in vivo*.[45]

Moreover, there have been many other nanomaterials that are widely applied for multiple purposes, and interestingly, we can extend them as potential nanoscale delivery carriers by proper design of their structures and properties. Functionalized carbon nanotubes (graphene oxides) can be used as the carrier for the delivery of therapeutic molecules due to their large surface area and ease to cross cell membranes. Liu et al.[7] prepared gelatin functionalized graphene nanosheets (gelatin-GSN) that were used in cellular imaging and drug delivery. The DOX-loaded gelatin-GSN exhibited a low toxicity, high loading capacity via the large surface area / strong π–π conjugation, and gelatin-mediated sustained release *in vitro*, providing a new pathway to modify graphene with biocompatibility in biological applications. Metal-organic frameworks (MOF) are potential porous materials that could be used in biomedical applications,[46] with adjustable pore size and surface properties.[47] An et al.[48] have constructed a porous bio-MOF and used Na cations to trigger procainamide release by tuning the ionic interactions. Nanofibers generate linear morphologies, smooth surfaces and clear nanostructures, which realizes a gradient distribution of the drug for potential controlled release.[49] Dendrimers with high molecular weights (> 20 000 Da) have also been applied as drug carriers to improve the therapeutic efficacy.[50] Padilla et al.[51] have evaluated various dendritic architectures (monomer unit 2,2-bis(hydroxymethyl) propanoic acid) for their suitability as drug carriers *in vitro* and *in vivo*, and showed that the half-life of DOX attached to an appropriate high molecular weight polymer was enhanced compared the free drug.

In all, all macromolecular systems exhibit promising characteristics as an efficient polymeric drug carriers. By tuning hydrophobic or hydrophilic reservior volume, network space, porous or surface areas, we are able to precisely tune the cargo encapsulation as well as release by

rational designs of the polymeric materials. Our investigations on block copolymer micelle systems can be further integrated into those delivery systems, thus providing more understandings of complicated drug delivery. At the same time, gaining more background information of other drug delivery systems, as well as their interactions with the guest active compounds, will lead more fine-tuning design of BCMs for drug delivery purposes.

1.2 Stimuli-responsive Nanocarriers

External stimuli that have been exploited for controlled cargo release include redox chemistry, pH, light, enzymes, magnetic fields, and ultrasound.[10, 52] Temperature change is especially important for implementing programmed functions that respond to the human body. Therefore, in this section we highlight the developments in temperature-responsive BCMs and nanoparticles, with a focus on their design, drug release performance and therapeutic effects. The PEO-PCL BCM system we investigate presents an intriguing phase transition upon temperature change, especially near physiological temperature, which we will describe in Chapter 3.

Poly(N-isopropylacrylamide) (PNIPAAm) is a most well-known themoresposive polymer with a reproducible lower critical solution temperature (LCST).[53-54] Below the LCST, polymers are water soluble and the polymeric medium is swollen by encapsulated cargos. Above the LCST, a hydrophilic–hydrophobic transition occurs with the morphology change from coil-to-globule. During this transition, there have been shrinkage in polymer medium and thus the release of internal water and cargo molecules, stemming from the collapse of the polymer network (**Figure 1.3**).

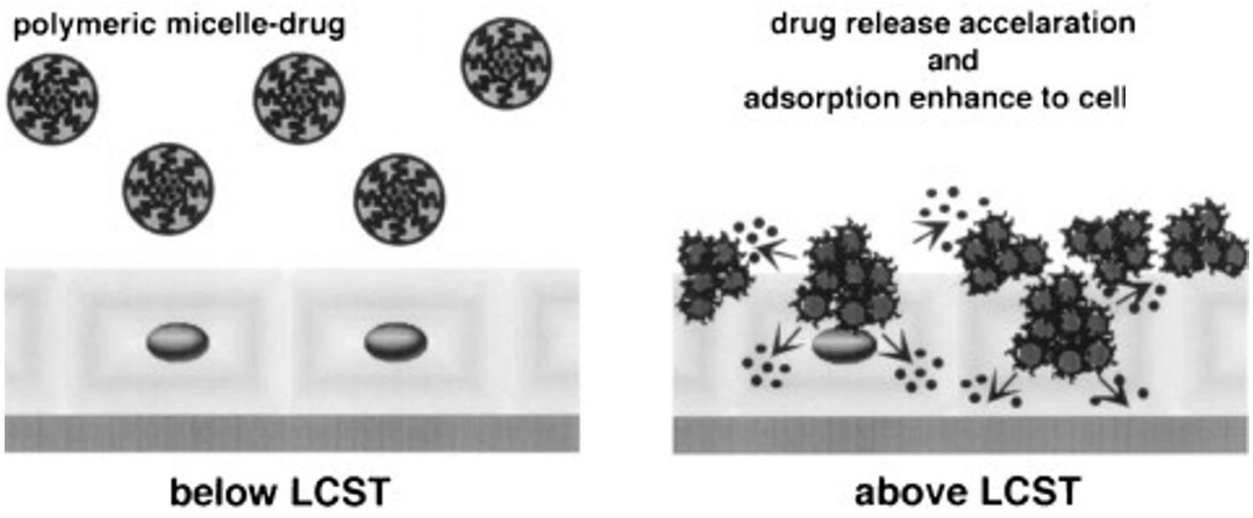

Figure 1.3. Drug release and interactions in micelles with PNIPAAm as shell-forming segments below and above LCST. Reproduced from Reference 55.[55]

More excitingly, dual and multi-stimuli responsive polymeric nanomaterials have been developed that respond to more than one signals, such as temperature / pH, temperature / pH /guest molecules and temperature / magnetic field.[56] The responses can occur either simultaneously or in a sequential manner at the pathological sites by designing different compartments or controlling the transport pathways in nanoparticles.

For example, Wei et al.[57] prepared diblock copolymer micelles with a PNIPAAm hydrophilic shell and a poly(10-undecenoic acid) hydrophobic core and they incorporated an anti-inflammation drug prednisone acetate into the BCMs. The release profile demonstrated a dramatic thermoresponsive switching behavior and also a pH responsive behavior. The BCMs were not pH sensitive below the LCST, but became pH sensitive above the LCST. Therefore, this dual-responsive micelle has great potential to be a novel carrier for drug delivery *in vivo*.

Zhao et al.[58] designed a dual-emissive photoluminescence hydrogel, by doping europium organic complexes Eu(III)$(TTA)_3$Phen in PNIPAAm-co-PS core and quaternary ammonium

tetraphenyl ethylene derivatives (d-TPE) in PNIPAM-co-poly (acrylic acid) (PAA) shell, respectively. These two emissions decreased linearly with the increasing temperature from 10 to 80 ℃ and pH from 7.6 to 4. This smart dual-emission hydrogel introduced two fluorescent moieties and improved the signal detectability compared to single photoluminescence, which has potential in applications such as biological imaging and cancer diagnosis.

Hoare et al.[59] synthesized a nanocomposite based on PNIPAAm and magnetite nanoparticles to achieve drug delivery by applying the magnetic field. They demonstrated the "on-demand" release of sodium fluorescein over multiple magnetic cycles and achieved 20-fold higher flux of sodium fluorescein when the temperature exceeded the volume phase transition temperature (40 ℃) of the nanogels. This bio-membrane has advantages of noncytotoxicity, biocompatibility and switchable flux, which greatly increases the flexibility of pharmacotherapy.

In summary, stimuli-responsive polymeric nanomaterials have excellent efficacy in both delivery and release of anti-cancer drugs. Dual and multi-stimuli responsive nanocarriers have tremendous potential for targeted cancer treatment with programmed site-specific features. In this dissertation, we discuss the temperature influence over dynamic stability and chain kinetics of BCMs in Chapters 3 – 4. The techniques and outcomes presented in these chapters will be helpful to investigate BCMs and other systems with temperature-based responses. In the forthcoming studies, thermo-responsive BCMs will be the model systems to study transitional behaviors and delivery features in polymeric nanocarriers.

1.3 Dynamic and Kinetic Studies of BCMs

BCMs have been the most extensively studied targeted cargo delivery carriers for years, and most studies have been focused on the static properties of BCMs at equilibrium, such as the overall stability or the size and structure of micelles. However, the polymer chains are rapidly

exchanging in BCMs, which also incur reassembly and disintegration.[60] Over the past decades, multiple studies have also been carried out to investigate chain kinetic behaviors in micelles. By understanding both dynamic and kinetic properties of BCMs, we obtained controlled design over nanocarriers that can be potentially applied not only in targeted drug delivery, but also other practical applications including foaming, coating and emulsification.

1.3.1 Unimer Exchange Process

A critical issue in understanding of the self-assembling behavior of BCMs is the chain exchange kinetics between individual micellar entities in the thermodynamic equilibrium. Here we review studies using small-angle neutron scattering, simulations and NMR to study the unimer exchange kinetics in BCMs. In Chapter 2, we will describe additional studies using NMR as a main tool, and in Chapter 4 we will propose a novel method to probe unimer exchange kinetics.

Zinn et al.[61] monitored the chain exchange kinetics of n-alkyl-PEO BCMs by time-resolved small angle neutron scattering (TR-SANS). By modeling the time-dependent scattering pattern after mixing H-H micelles and H-D micelles with a core-shell model, they confirmed the single exponential time decay, which agreed with the prediction of the Aniansson and Wall model.[62] Their findings support that chain exchange between the micelles is governed by the unimer expulsion process.

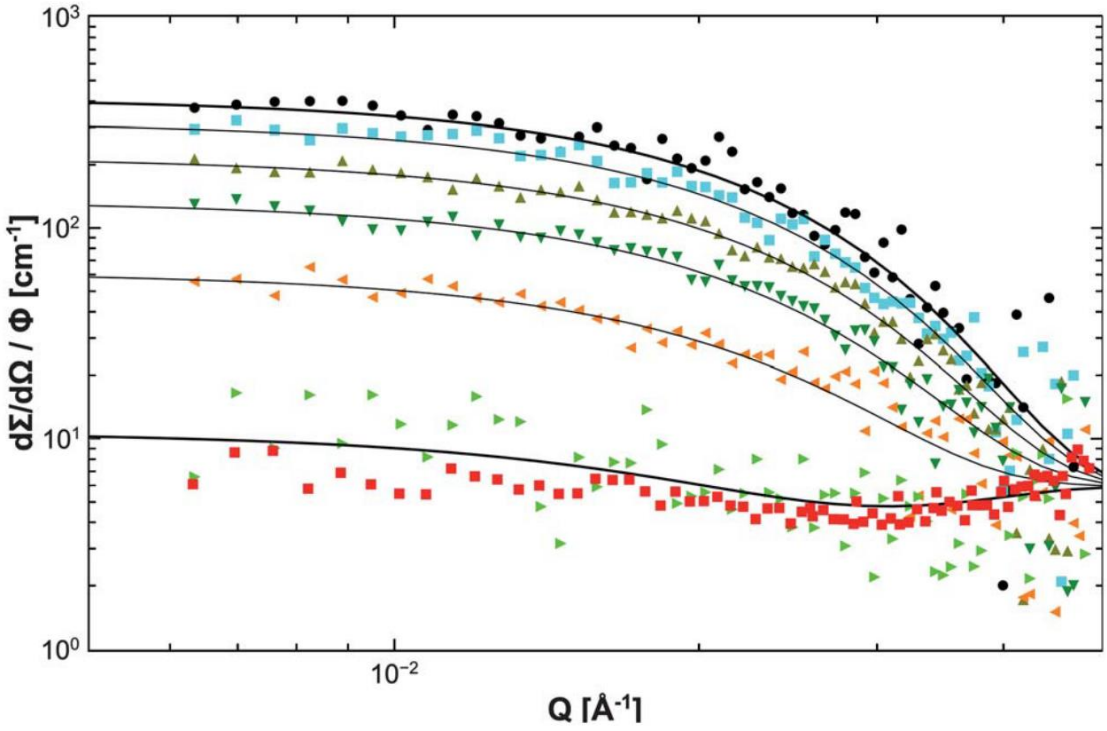

Figure 1.4. Time evolution of normalized absolute scattering cross section of C_{24}–PEO_5 BCMs after mixing. The data curves show the time evolution of normalized absolute neutron scattering cross-section of C_{24}-PEO_5 BCMs after mixing of deuterated and protonated micelle samples. Solid lines display fits of the core-shell model with $f(t)$ as variable parameter. Time evolution from top to bottom: t = 0.05 s, 5.6 s, 14.7 s, 25.2 s, 42.4 s, 95.0 s. Reproduced from Reference 61.

Prhashanna et al.[63] depicted the chain exchange kinetics between micelles formed by tadpole-shaped (with a loop-shaped hydrophobic block) and linear hydrophilic diblock copolymers using dissipative particle dynamics simulations. They found that the chain exchange kinetics were affected by the hydrophobicity, which resulted from the variations in chain architectures: a tadpole polymer had less hydrophobic blocks and exhibited a higher CMC, smaller aggregation number, and faster chain exchange kinetics. Also, the exchange kinetics of both components were affected by mixing, i.e. pure tadpole micelles > mixed micelles > pure linear micelles.

Schönhoff et al.[64] scrutinized the equilibrium dynamics of $C_{12}(EO)_5$ surfactant exchange between an adsorption layer on polystyrene latex particles and aqueous solution by pulsed field gradient (PFG) NMR. They described the region of intermediate exchange by a two-site model. The rates of monomer going into and leaving a micelle in equilibrium were given by the equation: $k_+ \, cmc = k_- \, N^{mic}$ (where N^{mic} was the aggregation number, k_+ the monomer incorporation rate, and k_- the monomer desorption rate). They identified the fast adsorption rates of micelles on latex layer on the order of 10 ms, which was corresponding to diffusion controlled adsorption. PFG-NMR probes the exchange time in ms, and is an efficient route to investigate equilibrium adsorption dynamics of surfactants beyond the diffusion limit, where the adsorption is kinetically controlled.

PFG-NMR is a powerful tool to probe soft matter behaviors. Nivaggioli et al.[65] have also studied the solubilization of aromatic molecules in Pluronic® micelles using NMR. Principles and more examples will be covered in Chapter 2.

1.3.2 Morphology Evolution

The self-assembling of BCMs provides a simple and tunable scheme with versatility and control over size or shape. To have a better control to tune BCM dynamics, it is crucial to obtain a detailed understanding of the dependence of morphology upon mixed solvents, polymer concentration, and block ratio, thereby providing guidance to optimize the preparation conditions to produce uniform and reproducible self-assemblies in solution. Techniques that can monitor morphological evolution include but are not limited to small angle X-ray scattering (SAXS), eletron microscopy (EM), dynamic light scattering (DLS), small angle neutron scattering (SANS), and nuclear magnetic resonance (NMR). In this section, we will review how the self-assembled structures are evolved using these techniques. In Chapter 3, we will introduce a BCM system in

mixed cosolvents (water / THF) and its dependence upon temperature and solvent composition using NMR.

Bang et al.[66] examined shape changes of a poly(styrene-b-isoprene) diblock copolymer dissolved in 1 vol % of solvents with varied selectivities for styrene, including dibutyl phthalate (DBP), diethyl phthalate (DEP) and dimethyl phthalate (DMP). The morphology changed from spheres to cylinders to vesicles, which was monitored by small angle X-ray scattering and cryo-TEM. Both techniques show good agreement with theory and indicate the importance of solvent selectivity in micellar morphologies.

Kelley et al.[67] highlighted the influence of cosolvent preparation methods (water / THF) on the micelle stability and size growth of polybutadiene-b-ethylene oxide (PEO-PB) BCMs (**Figure 1.5)**. They used multiple approaches, including DLS, cryo-TEM, SAXS and SANS to characterize BCMs prepared by common cosolvent mixtures, and led to quantitative investigations to reveal the mechanisms that affect micelles stability.

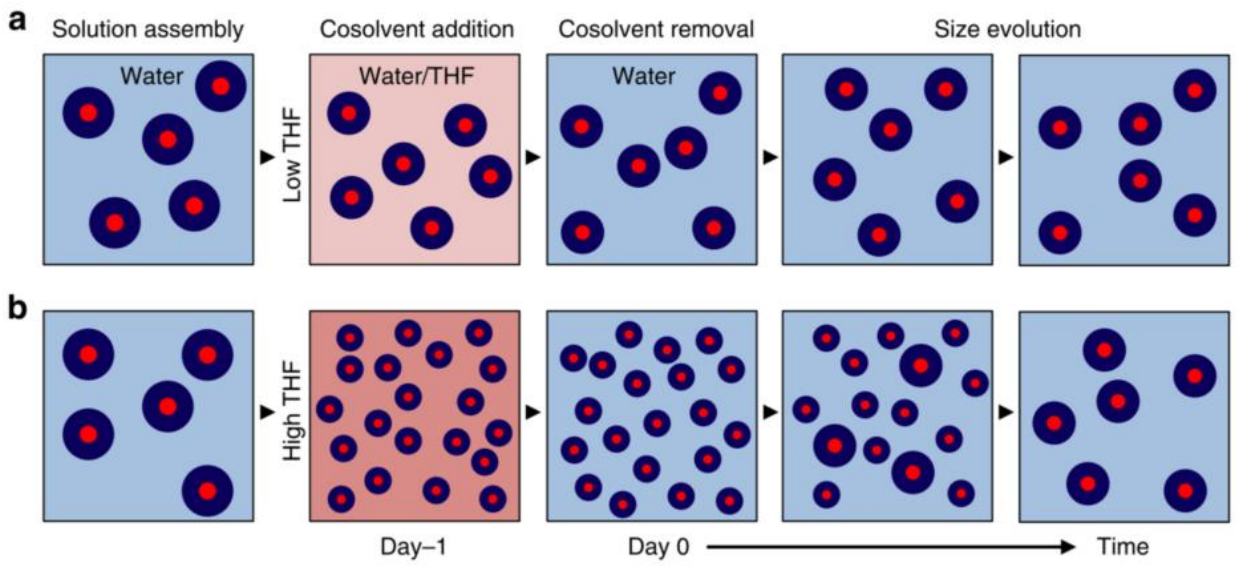

Figure 1.5. Schematic representation of changes in micelle size after cosolvent addition and removal (water / THF). (a) PB-PEO micelles in water decrease in size with THF cosolvent addition (< 10 vol %) and remain kinetically trapped after solvent is exchanged to water. Micelles prepared in solutions containing low THF contents are not perturbed far from their equilibrium size and do not undergo size revolution significantly. (b) Increasing the THF content (e.g. in 40 vol %) and subsequently remove the cosolvent perturbs the micelles far from their equilibrium size in water, leading to size relaxation through a bimodal pathway. Reproduced from Reference 67.

Ku et al.[68] prepared porous particles with tunable nanostructures and porosities using polystyrene-b-poly(4-vinyl pyridine) (PS-b-P4VP) polymers. By tuning the concentration of surfactant (sodium dodecyl sulfate (SDS)) and the volume fraction of P4VP (f_{P4VP}), they identified the interfacial instability that induced by the coadsorption of polymer and SDS at the droplet surface in emulsion, thus leading to the desired block copolymer particles. Those porous particles also demonstrated × 10 times higher loading efficiency of the dye molecules compared with

nonporous ones. Explorations of porous particles with a high surface area and stimuli-responsive functional groups could be targeted for selective uptake and release of active molecules.

Shen et al.[69] studied the thermodynamics of "crew-cut" micelles (with a large core and a relatively short corona) formed by polystyrene-b-poly (acrylic acid) (PS-b-PAA) in selective solvents DMF and H_2O. They used the UV-vis and DLS to measure the CMC, and estimated thermodynamic functions from ln(*C*/wt %) versus T_{CMT}^{-1} plots. They investigated the effects of water content, NaCl content, and the PS and PAA block lengths on the thermodynamic functions, including the standard Gibbs free energy (ΔG°), the standard enthalpies (ΔH°) and the standard entropies (ΔS°) of polymer chains per mole transfer from the ideal dilute polymer solution to the micelles. Moreover, the driving force for micellization changed from enthalpy only, to enthalpy with entropy, and eventually to entropy only as the water content increased. This dissertation discusses both dynamic and kinetic changes in BCM systems and will further studies in more complicated micelle systems and thermodynamic functions.

1.4 Conclusions

Current developments in chemistry, polymer science and biomedicine have accelerated the rise of new anti-cancer formulations, in which block copolymers contribute tremendously. This chapter introduces novel targeted cargo delivery carriers based on block copolymers include micelles, hydrogels, nanoparticles, liposomes, drug-polymer conjugates, graphite nanosheets, nanofibers, MOFs and dendrimers. All nanocarriers have exhibited excellent stability, as well as controlled / targeting cargo partitioning and release, which sheds lights on the proper design of block copolymer micelles (BCMs) we mainly study in this dissertation. We also discuss the dynamic and kinetic properties of BCMs, for example, the stability at equilibrium, unimer chain exchange and morphology change upon varying solvent properties (including mixed-solvent

compositions). We are able to have a controlled design of the polymer structures and thereby programmed properties applied in cargo delivery. To summarize, detailed understanding of BCMs is necessary for their development as novel delivery carriers. Chapter 2 will focus on theory and methods of NMR as applied to soft matters. Chapters 3 – 6 present new results of block copolymer micelles using NMR and Chapter 7 discusses how we can use NMR as a potent tool to understand ion-containing polymer systems with combination of other techniques.

References

1. Ulbrich, K.; Holá, K.; Šubr, V.; Bakandritsos, A.; Tuček, J.; Zbořil, R., Targeted Drug Delivery with Polymers and Magnetic Nanoparticles: Covalent and Noncovalent Approaches, Release Control, and Clinical Studies. *Chem. Rev.* **2016,** *116* (9), 5338-5431.
2. Basak, R.; Bandyopadhyay, R., Encapsulation of Hydrophobic Drugs in Pluronic F127 Micelles: Effects of Drug Hydrophobicity, Solution Temperature, and pH. *Langmuir* **2013,** *29* (13), 4350-4356.
3. Kiene, K.; Porta, F.; Topacogullari, B.; Detampel, P.; Huwyler, J., Self-assembling chitosan hydrogel: A drug-delivery device enabling the sustained release of proteins. *J. Appl. Polym. Sci* **2018,** *135* (1), 45638-n/a.
4. Zhang, L.; Li, Y.; Jin, Z.; Yu, J. C.; Chan, K. M., An NIR-triggered and thermally responsive drug delivery platform through DNA/copper sulfide gates. *Nanoscale* **2015,** *7* (29), 12614-12624.
5. Yavuz, M. S.; Cheng, Y.; Chen, J.; Cobley, C. M.; Zhang, Q.; Rycenga, M.; Xie, J.; Kim, C.; Song, K. H.; Schwartz, A. G.; Wang, L. V.; Xia, Y., Gold nanocages covered by smart polymers for controlled release with near-infrared light. *Nat. Mater.* **2009,** *8* (12), 935-939.
6. Belhadj, Z.; Ying, M.; Cao, X.; Hu, X.; Zhan, C.; Wei, X.; Gao, J.; Wang, X.; Yan, Z.; Lu, W., Design of Y-shaped targeting material for liposome-based multifunctional glioblastoma-targeted drug delivery. *J. Control. Release* **2017,** *255*, 132-141.
7. Liu, K.; Zhang, J.-J.; Cheng, F.-F.; Zheng, T.-T.; Wang, C.; Zhu, J.-J., Green and facile synthesis of highly biocompatible graphene nanosheets and its application for cellular imaging and drug delivery. *J. Mater. Chem* **2011,** *21* (32), 12034-12040.
8. Shen, Y.; Jin, E.; Zhang, B.; Murphy, C. J.; Sui, M.; Zhao, J.; Wang, J.; Tang, J.; Fan, M.; Van Kirk, E.; Murdoch, W. J., Prodrugs Forming High Drug Loading Multifunctional Nanocapsules for Intracellular Cancer Drug Delivery. *J. Am. Chem. Soc* **2010,** *132* (12), 4259-4265.

9. Nicolai, T.; Colombani, O.; Chassenieux, C., Dynamic polymeric micelles versus frozen nanoparticles formed by block copolymers. *Soft Matter* **2010,** *6* (14), 3111-3118.
10. Bae, Y.; Fukushima, S.; Harada, A.; Kataoka, K., Design of Environment-Sensitive Supramolecular Assemblies for Intracellular Drug Delivery: Polymeric Micelles that are Responsive to Intracellular pH Change. *Angew. Chem. Int. Ed.* **2003,** *42* (38), 4640-4643.
11. Chen, C.; Geng, J.; Pu, F.; Yang, X.; Ren, J.; Qu, X., Polyvalent Nucleic Acid/Mesoporous Silica Nanoparticle Conjugates: Dual Stimuli-Responsive Vehicles for Intracellular Drug Delivery. *Angew. Chem. Int. Ed.* **2011,** *50* (4), 882-886.
12. Cui, Y.; Zhang, M.; Zeng, F.; Jin, H.; Xu, Q.; Huang, Y., Dual-Targeting Magnetic PLGA Nanoparticles for Codelivery of Paclitaxel and Curcumin for Brain Tumor Therapy. *ACS Appl. Mater. Interfaces* **2016,** *8* (47), 32159-32169.
13. Wang, L.-J.; Zhou, X.-J.; Zhang, X.-H.; Du, B.-Y., Enhanced Mechanophore Activation within Micelles. *Macromolecules* **2016,** *49* (1), 98-104.
14. McBain, J., Mobility of highly-charged micelles. *Trans. Faraday Soc* **1913,** *9*, 99-101.
15. Lund, R.; Willner, L.; Richter, D., Kinetics of Block Copolymer Micelles Studied by Small-Angle Scattering Methods. In *Controlled Polymerization and Polymeric Structures*, Abe, A.; Lee, K.-S.; Leibler, L.; Kobayashi, S., Eds. Springer International Publishing: **2013**; Vol. 259, pp 51-158.
16. Ma, J.; Guo, C.; Tang, Y.; Xiang, J.; Chen, S.; Wang, J.; Liu, H., Micellization in aqueous solution of an ethylene oxide–propylene oxide triblock copolymer, investigated with 1H NMR spectroscopy, pulsed-field gradient NMR, and NMR relaxation. *J. Colloid. Inter. Sci.* **2007,** *312* (2), 390-396.
17. Jones, M.-C.; Leroux, J.-C., Polymeric micelles – a new generation of colloidal drug carriers. *Eur. J. Pharm. Biopharm.* **1999,** *48* (2), 101-111.
18. Moroi, Y., *Micelles Theoretical and Applied Aspects*. **1992**.
19. Oerlemans, C.; Bult, W.; Bos, M.; Storm, G.; Nijsen, J. F. W.; Hennink, W. E., Polymeric Micelles in Anticancer Therapy: Targeting, Imaging and Triggered Release. *Pharm. Res.* **2010,** *27* (12), 2569-2589.
20. Liaw, J.; Aoyagi, T.; Kataoka, K.; Sakurai, Y.; Okano, T., Visualization of PEO-PBLA-Pyrene Polymeric Micelles by Atomic Force Microscopy. *Pharm. Res.* **1998,** *15* (11), 1721-1726.
21. Nakamura, K.; Endo, R.; Takeda, M., Surface properties of styrene–ethylene oxide block copolymers. *J. Polym. Sci. B. Polym. Phys.* **1976,** *14* (7), 1287-1295.
22. Topel, Ö.; Çakır, B. A.; Budama, L.; Hoda, N., Determination of critical micelle concentration of polybutadiene-block-poly(ethyleneoxide) diblock copolymer by fluorescence spectroscopy and dynamic light scattering. *J. Mol. Liq.* **2013,** *177*, 40-43.

23. Kalyanasundaram, K.; Thomas, J. K., Environmental effects on vibronic band intensities in pyrene monomer fluorescence and their application in studies of micellar systems. *J. Am. Chem. Soc* **1977,** *99* (7), 2039-2044.
24. Mills, A. J.; Wilkie, J.; Britton, M. M., NMR and Molecular Dynamics Study of the Size, Shape, and Composition of Reverse Micelles in a Cetyltrimethylammonium Bromide (CTAB)/n-Hexane/Pentanol/Water Microemulsion. *J. Phys. Chem. B.* **2014,** *118* (36), 10767-10775.
25. Douglass, B. S.; Colby, R. H.; Madsen, L. A.; Callaghan, P. T., Rheo-NMR of Wormlike Micelles Formed from Nonionic Pluronic Surfactants. *Macromolecules* **2008,** *41* (3), 804-814.
26. Dimitrov, I.; Trzebicka, B.; Müller, A. H. E.; Dworak, A.; Tsvetanov, C. B., Thermosensitive water-soluble copolymers with doubly responsive reversibly interacting entities. *Prog. Polym. Sci.* **2007,** *32* (11), 1275-1343.
27. Yu, Y. S.; Eisenberg, A., Control of morphology through polymer-solvent interactions in crew-cut aggregates of amphiphilic block copolymers. *J. Am. Chem. Soc* **1997,** *119* (35), 8383-8384.
28. Israelachvili, J., Self-Assembly in Two Dimensions: Surface Micelles and Domain Formation in Monolayers. *Langmuir* **1994,** *10* (10), 3774-3781.
29. Holder, S. J.; Sommerdijk, N. A. J. M., New micellar morphologies from amphiphilic block copolymers: disks, toroids and bicontinuous micelles. *Polym. Chem*. **2011,** 2 (5), 1018-1028.
30. Yuan, J.; Li, Y.; Li, X.; Cheng, S.; Jiang, L.; Feng, L.; Fan, Z., The “crew-cut” aggregates of polystyrene-b-poly(ethylene oxide)-b-polystyrene triblock copolymers in aqueous media. *Eur. Polym. J.* **2003,** *39* (4), 767-776.
31. Deng, C.; Jiang, Y.; Cheng, R.; Meng, F.; Zhong, Z., Biodegradable polymeric micelles for targeted and controlled anticancer drug delivery: Promises, progress and prospects. *Nano Today* **2012,** *7* (5), 467-480.
32. Peppas, N. A.; Keys, K. B.; Torres-Lugo, M.; Lowman, A. M., Poly(ethylene glycol)-containing hydrogels in drug delivery. *J. Control. Release* **1999,** *62* (1), 81-87.
33. Harris, J. M., *Poly(ethylene glycol) Chemistry: Biotechnical and Biomedical Applications*. Plenum Press: **1992**.
34. Lutz, P.; Rempp, P., New developments in star polymer synthesis. Star-shaped polystyrenes and star-block copolymers. *Die Makromolekulare Chemie* **1988,** *189* (5), 1051-1060.
35. Graham, N. B., *Hydrogels in Medicine and Pharmacy*. CRC Press: **1987**; p 95-113.
36. Guo, X.; Li, D.; Yang, G.; Shi, C.; Tang, Z.; Wang, J.; Zhou, S., Thermo-triggered Drug Release from Actively Targeting Polymer Micelles. *ACS Appl. Mater. Interfaces* **2014,** *6* (11), 8549-8559.
37. Mohamed Daoud, C. E. W., *Soft Matter Physics*. **1999**; p 201-216.
38. Meier, M. A. R.; Aerts, S. N. H.; Staal, B. B. P.; Rasa, M.; Schubert, U. S., PEO-b-PCL Block Copolymers: Synthesis, Detailed Characterization, and Selected Micellar Drug

Encapsulation Behavior. In *Macromol. Rapid Commun.*, WILEY-VCH Verlag: **2005**; Vol. 26, pp 1918-1924.

39. Han, Y.; Zhang, Z.; Smith, G. S.; Do, C., Effect of nucleoside analogue antimetabolites on the structure of PEO-PPO-PEO micelles investigated by SANS. *Phys. Chem. Chem. Phys.* **2017,** *19* (24), 15686-15692.

40. Bae, Y. H.; Huh, K. M.; Kim, Y.; Park, K.-H., Biodegradable amphiphilic multiblock copolymers and their implications for biomedical applications. *J. Control. Release* **2000,** *64* (1–3), 3-13.

41. Malam, Y.; Loizidou, M.; Seifalian, A. M., Liposomes and nanoparticles: nanosized vehicles for drug delivery in cancer. *Trends Pharmacol. Sci.* **2009,** *30* (11), 592-599.

42. Hajos, F.; Stark, B.; Hensler, S.; Prassl, R.; Mosgoeller, W., Inhalable liposomal formulation for vasoactive intestinal peptide. *Int. J. Pharm.* **2008,** *357* (1), 286-294.

43. Vyas, S. P.; Quraishi, S.; Gupta, S.; Jaganathan, K. S., Aerosolized liposome-based delivery of amphotericin B to alveolar macrophages. *Int. J. Pharm.* **2005,** *296* (1), 12-25.

44. Lian, T.; Ho, R. J. Y., Trends and Developments in Liposome Drug Delivery Systems. *J. Pharm. Sci.* **2001,** *90* (6), 667-680.

45. Yan, J.; He, W.; Yan, S.; Niu, F.; Liu, T.; Ma, B.; Shao, Y.; Yan, Y.; Yang, G.; Lu, W.; Du, Y.; Lei, B.; Ma, P. X., Self-Assembled Peptide–Lanthanide Nanoclusters for Safe Tumor Therapy: Overcoming and Utilizing Biological Barriers to Peptide Drug Delivery. *ACS Nano* **2018,** *12* (2), 2017-2026.

46. Kitagawa, S.; Kitaura, R.; Noro, S.-i., Functional Porous Coordination Polymers. *Angew. Chem. Int. Ed.* **2004,** *43* (18), 2334-2375.

47. Zhou, H.-C.; Long, J. R.; Yaghi, O. M., Introduction to Metal–Organic Frameworks. *Chem. Rev.* **2012,** *112* (2), 673-674.

48. An, J.; Geib, S. J.; Rosi, N. L., Cation-Triggered Drug Release from a Porous Zinc−Adeninate Metal−Organic Framework. *J. Am. Chem. Soc* **2009,** *131* (24), 8376-8377.

49. Yu, D.-G.; Li, X.-Y.; Wang, X.; Yang, J.-H.; Bligh, S. W. A.; Williams, G. R., Nanofibers Fabricated Using Triaxial Electrospinning as Zero Order Drug Delivery Systems. *ACS Appl. Mater. Interfaces* **2015,** *7* (33), 18891-18897.

50. Ngoc Quyen, T.; Cuu Khoa, N.; Thi Phuong, N., Dendrimer-based nanocarriers demonstrating a high efficiency for loading and releasing anticancer drugs against cancer cells in vitro and in vivo. *Advances in Natural Sciences: Nanoscience and Nanotechnology* **2013,** *4* (4), 045013.

51. Padilla De Jesús, O. L.; Ihre, H. R.; Gagne, L.; Fréchet, J. M. J.; Szoka, F. C., Polyester Dendritic Systems for Drug Delivery Applications: In Vitro and In Vivo Evaluation. *Bioconjugate Chemistry* **2002,** *13* (3), 453-461.

52. Mura, S.; Nicolas, J.; Couvreur, P., Stimuli-responsive nanocarriers for drug delivery. *Nature Materials* **2013,** *12*, 991.
53. Karimi, M.; Sahandi Zangabad, P.; Ghasemi, A.; Amiri, M.; Bahrami, M.; Malekzad, H.; Ghahramanzadeh Asl, H.; Mahdieh, Z.; Bozorgomid, M.; Ghasemi, A.; Rahmani Taji Boyuk, M. R.; Hamblin, M. R., Temperature-Responsive Smart Nanocarriers for Delivery Of Therapeutic Agents: Applications and Recent Advances. *ACS Appl. Mater. Interfaces* **2016,** *8* (33), 21107-21133.
54. Voets, I. K.; Moll, P. M.; Aqil, A.; Jérôme, C.; Detrembleur, C.; Waard, P. d.; Keizer, A. d.; Stuart, M. A. C., Temperature Responsive Complex Coacervate Core Micelles With a PEO and PNIPAAm Corona. *J. Phys. Chem. B.* **2008,** *112* (35), 10833-10840.
55. Wei, H.; Cheng, S.-X.; Zhang, X.-Z.; Zhuo, R.-X., Thermo-sensitive polymeric micelles based on poly(N-isopropylacrylamide) as drug carriers. *Prog. Polym. Sci.* **2009,** *34* (9), 893-910.
56. Cheng, R.; Meng, F.; Deng, C.; Klok, H.-A.; Zhong, Z., Dual and multi-stimuli responsive polymeric nanoparticles for programmed site-specific drug delivery. *Biomaterials* **2013,** *34* (14), 3647-3657.
57. Wei, H.; Zhang, X.-Z.; Cheng, H.; Chen, W.-Q.; Cheng, S.-X.; Zhuo, R.-X., Self-assembled thermo- and pH responsive micelles of poly(10-undecenoic acid-b-N-isopropylacrylamide) for drug delivery. *J. Control. Release* **2006,** *116* (3), 266-274.
58. Zhao, Y.; Shi, C.; Yang, X.; Shen, B.; Sun, Y.; Chen, Y.; Xu, X.; Sun, H.; Yu, K.; Yang, B.; Lin, Q., pH- and Temperature-Sensitive Hydrogel Nanoparticles with Dual Photoluminescence for Bioprobes. *ACS Nano* **2016,** *10* (6), 5856-5863.
59. Hoare, T.; Santamaria, J.; Goya, G. F.; Irusta, S.; Lin, D.; Lau, S.; Padera, R.; Langer, R.; Kohane, D. S., A Magnetically Triggered Composite Membrane for On-Demand Drug Delivery. *Nano Lett.* **2009,** *9* (10), 3651-3657.
60. Prhashanna, A.; Khan, S. A.; Chen, S. B., Kinetics of Chain Exchange between Diblock Copolymer Micelles. *Marcomol. Theory Simul* **2016,** *25* (4), 383-391.
61. Zinn, T.; Willner, L.; Lund, R.; Pipich, V.; Richter, D., Equilibrium exchange kinetics in n-alkyl-PEO polymeric micelles: single exponential relaxation and chain length dependence. *Soft Matter* **2012,** *8* (3), 623-626.
62. Aniansson, E. A. G.; Wall, S. N., Kinetics of step-wise micelle association. *J. Phys. Chem.* **1974,** *78* (10), 1024-1030.
63. Prhashanna, A.; Dormidontova, E. E., Tadpole and Mixed Linear/Tadpole Micelles of Diblock Copolymers: Thermodynamics and Chain Exchange Kinetics. *Macromolecules* **2017,** *50* (4), 1740-1748.
64. Schönhoff, M.; Söderman, O., PFG-NMR Diffusion as a Method To Investigate the Equilibrium Adsorption Dynamics of Surfactants at the Solid/Liquid Interface. *J. Phys. Chem. B.* **1997,** *101* (41), 8237-8242.

65. Nivaggioli, T.; Tsao, B.; Alexandridis, P.; Hatton, T. A., Microviscosity in Pluronic and Tetronic Poly(ethylene oxide)-Poly(propylene oxide) Block Copolymer Micelles. *Langmuir* **1995,** *11* (1), 119-126.
66. Bang, J.; Jain, S.; Li, Z.; Lodge, T. P.; Pedersen, J. S.; Kesselman, E.; Talmon, Y., Sphere, Cylinder, and Vesicle Nanoaggregates in Poly(styrene-b-isoprene) Diblock Copolymer Solutions. *Macromolecules* **2006,** *39* (3), 1199-1208.
67. Kelley, E. G.; Murphy, R. P.; Seppala, J. E.; Smart, T. P.; Hann, S. D.; Sullivan, M. O.; Epps, T. H., Size evolution of highly amphiphilic macromolecular solution assemblies via a distinct bimodal pathway. *Nat Commun* **2014,** *5*.
68. Ku, K. H.; Shin, J. M.; Klinger, D.; Jang, S. G.; Hayward, R. C.; Hawker, C. J.; Kim, B. J., Particles with Tunable Porosity and Morphology by Controlling Interfacial Instability in Block Copolymer Emulsions. *ACS Nano* **2016,** *10* (5), 5243-5251.
69. Shen, H.; Zhang, L.; Eisenberg, A., Thermodynamics of Crew-Cut Micelle Formation of Polystyrene-b-Poly(acrylic acid) Diblock Copolymers in DMF/H2O Mixtures. *J. Phys. Chem. B.* **1997,** *101* (24), 4697-4708.

Chapter 2: Molecular Translational Motion and NMR Diffusometry

Abstract

This chapter will briefly present the basic theories of translational motion and principles of NMR diffusometry. Chapter 1 introduces a range of polymeric materials, which have played important roles as drug delivery agents, local sensors and nanoreactors in heterogeneous-phase synthetic procedures. Among a multitude of techniques to study these materials, NMR serves as a potent and diverse tool due to its non-destructive nature, its chemical specificity, and its isotope selectivity, thereby enabling acquisition of valuable molecular information, such as structure, interactions, dynamics, binding affinity, exchange kinetics and mobilities. An important concept in NMR methodology is the magnetic field *gradient,* which is applied to provide translational diffusion information, and also structural information (e.g. restricted diffusion in the range of 0.1 – 100 μm) during the NMR time scale. In all, by using NMR diffusometry, which is also known as pulsed-field-gradient (PFG) NMR, we are able to perform detailed qualitative and quantitative study of block copolymer micelles, and other polymeric systems to reveal their complex dynamic properties.

2.1 Introduction

2.1.1 Principles of NMR

The Nuclear Magnetic Resonance (NMR) initial longitudinal magnetization has coherence order $p = 0$ with the coherence order signifying the multiple of the *Larmor* frequency describing the free precession of the respective density matrix element. The rf pulses can change p and a 90° rf pulse transforms longitudinal into transverse magnetization ($p = +1$ and -1) in equal amounts and only signals corresponding to $p = -1$ will give a detectable signal.[1] In a system of coupled

spins or in which the spin quantum number is larger than 1/2, subsequent 90° pulses can generate multiple quantum coherences. (i.e. $p > +1$ or $p < -1$).

The NMR signal that is detected is the projection of the spin magnetization ($p = -1$ coherences) onto the x-y plane. The quadrature detector detects the signal and determines the nuclear spin precession.[2] According to the Euler's formula:

$$\exp(i\Phi) = \cos(\Phi)+i\sin(\Phi) \tag{2.1}$$

The signal intensity from a spin is proportional to the real component. The real component is $\cos(\Phi)$ and Φ is the phase angle of the spin in the x-y plane. In the NMR experiment, *I(t)* is the signal acquired at time *t* after initial excitation, which is obtained from the product of the volume integral $M(\boldsymbol{r})$ (i.e. bulk magnetization at point $\boldsymbol{r}$), multiplies the instantaneous phase of the magnetization $\Phi(\boldsymbol{r},t)$.[3-4]

$$I(t) = \int M(r)e^{i\phi(r,t)}dV \tag{2.2}$$

The signal attenuation of the NMR signal due to the distribution of Φ is given by:

$$I(t)=\int_{-\infty}^{\infty} P_{\phi}(\phi,t)e^{i\phi}d\phi \tag{2.3}$$

where $P_{\Phi}(\Phi,t)$ is the relative phase-distribution function; $P_{\Phi}(\Phi,t)$ is normalized and thus,

$$\int_{-\infty}^{\infty} \mathrm{P}_{\phi}(\phi,t)d\phi = 1 \tag{2.4}$$

When all the spins are coherently oriented along $\Phi = 0$, which corresponds to $P_{\Phi}(\Phi,t) = \delta(\Phi)$, where is the delta function and there will be zero attenuation, i.e. maximum signal.

$$I(t)=\int_{-\infty}^{\infty} \delta(\phi)e^{i\phi}d\phi=1 \tag{2.5}$$

The energy of the nuclear spins is dominated by the longitudinal field *Zeeman* interaction.[5] Due to the coherence times that spin ensembles exhibit, many other weak interaction terms can be

seen from NMR.[3-4] That is why NMR is a powerful tool to probe inter- and intra- molecular interactions in liquids. In solids, the dipolar interactions between spins strongly broadens the linewidth in NMR, therefore the transverse magnetization coherence is disturbed in a few tens of microseconds after formation.[6]

Since the 1970s, NMR has been used in colloidal and interfacial studies. NMR spectroscopy not only provides detailed micellar structural information, but also probes molecular interactions, arrangements and dynamics of micelles intravarious phases.[7] NMR serves as a versatile tool for block copolymer micelles (BCMs) by quantitative and qualitative measurements of spin-lattice relaxation time (T_1), spin-spin relaxation time (T_2) and diffusion coefficients (D),[8-9] which investigates molecular dynamic information on multiple time and length scales.[10] T_1 describes the time for net magnetization to relax back to equilibrium along the z-axis. T_2 describes time for net magnetization decoherence in the transverse x-y plane. Diffusion coefficient describes the mobility and will be introduced more in next two sessions.[11] In this dissertation, NMR is a main pathway to provide direct information of structural and dynamical behavior of micelles, unimers, cargos and solvents.

In NMR magnets, the manufacturers provide a magnetic field as homogeneous as possible in the sample space region, with the incorporation of 1st, 2nd, and higher order shimming coils to correct fine line-shapes. However, it is inevitable that there may occur some variations in spectrometer magnetic field along the longitudinal axis (B_0) across the sample area, which broadens a few Hz in the ^{1}H NMR spectrum. Note that this broadening effect can distort the NMR spectrum severely when the acquisition bandwidth is narrow. The additional broadening caused by B_0 field inhomogeneity can result in FID decay more rapidly than spin-spin relaxation (T_2) effects. The resultant time constant is usually labelled T_2*. The coherence loss from T_2 relaxation

is random and irreversible while that caused by the field inhomogeneity is ordered.[3, 12] Moreover, the coherence loss arises from inhomogeneous broadening can be refocused by applying an appropriate pulse sequence. Typically, the inhomogeneous broadening is caused by local differences in the Hamiltonian between the spin packets (isochromats). To the contrary, the homogenous broadening is common to each spin packet and is irreversible, which arises from the random motion of spins.[13] Throughout this dissertation, we assume the B_0 field is homogenous and well-shimmed. Therefore, the line-broadening is related with random motion (T_2-related) only.

2.1.2 Translational Motion

In a molecular system, the mean translational kinetic energy is given by the equipartition principle and is on the order of kT (where k is the Boltzmann constant and T is temperature). The distance molecules travel is described by the mean-square displacement (MSD) and varies with aggregation state due to the varying degree of hindrance (obstruction) presented by other molecules. If a species has a sufficient concentration by itself, its motion will also be affected by its own obstruction.[14]

Translational diffusion is the random thermal motion of molecules and is one of the most fundamental and important transport form. The stochastic molecular motion in a pure liquid at thermal equilibrium is termed *self-diffusion* and is characterized by a diffusion coefficient D ($m^2\ s^{-1}$) (**Figure 2.1**). In a multi-component system, each component has its own individual diffusion coefficient (D_i), which is related with its size, bulk viscosity and temperature. In the block copolymer micelle (BCM) systems we are studying, typical self-diffusion coefficients for BCMs range from $10^{-11} – 10^{-12}\ m^2\ s^{-1}$, for free unimer chains range from $10^{-10} – 10^{-11}\ m^2\ s^{-1}$ and for cargos range from $10^{-10} – 10^{-11}\ m^2\ s^{-1}$, depending upon the temperature, solvent properties and whether or not cargos are trapped in micelle cores.[15]

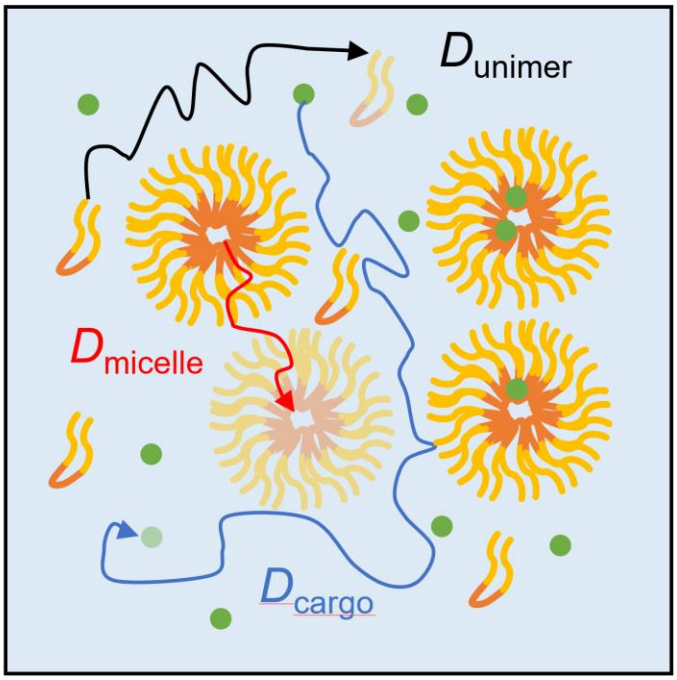

Figure 2.1. A schematic of stochastic molecular motion path of micelles (in red), unimer chains (in black) and cargos (in blue) in aqueous solution at thermal equilibrium.

Translational diffusion measurements have associated with a characteristic timescale termed Δ (i.e. "observation" or "diffusion" time). In enclosed porous structures, Δ determines and limits the dynamic information we get in the systems being studied. For example, a particle undergoes (1) isotropic free diffusion and (2) restricted diffusion in spheres (radius r) in **Figure 2.2**. To describe the effects of restriction on diffusion measurements, the dimensionless variable ξ, is defined in the Equation 2.6:

$$\xi = \frac{D\Delta}{r^2} \tag{2.6}$$

For the block copolymer micelle systems investigated in this thesis, we also investigated if there is any possible restricted diffusion in these self-assembled structures. In Chapter 4, we varied the Δ and observed constant D values, which indicates the isotropy and homogeneity of the

system. Moreover, varying Δ in diffusion can be further applied in the self-assembled gel systems to understand network crosslinking.

Diffusion measurements in restricted geometries can be divided into three regimes based upon the size of the mean-square displacement (MSD) compared to the pore size. (1) The "short time" or "free diffusion" limit ($\xi << 1$ or short Δ); in this limit the particle does not travel far enough to reach boundaries in pores during Δ, thus it feels no restrictions during diffusion and the measurements performed within Δ indicates the true diffusion coefficient (D^0). (2) The "crossover regime" from short- to long-time diffusion ($\xi \approx 1$); in this regime some of the particles can feel the effects of restrictions and the D measured is a function of Δ (D_{app}). The fraction of particles that reaches the boundary depends on the surface-to-volume ratio of the pore (S_p/V_p). (3) The "long-time" limit ($\xi >> 1$ or long Δ); in this regime all the particles experience the restriction boundaries and the displacement of particle is not dependent of Δ but only relies on r. In NMR diffusion measurements (with typical timescale of Δ = 10 – 1000 ms) and on small molecules with rapid diffusion (e.g., water), this indicates that restricted diffusion could become apparent in structures with length scales $\leqslant$ 100 μm.

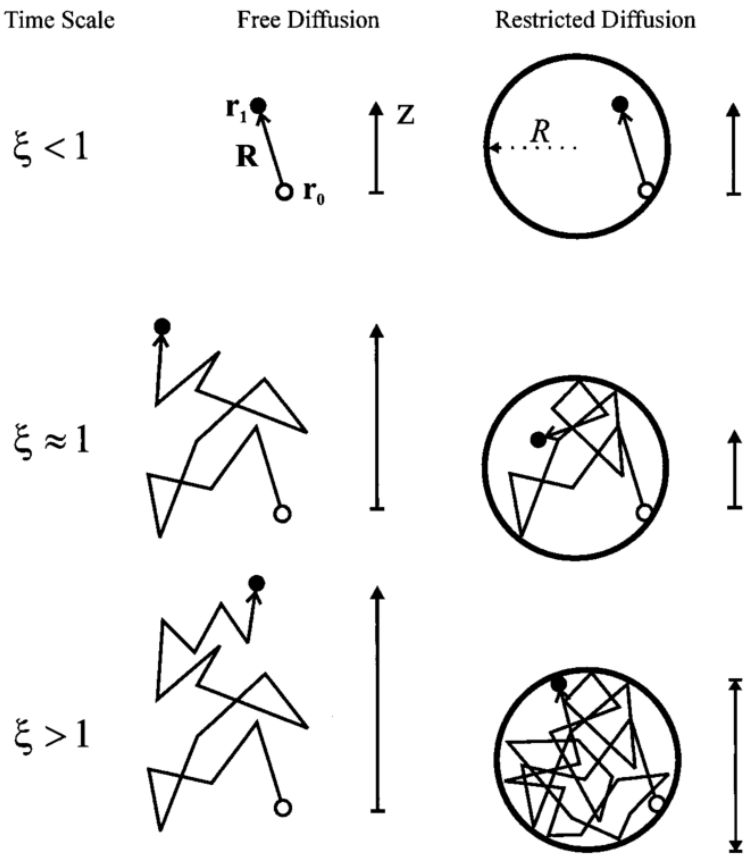

Figure 2.2. A schematic by comparing the effects of measurement timescale in free and restricted diffusion. The displacement of a species in the *z* direction (vertical) is measured by observing its starting position r_0 (open circle) at $t = 0$ and then at ending position r_1 (closed circle) at $t = \Delta$. **R** contributes to the displacement between the initial and final positions and the *Z* with vertical arrows represents the displacement of particle at vertical direction. At long diffusion times ($\xi >> 1$), the maximum displacement in restricted geometry is limited by the sphere boundary (i.e. radius). Reproduced from Reference 16.[16]

2.1.3 NMR Diffusometry

Various techniques have been developed for investigating molecular diffusion, including nuclear magnetic resonance,[17] dynamic light scattering,[18] neutron scattering,[19] fluorescence,[20]

capacity intermittent titration techniques,[21] attenuated total reflection infrared spectroscopy,[22] and centrifuge methods.[23] Those methods are usually limited to the sample preparation, experimental difficulty and concentration range. Besides those methods, NMR provides as an efficient tool to probe molecular dynamics in chemical and bio-logical systems, with the advantages such as non-invasive, non-perturbative and no requirement to label probe molecules. More importantly, NMR methods allow a direct measurement of diffusion coefficient (*D*) at different physical conditions, including high pressures or high temperatures. NMR diffusion measurements are applicable to any molecular concentration as long as there is a sufficient signal-to-noise ratio for NMR detection, where other methods could be possibly precluded.

The NMR spin-echo has been used in the diffusion measurements since its discovery by Hahn in 1950.[24] The application of static magnetic gradients (e.g. steady gradient spin-echo, SGSE NMR) have been used for diffusion measurements of water and polymers.[25] In 1965, it was improved by Stejskal and Tanner[26] by applying the magnetic gradients as pulses in the spin-echo sequence (i.e. pulsed gradient spin-echo, PGSE NMR). All the spin systems mentioned here, we assume to be at thermal equilibrium (i.e. M_0) when the pulse sequences were implemented. Here, the terms "spin" and "particle" convey the same meanings as the diffusing particles always contain nuclear spins. The imposition of magnetic field gradient pulses allows appropriate measurements of NMR diffusion and flow. Bloch-Torrey theory[27-28] equations describe the relationship between spin-echo attenuation, diffusion and gradient pulses. However, their full solutions become mathematically intractable for more complicated systems. Thus, we apply approximations and two of the most commonly used are: Short Gradient Pulse[29](SGP) and the Gaussian Phase Distribution[30] (GPD) approximations. The solutions derived using each of the methods to measure free isotropic diffusion is subject to correct boundary conditions. The SGP approximation is the

most easily method to express the relationship between experimental variables and the PGSE experiment. Thus, SGP is the first method relating the spin-echo attenuation to the experimental parameters we examine. Except the most commonly used sequences in PFG NMR, i.e. the Hahn spin-echo sequence[31] (SE) and the stimulated echo sequence[32] (STE), there have been other sequences such as Carr-Purcell-Meiboom-Gill[33-34] sequences (CPMG) and the related oscillating gradient experiments[35-36] (OGSE).

Magnetic field gradients are of great importance in PFG NMR and magnetic resonance imaging (MRI). They allow variations in magnetic gradient fields to encode spin spatial positions, that is, the gradient is to generate spatially distributed *Larmor* frequency along with its associated phase shift ω_0 (**r**)t, which can be detected to yield spatial (position) information for translational motion in PFG diffusometry and MRI. **Figure 2.3** schematically illustrates the PFG NMR pulse sequence design and measurement of molecular diffusion using an external magnetic gradient.

In a pulsed-gradient spin echo (PGSE) sequence, the first 90 ° pulse rotates the net magnetization from the z-direction to the x-y plane. After the RF pulse, all spins precess with the same frequency ($\omega_0 = \gamma B_0$) under B_0 (static magnetic field). When the 1st gradient pulse is applied, spins precess with position-dependent angular frequency ω_0 (z) = γB_0 + γzg, which results in a spatially distributed phase angle Ø(z) = $\gamma B_0 \delta$ + γzgδ at the end of the 1st gradient pulse δ. Ø(z) varies continuously in space and forms a helix profile along the gradient direction (z-direction in this schematic). If molecules do not experience translational motion during the diffusion time period Δ (the delay between the 1st and 2nd gradient pulses), the 180 °RF pulse will invert the helix phase, then the 2nd gradient pulse of the exactly same strength and duration as the 1st gradient pulse rewinds the helix, and produces a total signal where all the spin refocus into phase again (which is denoted as I_0).

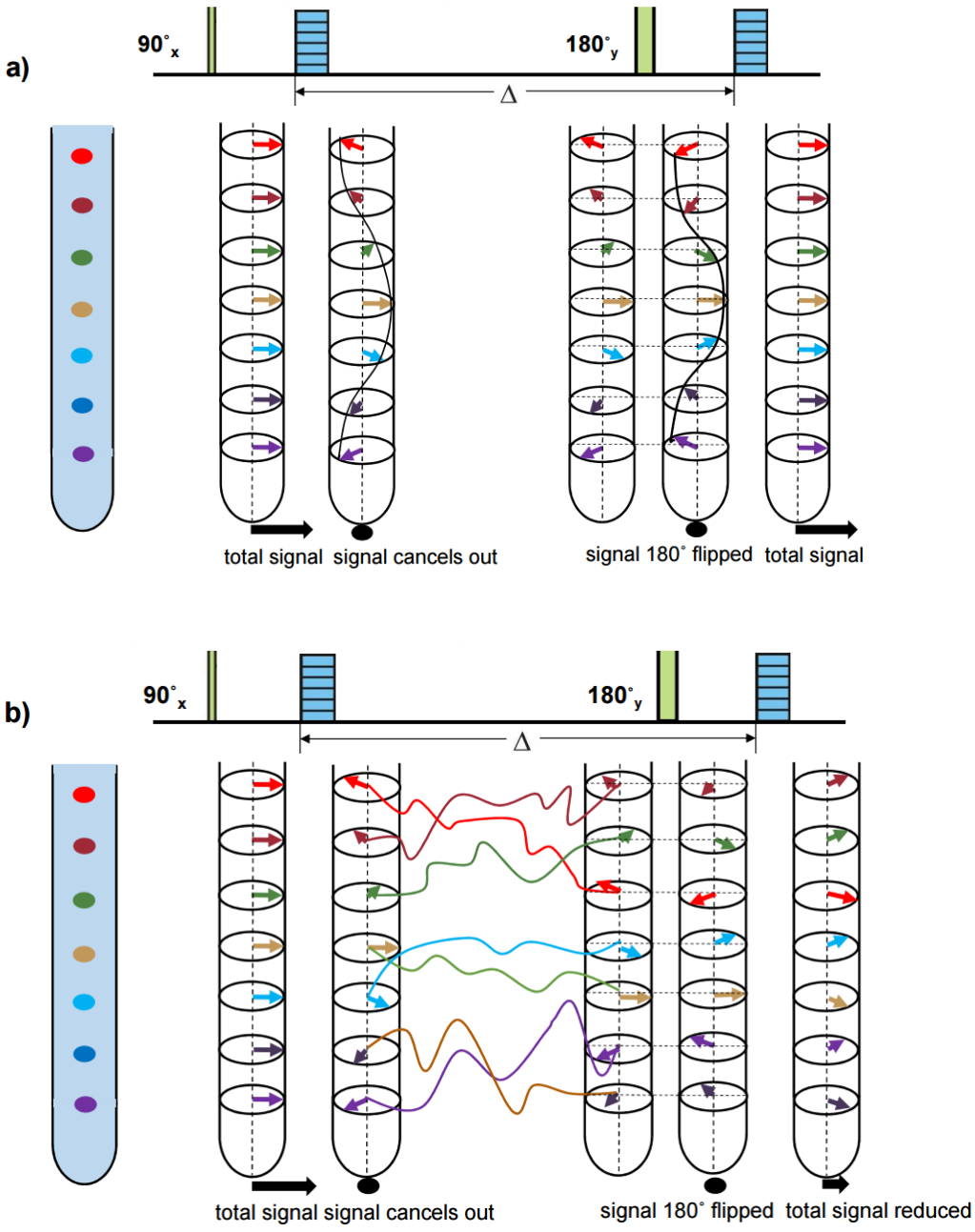

Figure 2.3. PFG spin echo (PGSE) sequence with one 90° and one 180 °pulses and two gradient pulses to dephase and refocus the nuclei spins. Δ is the time interval between the leading edges of gradient pulses. Effects of gradient pulses for nuclei (a) a total signal reappears with a refocusing gradient if there is no diffusion, (b) a total signal reduces with a refocusing gradient if there is diffusion.

However, if there are translational molecular motions during Δ, which is mostly common due to *Brownian* motion of molecules, a distribution of phases encoded with the history of the motions will dephase the complete refocus of the spins after the 2nd gradient pulse, resulting in a loss of magnetization phase coherence and a decrease in NMR signal intensity (denoted as *I*).

Besides measurements of a sample with a single species, we also have many interests in mixtures of species with various molecular weights or sizes. Moreover, macromolecular systems such as polymers (e.g. synthetic and natural) may form polydisperse systems, which can present challenges for PFG NMR measurements. As the diffusion coefficient of a molecule is correlated to its molecular weight through its effective hydrodynamics radius via the Einstein-Sutherland Equation,[37] diffusion measurements can work with mixtures of various species and polydisperse systems of the same species (will discuss more in Chapter 3). Thus, we can resolve differences in signal attenuation between the components in complex systems, which is termed "NMR Chromatography".[38-39]

The analysis would be simplest when the difference species have isolated resonances in the NMR spectrum. However, it is common that the resonances of difference species are overlapped. For a discrete system of N_d freely diffusing species with individual diffusion coefficient D_i, each species is characterized by a signal relaxation time T_{2i}. We can acquire the echo signal amplitude with a Hahn spin-echo-based sequence can be described by a decaying multi-exponential function below:[3, 15]

$$I(q,2\tau)=\sum_{i}^{N_D} M_{0,i}\exp(\frac{-2\tau}{T_{2i}})\exp(-bD_i) \tag{2.7}$$

where $M_{0,i}$ is the equilibrium magnetization for the *i*th species in the sample. In a polydisperse system with a single monomer species: $M_{0,i}$ is proportional to $M_{Wi}n_i$; where M_{Wi} is the molar mass

of the *i*th aggregate species, n_i is the number of these molecules present. The analysis of polymeric samples is complicated as the spectra of the different oligomers are completely superimposable.

As indicated by Equation 2.7 the PGSE attenuation curves of mixtures and polydisperse samples tend to be non-exponential. This may be not apparent depends on samples, for example, diffusion difference, degree of polydispersity or relative population of different species. Different molecular weights and mobility of polydisperse species can result in different relaxation rates, therefore the observed echo signal is not only weighted by the respective concentrations. We obtain the following equation by normalizing Equation 2.7:

$$\mathrm{E(q,\Delta)}=\frac{S(q,2\tau)}{S(0,2\tau)}=\frac{\sum_{i}^{N_D} M_{0,i}\exp(\frac{-2\tau}{T_{2i}})\exp(-bD_i)}{\sum_{i}^{N_D} M_{w,i}n_i\exp(\frac{-2\tau}{T_{2i}})} \tag{2.8}$$

Non-exponential decays have been observed in synthetic polymer systems to indicate polydispersity, but it has not been noted in PGSE measurement of proteins. Only a single "average" diffusion coefficient can be obtained from the data, even for concentrated samples of proteins such as lysozyme. Thus, in some systems, there is some process that results in ensemble averaging of diffusion coefficients of the different oligomeric species on microscopic scale. The averaging process can be approximated by taking the cumulant expansion:

$$\ln(I(q,\Delta)) = -b[D]_w + \frac{b^2}{2}([D]^2{}_w - [D^2]_w) \tag{2.9}$$

where $[D]_w$ is the mass-averaged diffusion coefficient defined by:

$$[D]_w = \frac{\sum_{i=1}^{N_D} M_{w,i}n_iD_i}{\sum_{i=1}^{N_D} M_{w,i}n_i} \tag{2.10}$$

The second term indicates the degree of polydispersity and would become evident as non-linearity in the attenuation plot (ln(*I*) vs. *b*), especially at large values of *b*. Although the exchange between different large oligomeric units is likely to be slow on the timescale of Δ, the final equation for the apparent diffusion coefficient is mathematically equivalent to that of the case of fast exchange:

$$I\,(\mathrm{q}, \Delta) = \exp\,(-b[D]_{\mathrm{w}}) \tag{2.11}$$

In NMR, there are mainly two ways to determine the self-diffusion coefficients by (1) analyzing nuclear spin relaxation data (2) magnetic field gradient NMR. Relaxation-based measurements are based on sensitivity of nuclear spin relaxation to the motions on the timescale of reorientation correlation time (τ_c) of the species. τ_c is usually in the ps to ns timescale in solution state and can be related to the solution viscosity and finally to the translational motion (i.e. diffusion coefficient) by Debye equation:[40]

$$\tau_c = \frac{4\pi\eta r_s^{\,3}}{3kT} \tag{2.12}$$

as well as the Einstein-Sutherland equation:[37]

$$D = \frac{kT}{6\pi\eta r_s} \tag{2.13}$$

In this spin-relaxation analysis, there are a couple of assumptions need to be made. Firstly, the relaxation mechanism of the probe species needs to be known and the intermolecular contributions can be separated from the intra-molecular contributions. Secondly, only spherical molecules can be described by a single correlation time for its reorientation dynamics. Thirdly, the bulk solution should be continuous for the probe molecules to validate the Debye equation. For example, a small probe species is used in biological milieux since the solution normally has a large macromolecule component (e.g. the cytoplasm of red blood cells).

The second method, pulsed-field-gradient (PFG) NMR provide a measurement of the translational self-diffusion coefficient as against methods such as dynamic light scattering or neutron scattering techniques. There have been numerous studies by using NMR methods to investigate soft matter. Lindman[41] and Stilbs[42] employed PFG NMR to obtain multicomponent diffusion data for various microemulsion systems and determine organic counterion binding to micelles. Stilbs et al.[43-44] also further studied the solubilization equilibria in surfactant micelles (e.g. sodium dodecyl sulfate). Typical spectra of signal attenuation in NMR diffusometry is shown in **Figure 2.4**.

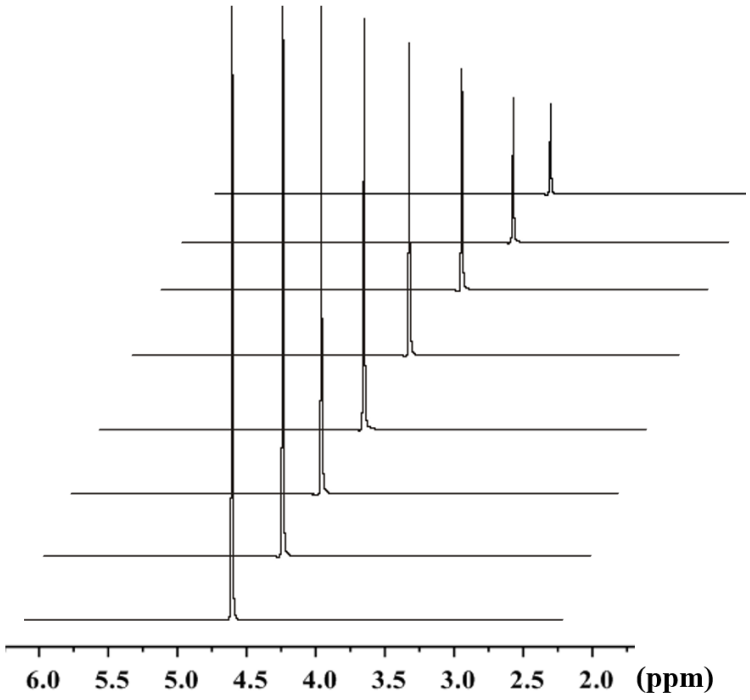

Figure 2.4. Example of signal attenuation of HPLC water in a ^{1}H NMR diffusometry experiment. *D* can be accurately measured for H_2O of 2.2×10^{-9} m^2 s^{-1}, which is < 3% error compared to the reference value. In one pulse sequence, we can measure a range of species, including solvent and polymers. Detailed diffusion measurements on BCM systems will be covered through Chapters 3-6.

In the next chapters, we will introduce more PFG NMR to investigate block copolymer systems, and we remark NMR and other techniques are complementary to study soft matter on different timescales.

2.2 Conclusions

In summary, NMR diffusometry (pulsed-field-gradient NMR) provides a straightforward way to obtain the translational motion information of nuclear spins. The modeling to extract information regarding the diffusion process and relevant chemical structures and morphologies can be complicated depending on the types of geometries present or the presence or absence of anisotropy in such systems. For all the systems we discuss in the latter chapters, the complications are ignored as for diluted polymeric systems.

This chapter quickly reviews basic NMR diffusometry to study translational motion and molecular interactions. It will be the major method to investigate dynamic (Chapter 3) and cargo partitioning behaviors (Chapter 5) in block copolymer micelles, as well as other functionalized polymer systems (Chapter 6 and 7). Not only can PFG NMR be applied to polymers, but it also can be extended to more complex systems such as restricted porous media and exchange of trapped cargos, to investigate structure and dynamics in a comprehensive way.

References

1. Aigner, C. S.; Clason, C.; Rund, A.; Stollberger, R., Efficient high-resolution RF pulse design applied to simultaneous multi-slice excitation. *J. Magn. Reson.* **2016,** *263*, 33-44.
2. Cujia, K. S.; Boss, J. M.; Herb, K.; Zopes, J.; Degen, C. L., Tracking the precession of single nuclear spins by weak measurements. *Nature* **2019,** *571* (7764), 230-233.
3. Callaghan, P. T., *Principles of nuclear magnetic resonance microscopy*. Oxford University Press on Demand: **1993**.
4. Levitt, M. H., *Spin Dymamics Basics of Nulcear Magnetic Resonance*. John Wiley&Sons, Ltd: **2011**.
5. Yao, W.; Liu, R.-B.; Sham, L. J., Theory of electron spin decoherence by interacting nuclear spins in a quantum dot. *Phys. Rev. B* **2006,** *74* (19), 195301.

6. Pines, D.; Slichter, C. P., Relaxation Times in Magnetic Resonance. *Phys. Rev.* **1955,** *100* (4), 1014-1020.
7. Wong, T. C., Micellar Systems: Nuclear Magnetic Resonance Spectroscopy. In *Encyclopedia of Surface and Colloid Science, Second Edition*, **2006**; pp 3738-3756.
8. J.P.Fraissard, H. A. R., *Magnetic Resonace in Colloid and Interface Science*. Springer-Verlag New York Inc.: **1979**.
9. Furó, I., NMR spectroscopy of micelles and related systems. *J. Mol. Liq.* **2005,** *117* (1–3), 117-137.
10. Steinbeck, C. A.; Chmelka, B. F., Rapid 1H {13C}-resolved diffusion and spin-relaxation measurements by NMR spectroscopy. *J. Am. Chem. Soc* **2005,** *127* (33), 11624-11635.
11. Bilia, A. R.; Bergonzi, M. C.; Vincieri, F. F.; Nostro, P. L.; Morris, G. A., A diffusion-ordered NMR spectroscopy study of the solubilization of artemisinin by octanoyl-6-O-ascorbic acid micelles. *J. Pharm. Sci.* **2002,** *91* (10), 2265-2270.
12. Golman, K.; in 't Zandt, R.; Thaning, M., Real-time metabolic imaging. *Proc. Natl. Acad. Sci.* **2006,** *103* (30), 11270-11275.
13. Keeler, J.; Neuhaus, D., Comparison and evaluation of methods for two-dimensional NMR spectra with absorption-mode lineshapes. *J. Magn. Reson.* **1985,** *63* (3), 454-472.
14. Söderman, O.; Price, W. S.; Schönhoff, M.; Topgaard, D., NMR diffusometry applied to liquids. *J. Mol. Liq.* **2010,** *156* (1), 38-44.
15. Price, W. S., *NMR studies of translational motion: principles and applications*. Cambridge University Press: **2009**.
16. Price, W. S., Pulsed-field gradient nuclear magnetic resonance as a tool for studying translational diffusion: Part 1. Basic theory. *Concepts. Magn. Reson* **1997,** *9* (5), 299-336.
17. Schönhoff, M.; Söderman, O., PFG-NMR Diffusion as a Method To Investigate the Equilibrium Adsorption Dynamics of Surfactants at the Solid/Liquid Interface. *J. Phys. Chem. B.* **1997,** *101* (41), 8237-8242.
18. Schillen, K.; Brown, W.; Johnsen, R. M., Micellar Sphere-to-Rod Transition in an Aqueous Triblock Copolymer System - A Dynamic Light-Scattering Study of Translational and Rotational Diffusion. *Macromolecules* **1994,** *27* (17), 4825-4832.
19. Chudley, C. T.; Elliott, R. J., Neutron Scattering from a Liquid on a Jump Diffusion Model. *Proc. Phys. Soc.* **1961,** *77* (2), 353.
20. Müller, C. B.; Loman, A.; Pacheco, V.; Koberling, F.; Willbold, D.; Richtering, W.; Enderlein, J., Precise measurement of diffusion by multi-color dual-focus fluorescence correlation spectroscopy. *EPL* **2008,** *83* (4), 46001.
21. Tang, X.-C.; Song, X.-W.; Shen, P.-Z.; Jia, D.-Z., Capacity intermittent titration technique (CITT): A novel technique for determination of Li+ solid diffusion coefficient of LiMn2O4. *Electrochim. Acta* **2005,** *50* (28), 5581-5587.

22. Lyon, S. B.; Philippe, L.; Tsuousoglou, E., Direct measurements of ionic diffusion in protective organic coatings. *Transactions of the IMF* **2006,** *84* (1), 23-27.
23. Minton, A. P., Analytical centrifugation with preparative ultracentrifuges. *Analytical Biochemistry* **1989,** *176* (2), 209-216.
24. Hahn, E. L., Spin Echoes. *Phys. Rev.* **1950,** *80* (4), 580-594.
25. Kimmich, R., Main-Field Gradient NMR Diffusometry. In *NMR: Tomography, Diffusometry, Relaxometry*, Kimmich, R., Ed. Springer Berlin Heidelberg: Berlin, Heidelberg, **1997**; pp 179-190.
26. Stejskal, E.; Tanner, J., Spin diffusion measurements: spin echoes in the presence of a time-dependent field gradient. *J. Chem. Phys.* **1965,** *42* (1), 288-292.
27. Barzykin, A. V., Theory of Spin Echo in Restricted Geometries under a Step-wise Gradient Pulse Sequence. *J. Magn. Reson.* **1999,** *139* (2), 342-353.
28. Weisskoff, R.; Zuo, C. S.; Boxerman, J. L.; Rosen, B. R., Microscopic susceptibility variation and transverse relaxation: Theory and experiment. *Magn. Reson. Med.* **1994,** *31* (6), 601-610.
29. Linse, P.; Soderman, O., The Validity of the Short-Gradient-Pulse Approximation in NMR Studies of Restricted Diffusion. Simulations of Molecules Diffusing between Planes, in Cylinders and Spheres. *J. Magn. Reson.* **1995,** *116* (1), 77-86.
30. Resing, H. A., Apparent Phase—Transition Effect in the NMR Spin—Spin Relaxation Time Caused by a Distribution of Correlation Times. *J. Chem. Phys.* **1965,** *43* (2), 669-678.
31. Bottomley, P. A.; Hardy, C. J., Two-dimensional spatially selective spin inversion and spin-echo refocusing with a single nuclear magnetic resonance pulse. *J. Appl. Phys* **1987,** *62* (10), 4284-4290.
32. Merboldt, K.-D.; Hanicke, W.; Frahm, J., Self-diffusion NMR imaging using stimulated echoes. *J. Magn. Reson.* **1985,** *64* (3), 479-486.
33. van Dusschoten, D.; Moonen, C. T. W.; de Jager, P. A.; Van As, H., Unraveling diffusion constants in biological tissue by combining Carr-Purcell-Meiboom-Gill imaging and pulsed field gradient NMR. *Magn. Reson. Med.* **1996,** *36* (6), 907-913.
34. Hürlimann, M. D.; Griffin, D. D., Spin Dynamics of Carr–Purcell–Meiboom–Gill-like Sequences in Grossly Inhomogeneous B0 and B1 Fields and Application to NMR Well Logging. *J. Magn. Reson.* **2000,** *143* (1), 120-135.
35. Schachter, M.; Does, M. D.; Anderson, A. W.; Gore, J. C., Measurements of Restricted Diffusion Using an Oscillating Gradient Spin-Echo Sequence. *J. Magn. Reson.* **2000,** *147* (2), 232-237.
36. Parsons Jr., E. C.; Does, M. D.; Gore, J. C., Temporal diffusion spectroscopy: Theory and implementation in restricted systems using oscillating gradients. *Magn. Reson. Med.* **2006,** *55* (1), 75-84.

37. Poo, M.-m.; Cone, R. A., Lateral diffusion of rhodopsin in the photoreceptor membrane. *Nature* **1974,** *247*, 438.
38. Pemberton, C.; Hoffman, R. E.; Aserin, A.; Garti, N., NMR Chromatography Using Microemulsion Systems. *Langmuir* **2011,** *27* (8), 4497-4504.
39. Pemberton, C.; Hoffman, R.; Aserin, A.; Garti, N., New insights into silica-based NMR "chromatography". *J. Magn. Reson.* **2011,** *208* (2), 262-269.
40. Debye, P.; Edwards, J. O., Long-Lifetime Phosphorescence and the Diffusion Process. *J. Chem. Phys.* **1952,** *20* (2), 236-239.
41. Lindman, B.; Stilbs, P.; Moseley, M. E., Fourier transform nmr self-diffusion and microemulsion structure. *J. Colloid. Inter. Sci.* **1981,** *83* (2), 569-582.
42. Stilbs, P.; Lindman, B., Determination of organic counterion binding to micelles through Fourier transform NMR self-diffusion measurements. *J. Phys. Chem.* **1981,** *85* (18), 2587-2589.
43. Stilbs, P., A comparative study of micellar solubilization for combinations of surfactants and solubilizates using the fourier transform pulsed-gradient spin—echo NMR multicomponent self—diffusion technique. *J. Colloid. Inter. Sci.* **1983,** *94* (2), 463-469.
44. Stilbs, P., Micellar breakdown by short-chain alcohols. A multicomponent FT-PGSE-NMR self-diffusion study. *J. Colloid. Inter. Sci.* **1982,** *89* (2), 547-554.

Chapter 3: Mapping Coexistence Phase Diagrams of Block Copolymer Micelles and Free Unimer Chains

Reprinted with permission from Xiuli Li, Tyler. J. Cooksey, Bryce. E. Kidd, Megan. L. Robertson, Louis. A. Madsen. Macromolecules **2018** 51 (20), 8127-8135 © 2018, American Chemical Society.

Abstract

Block copolymer micelles can carry molecular cargo in a nanoscopic package that is tunable via polymer structure in combination with cargo and/or solution properties. We use NMR spectroscopy and diffusometry to investigate spherical micelles that self-assemble from diblock poly(ethylene oxide)-b-(ε-caprolactone) (PEO-PCL) at 1% wt/vol in D_2O-THF-d_8 mixed solvents. For two series of micelles with block masses of 2 and 3 kg/mol (PEO and PCL, respectively), and 5 and 8 kg/mol, we quantify diffusion coefficients and relative populations of micelles and free unimers over a range of temperature (21 – 50 ˚C) and solvent composition (10 – 100 vol % THF-d_8). Micelles and free unimers coexist over surprisingly large areas of these micelle-unimer phase diagrams, and with a large variation of relative populations. This study provides a new avenue for understanding how inter- and intramolecular interactions fundamentally affect unimer exchange, cargo release, the thermodynamics of chain partitioning, and the tuning of micelle structure and dynamics.

3.1 Introduction

Block copolymer micelles (BCMs) have been favored in a multitude of applications such as tailored nanoreactors,[1] tissue engineering[2] and drug delivery.[3] In particular, BCMs have been applied as novel and promising carriers in targeted drug delivery because of their prolonged circulation time, *in vivo* degradability, low critical micelle concentration and controllable

functionalities.[4-7] For example, biodegradable BCMs have been employed in controlled delivery of hydrophobic anticancer drugs, e.g., paclitaxel and doxorubicin, and there have been many micellar drug formulations approved for clinical trials.[2, 8-9] In terms of fundamentally understanding amphiphilic BCM systems, micellar solution morphology depends not only on *polymer characteristics*, including polymer chain length and relative proportions of hydrophilic and hydrophobic blocks.[10-12] but also on *solution composition*, including choice of solvent, solute concentration, and the presence of additives.[13-14] Micelle structure and size are determined by balancing effects with three main influences: (1) interfacial tension between the core and corona blocks, (2) stretching force between core and corona blocks, and (3) interactive repulsion force among corona chains.[10, 15] Also critical for understanding solution properties and micelle dynamics, such as polymer chain and cargo exchange kinetics, are the populations of both free unimers and micelles in solution.[16-17]

The block copolymer poly(ethylene oxide)-*b*-(ε-caprolactone) (PEO-PCL) has enjoyed popularity in targeted cargo delivery for its capacity to self-assemble into spherical micelles in aqueous solution and solubilize relatively hydrophobic molecules into the micelle cores.[18] The hydrophilic PEO block forms the external shell and is non-biodegradable and biocompatible. The hydrophobic PCL block forms the inner core and provides a desirable matrix for long-term drug release.[19] There have been relatively few studies on the fundamental behaviors of PEO-PCL based micelles. Cho et al.[20] synthesized a series of PEO-PCL-PEO triblock copolymers and studied the effects of hydrophile-lipophile balance on the elasticity and stability of multiple emulsions. Schuetz et al.[21] studied the morphology of a PEO-PCL block copolymer from spherical micelles to vesicles by tuning the solvent ratio of THF and water, and demonstrated an effective design to

control the morphology of self-assemblies in solutions. Kim et al.[22] prepared PEO-PCL BCMs to load indomethacin and evaluated them as drug carriers for hydrophobic cargos.

However, none of the above studies explored the free unimer population in solution, and free unimer concentration strongly affects overall micellar dynamics and self-assembly. At equilibrium, the free unimer concentration is usually assumed to be equal to the critical micelle concentration (CMC). For BCMs, the CMC generally is 10^{-6} to 10^{-7} M,[23] below the detection sensitivity of traditional physical methods such as osmotic pressure, conductivity, and interfacial tension,[24] thus making measurements highly uncertain. Under nonequilibrium conditions, assembly of micelles can occur by a sudden jump in either temperature or in the mixed solvent composition, driven by over-saturation of free unimers in solution.[25] Moreover, it has been reported that block copolymer aggregation state and free unimer population can influence pharmacokinetics (e.g., elimination of polymer from the body) and biodistribution.[26-27] Also, BCMs have been applied in the synthesis of precisely-controlled functional nanomaterials, such as nanoparticles[28] or mesophase crystals[29]. For example, Fan et al.[29] have formulated nanocrystal (NC)-micelles as building block solution and further self-assembled them into 2- and 3-dimentional order arrays. Excessive unimers in solution would result in less defined micelles, thus less control over the particle final structures and collective properties, notably for the evaporation-induced self-assemblies that can be affected by temperature or solvents. More broadly, presence of free unimers in thermal-responsive BCMs for targeted drug delivery is also crucial in medicinal and biological applications, to discover the design rules, thermostability, cargo encapsulation and release of BCMs at body temperature (~37 °C). In all, unimer concentration can correlate with the aggregation number, diameter and cargo loading in BCM solution. Therefore, it is necessary to establish a reliable method to identify free unimers in aqueous solution and quantify their relative

concentration, thus providing insights into molecular interactions and the dynamics of unimer exchange between micelles.

In order to quantify free unimer populations and understand solution behavior in micellar systems, we employ NMR diffusometry.[30-31] This technique allows straightforward and high precision diffusion coefficient measurements of various mobile species in many types of polymeric systems.[16, 32-33] In general, NMR serves as a complement to other BCM characterization techniques and holds the advantages of elemental and molecular specificity, wide availability, easy sample preparation, and non-destruction of samples. NMR spectroscopy and diffusometry also have a broad history in characterizing colloidal and interfacial systems,[16, 33-41] and can reveal details not only of chemical structure but also of molecular interactions and dynamics in various phases.

In this work, we expand on our previous studies of PEO-PCL BCM solutions with two different polymer compositions,[16-17] in which we investigated structural and dynamical features over a range of time and length scales. The lower molecular weight polymer composition, termed the 2k series (or PEO_{2k}-PCL_{3k}), has PEO and PCL blocks of molecular weight 2 and 3 kg/mol, respectively. The higher molecular weight composition, termed the 5k series (or PEO_{5k}-PCL_{8k}), has PEO and PCL blocks of 5 and 8 kg/mol, respectively. In all cases, we formulate these systems at 1% wt/vol in mixtures of D_2O and a co-solvent, THF-d_8, to generate spherical micelles instead of other self-assemblies, e.g. worm-like micelles or vesicles, which provides a way to sensitively tune micelle structure and dynamics, as well as give insights as a model compound to mimic hydrophobic cargo in a micelle (such as a drug). Our NMR diffusometry[16] and SANS[17] studies demonstrated drastically varying structural and dynamic parameters of these systems as a function of THF-d_8 co-solvent content, indicating that we can fine tune micelle self-assembly.

This manuscript focuses on the additional effect of temperature on the presence and dynamics of micelles and free unimers in PEO-PCL micelle solutions at varying solvent composition. In contrast to conventional expectations, we observe broad coexistence regions of micelles and free unimers in both PEO-PCL series. In addition, we can apply NMR diffusometry to investigate the self-assembly of amphiphilic polymers from unimers into micelles and reveal important characteristics, e.g. critical micelle temperature or critical micelle concentration. **Figure 3.1** schematically introduces the evolution of micelle-unimer coexistence as a function of the variables (temperature and solvent composition) that we modulate in this study.

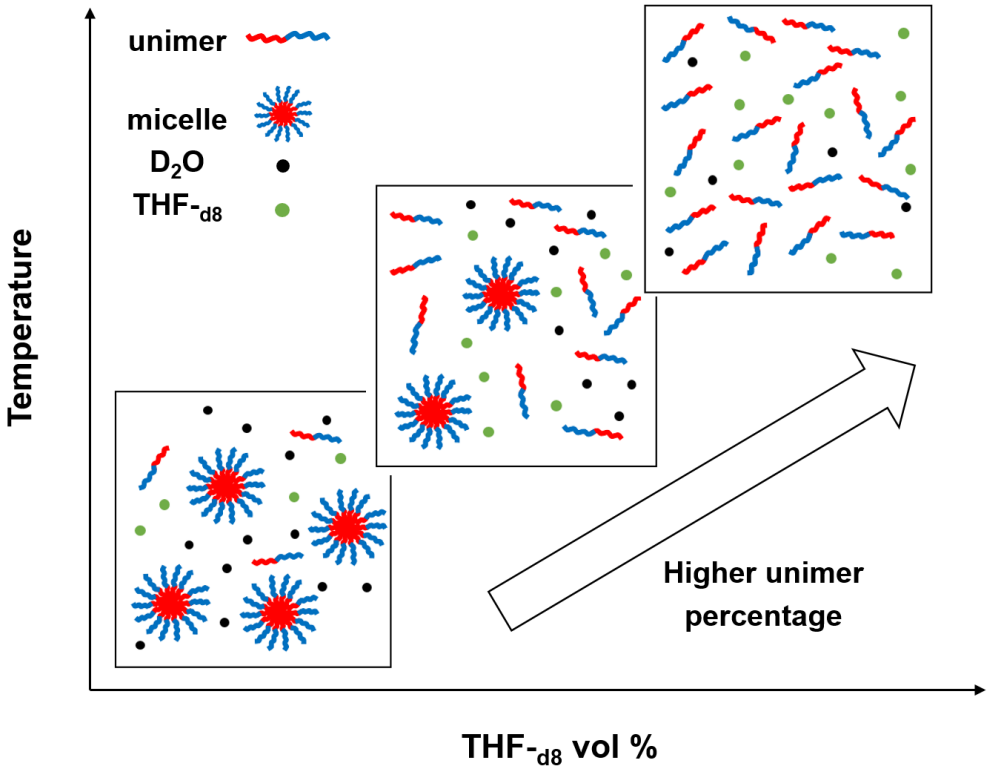

Figure 3.1. Illustration of block copolymer micelle (BCM) morphology changes with temperature and solvent composition. We observe the evolution of a free unimer fraction in solution with either increased temperature or THF-d_8 volume percentage in the solvent mixture, providing insightful information into controlled design of BCMs for various applications.

Building on these observations, we expect to provide insights into how these factors generally and significantly impact micelle structure and self-assembly, and thus enable controlled design of BCMs for drug delivery and other applications.

3.2 Experimental

3.2.1 Materials

Our procedures for the synthesis and characterization of poly(ethylene oxide-*b*-ε-caprolactone) (PEO-PCL) were previously published.[16-17] Briefly, PEO-PCL was synthesized through the ring-opening polymerization of ε-caprolactone from a methoxy-PEO initiator. The number-average molecular weight and dispersity were characterized by gel permeation chromatography, and a solvent switch method was used to prepare micelle solutions, following procedures reported previously by our group,[16-17] in which PEO-PCL was dissolved in THF-d_8 (1% wt/vol), followed by slow addition of D_2O using a syringe pump, followed by filtration. The solutions were then transferred to a 5 mm NMR tube and sonicated (Fisher Scientific model FS140H, Hampton, NH) for 30 min prior to data acquisition to minimize any possible aggregation. Four capillary tubes with outside diameter of 1 mm were placed in the tube to reduce thermal convection. Also, the tubes were flame sealed before the experiment to prevent solvent evaporation. Each sample tube was equilibrated for > 10 min prior to the first experiment at each temperature to make sure the sample is at thermal equilibrium. Samples are labeled 2k-X% (for 2k series) and 5k-X% (for 5k series) where "X" refers to the volume % of THF-d_8 in solution, which varies from 10 – 100%.

3.2.2 Pulsed-field-gradient (PFG) NMR Diffusometry

^{1}H PFG NMR diffusometry experiments were performed using a 400 MHz Bruker Avance III WB NMR spectrometer, equipped with a MIC probe and ^{1}H 5 mm coil coupled to a Diff60

single-axis (z-axis) gradient system. In an NMR diffusometry experiment, measured signal amplitude I as a function of gradient strength, g, was fit to the Stejskal-Tanner equation, [30, 42-43]

$$I = I_0 \exp[-\gamma^2 \delta^2 g^2 (\Delta - \delta/3) D] \quad (3.1)$$

where I_0 is the signal amplitude at $g = 0$, γ is the gyromagnetic ratio, δ is the effective gradient pulse length, Δ is the diffusion time between gradient pulses, and D is the self-diffusion coefficient. The "b" factor, which represents all known NMR-specific parameters and is useful for qualifying diffusion behaviors and artifacts, is given by $b = -\gamma^2 g^2 \delta^2 (\Delta - \delta/3)$. The simple and robust pulsed-gradient stimulated echo (PGSTE) sequence[30] was used with a 90 ° RF pulse length of 4.5 μs. A half sinusoid gradient pulse length of δ = 3.14 ms (effective rectangular pulse length = 2.00 ms), and post-gradient delay of 1.00 ms were used for ^{1}H diffusion measurements. The time scale of motion probed by this measurement is given by the diffusion time (Δ) in the PGSTE pulse sequence, which were varied from 10 – 200 ms. The unimers are not exchanging rapidly between solution and micelles over this range of time scales. In other words, the unimers are stable in each population at least up to 200 ms. Maximum gradient strengths were adjusted in the range 5 – 600 G cm^{-1} to achieve 90 – 99% signal attenuation in 16 – 32 steps. Sufficient signal-to-noise ratio (SNR) for each data point was achieved with 4 – 8 scans and acquisition times of 0.5 s (polymer signals) and 1.0 s (solvent signals) with 1 Hz line broadening. Relaxation delay times of 2.0 s were used for both polymer and solvent signals. Spin-lattice relaxation time (T_1) measurements using the same RF pulse lengths as above and the inversion-recovery sequence yielded T_1 values for PCL 6, PCL 2, PCL 3,5 and PCL 4 of 0.45 s, 0.46 s, 0.37 and 0.37s, respectively. The T_1 value of solvent water (residual H_2O in the D_2O) is 4.0 s. Spin-spin relaxation (T_2) measurements using the same RF pulse lengths as above and the CPMG sequence yielded T_2 values in the range of 0.03 to 1 s for all polymer resonances. The parameters used for the PGSTE experiments did not produce

significant differential signal intensity component weighting (including in 2-component fits, see below) due to T_1 and T_2 spin relaxation variations.

3.3 Results and Discussion

3.3.1 Proton NMR Spectroscopy and Spectral Linewidth

Detailed information of molecular environments can be gained from chemical shifts and linewidths observed in 1D ^{1}H NMR spectra. Chemical shift is mainly determined by covalently bound chemical structure, but is also influenced by weak intermolecular interactions such as hydrogen bonding, ring current effects, and solvent polarity.[44] In micellar systems, chemical shift can reveal important information such as interactions between molecules and/or ions.[40] In addition, monitoring changes in NMR linewidths can provide insights into micellar phase change and aggregations. Spin-spin relaxation time (T_2) generally reports on whether polymer chains are in a "rigid" or "mobile" environment. Broader linewidth (shorter T_2) indicates that polymer chains are less mobile, e.g., compared to solvent molecules. For example, in the NMR spectrum (**Figure 3.2**) obtained from the 5k-10% solution (10 vol % THF-d_8 and 90 vol % D_2O) at 21 ℃, the T_2 values for water (residual H_2O in the D_2O solvent), PEO, and PCL peaks are 6 s, 300 ms and 60 ms, respectively. Shorter T_2 values for PEO and PCL blocks demonstrate that the slower tumbling polymer chains are less mobile than the solvent. Moreover, PCL peaks have much shorter T_2 values compared to the PEO peak, which originates from the slower dynamics of PCL in the micelle cores.

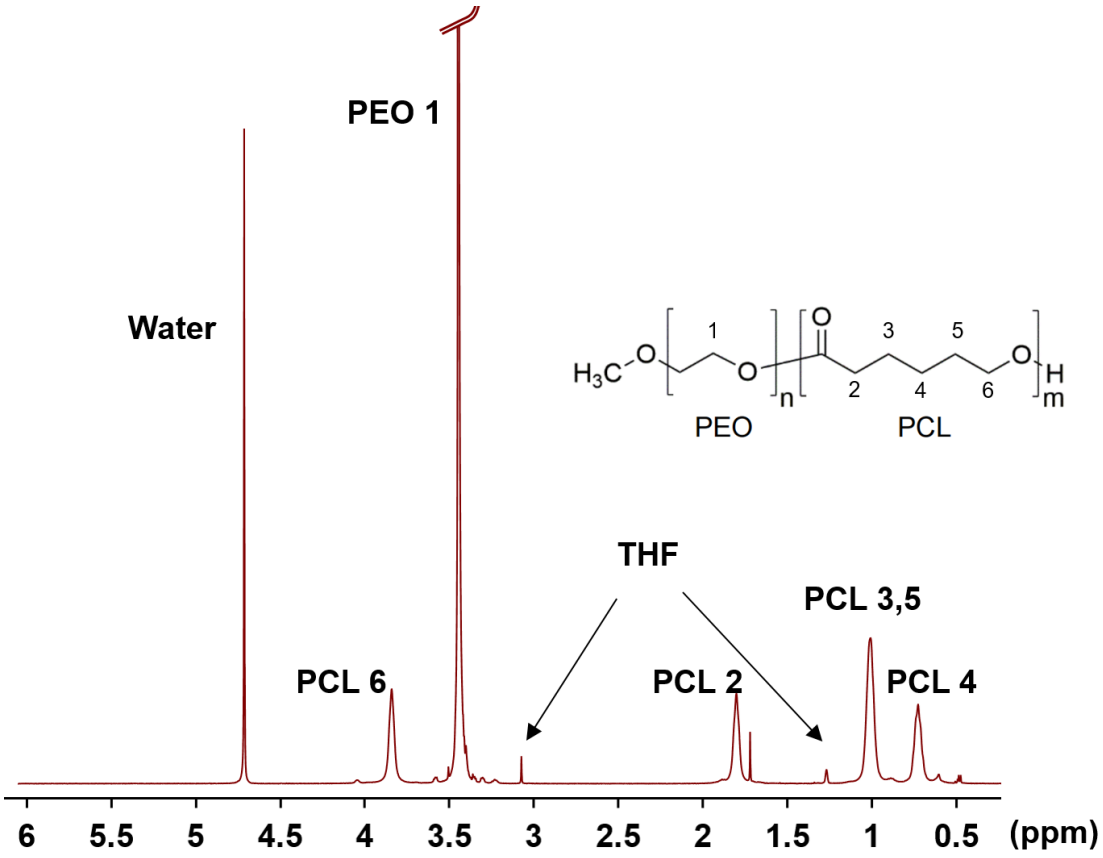

Figure 3.2. ^{1}H NMR spectrum of the 5k-10% micelle solution (PEO_{5k}-PCL_{8k} in 10 vol % THF-d_8: 90 vol % D_2O) at 25 ℃ and 600 MHz. Broader lines for both PEO and PCL peaks indicate that these polymer chains are in a less mobile environment compared to solvent, and that the PCL core has slower dynamics than the PEO corona. We can also probe molecular dynamics of PEO and PCL chains by measurement of spin-spin relaxation time (T_2).

Using NMR linewidth observation and T_2 measurement, we have also demonstrated the absence of core crystallization in these PEO-PCL BCMs. In NMR, broader linewidth or shorter T_2 value indicate that polymer chains are in a less mobile environment. In **Figure 3.3a**, all PCL signals remain as narrow peaks (no obvious broadening) at elevated temperatures, which suggests no core crystallization occurs upon heating. In **Figure 3.3b**, the increase of PCL T_2 value further supports there is no crystallization in this system.

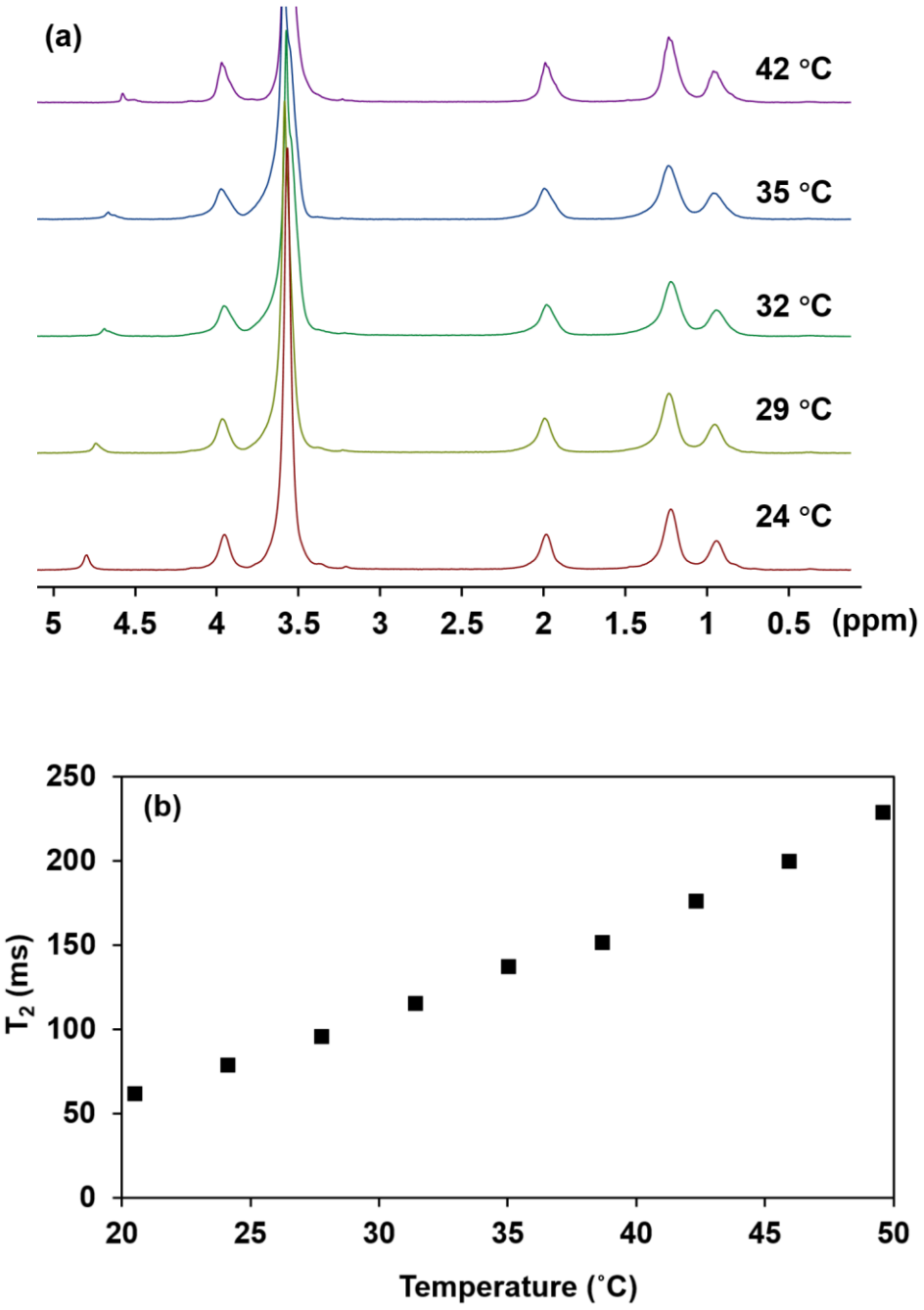

Figure 3.3. 1D ^{1}H NMR spectra overlay (a) and spin-spin relaxation time (T_2) (b) of PCL peaks in 5k series PEO-PCL micelle solutions at 10 vol % THF-d_8 in the range 21 – 50 ℃.

Typically, the NMR linewidth is inversely proportional to T_2 ($\upsilon_{1/2} = 1/\pi T_2$, $\upsilon_{1/2}$ = full width at half maximum). We did not observe narrowed PCL peaks in this system, which is because of

the multiplet splitting of PCL peaks and some modest magnetic field inhomogeneity (shims). In addition, other studies interpret NMR line shape and relaxation times to probe chain motions in membrane protein[1] and polymers.[2] Therefore, we can extend those NMR measurements as a sensitive tool to study the dynamic environment in macromolecules or nano crystallizers.

3.3.2 Effects of Temperature on Micelle-Unimer Coexistence at Fixed Solvent Composition

In our previous studies,[16-17] we sampled a range of solvent volume ratios for our binary solvent mixture starting with 10 to 100 vol % THF-d_8. By changing the mixed solvent (D_2O and THF-d_8) volume ratio, we gained insights into how micelle self-assembled structure, dynamics and unimer partitioning depend on the solvent environment.[16] Here we tune another important parameter to BCM structure and dynamics – temperature. **Figure 3.4a** shows increasing polymer diffusion coefficient as we increase temperature from 21 to 50 ℃, which is in accordance with the expected decrease in bulk viscosity. Significantly, when the temperature exceeds 35 ℃, we identify a second species that diffuses a factor of 4 faster than the previously observed polymer diffusion. This faster diffusion coefficient also increases monotonically with temperature. As in our previous study,[16] we attribute the slow diffusing component to micelles and the fast diffusing component to free unimer chains. Similarly, Fleischer et al.[45] have investigated a poly(ethylene oxide)/poly(propylene oxide)/poly(ethylene oxide) (PEO-PPO-PEO) P85 triblock copolymer using this method and identified macroscopic phase separation at 65 and 75 ℃ (10% wt/vol): one slow diffusion from the polymer-rich phase and one fast diffusion from polymer-poor phase. This NMR diffusometry method can resolve components of a single type of molecules in multi-diffusing environments (e.g., free unimers versus micelles) with high precision by the differences in NMR signal attenuation curve, which provides new insights into block copolymer behaviors, including micellization, gelation and phase separation.

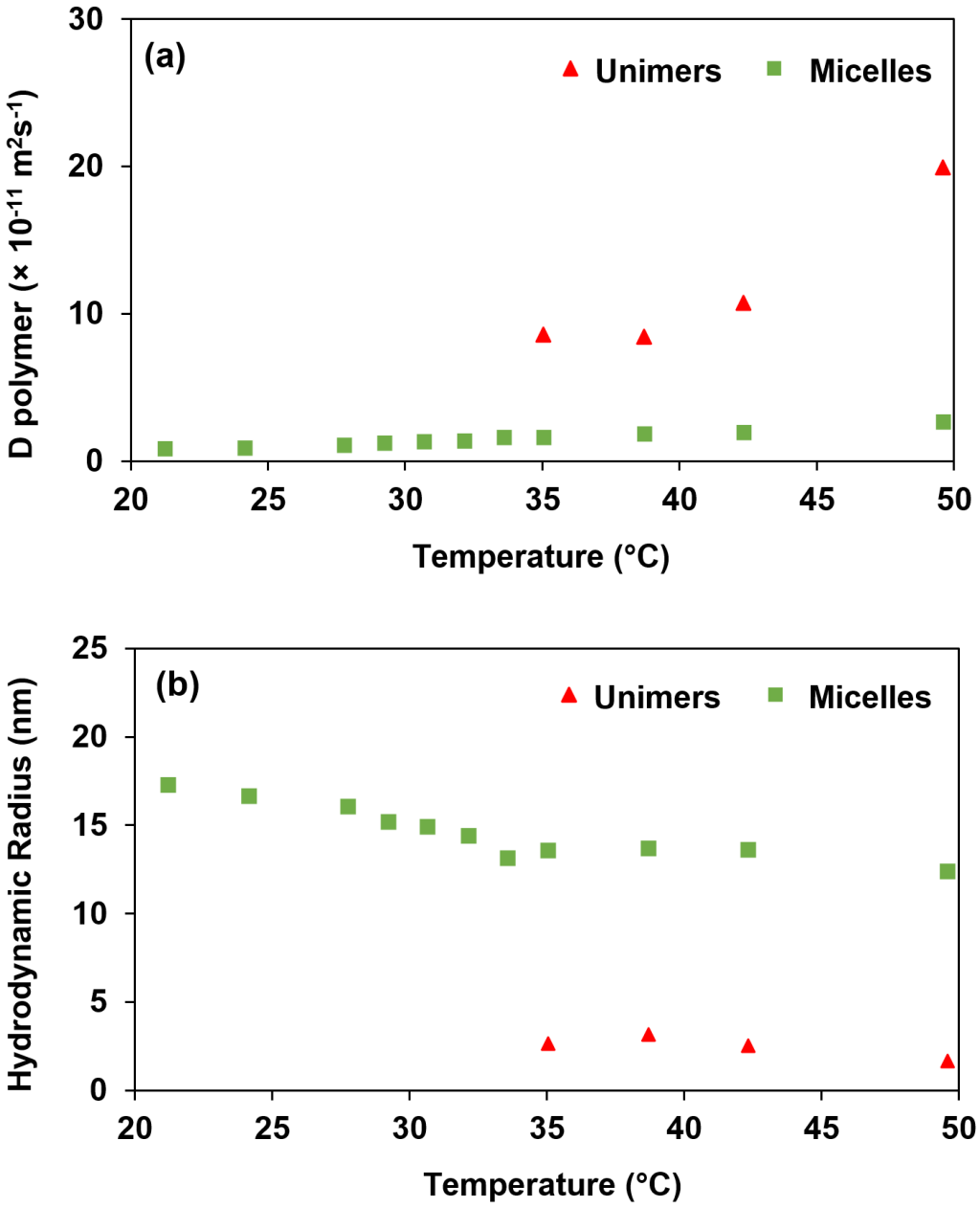

Figure 3.4. Diffusion coefficients (a) and hydrodynamic radii (b) of 5k-10% PEO-PCL BCM solutions at 21 – 50 ℃ obtained by ^{1}H NMR diffusometry. The slow-diffusing component (green squares) represents micelles and the fast-diffusing component (red triangles) represents free unimers, where the free unimer population rises with increased temperature.

Furthermore, we calculate the hydrodynamic radii of these species based on the Stokes-Einstein equation:

$$D = \frac{kT}{c\eta r_H} \tag{3.2}$$

where k is the Boltzmann constant, T is temperature, η is solution viscosity, r_H is hydrodynamic radius of the diffusing species, and c is a correction factor that depends on the relative size and shape of the diffusing species.[46] For spherical diffusing particles that are large compared with the surrounding fluid molecules (no-slip boundary conditions), c is 6π. For small diffusing particles (radii range: 2 – 6 Å), c is less than 6π.[47] For our micelles, r_H is large relative to solvent molecules, so we use $c = 6\pi$. For free unimers, this may not be as accurate an approximation, making r_H appear somewhat smaller than the actual size. We apply the Stokes−Einstein equation based on the assumption that free unimers and micelles are spheres in order to have a direct comparison of relative sizes between free unimers and micelles.

As shown in **Figure 3.4b**, the size of the micelles (green squares) varies from 12 – 17 nm. Decreasing micelle size with temperature likely results from dehydration of the PEO corona upon temperature elevation.[48-49] Here we compare with values of hydrodynamic radius of free unimers reported by Fleischer et al.[45] (10 ℃, 1 wt % of P85) and Bryskhe et al.[38] (10 ℃, 0.01 wt % of L121), which are 1.5 and 1.9 nm, respectively. We have a comparable average radius of ~ 2 nm of free unimers (red triangles). Therefore, we have identified the existence of a substantial population of free unimers in BCM solutions at elevated temperature, which we explore quantitatively next. The emergence of the free unimer population becomes easily visible in NMR diffusometry above approximately 5% of the total signal intensity, which corresponds to ~ 1×10^{-5} and ~ 4×10^{-6} M in solution for these PEO-PCL 2k and 5k series BCMs, respectively.

3.3.3 Micelle-Unimer Populations Assessed by NMR Diffusometry

In NMR diffusometry, we can detect multi-component diffusion when the species of interest is in different environments that exchange slowly on the diffusion time scale Δ (from a few ms to ~ 1 s), for example polymer chains residing both in micelles and in free solution. **Figure 3.5** shows NMR signal attenuation plots (also called Stejskal−Tanner plots) for 5k-10% micelle solution at 21 and 50 ℃, highlighting evolution of one-component and two-component signal decay curves, respectively. By plotting the natural log of normalized NMR signal intensity (I/I_0) versus the *b* factor in the Stejskal-Tanner equation (Equation 3.2), we are able to identify different components in the plots. A single linear regression suggests a single component fit, and the slope equals the diffusion coefficient (red dashed line). A bilinear dependence in the plot corresponds to more than one diffusing component (blue solid line), and in this case we observe a fast diffusing component (*free unimers*) that contributes to rapid signal decay at lower gradient strengths (steep slope), and a slow diffusing component (*micelles*) that decays slowly at higher gradient strengths (shallow slope).[50-53] Note that we did not detect any diffusing homopolymer (or short oligomer) component, which would diffuse substantially faster, indicating that block copolymer micelles are of high purity. We would also see continuous variations in diffusion curves if substantial amounts of smaller polymer fragments and/or a broad distribution of polymer molar mass were present in solution.

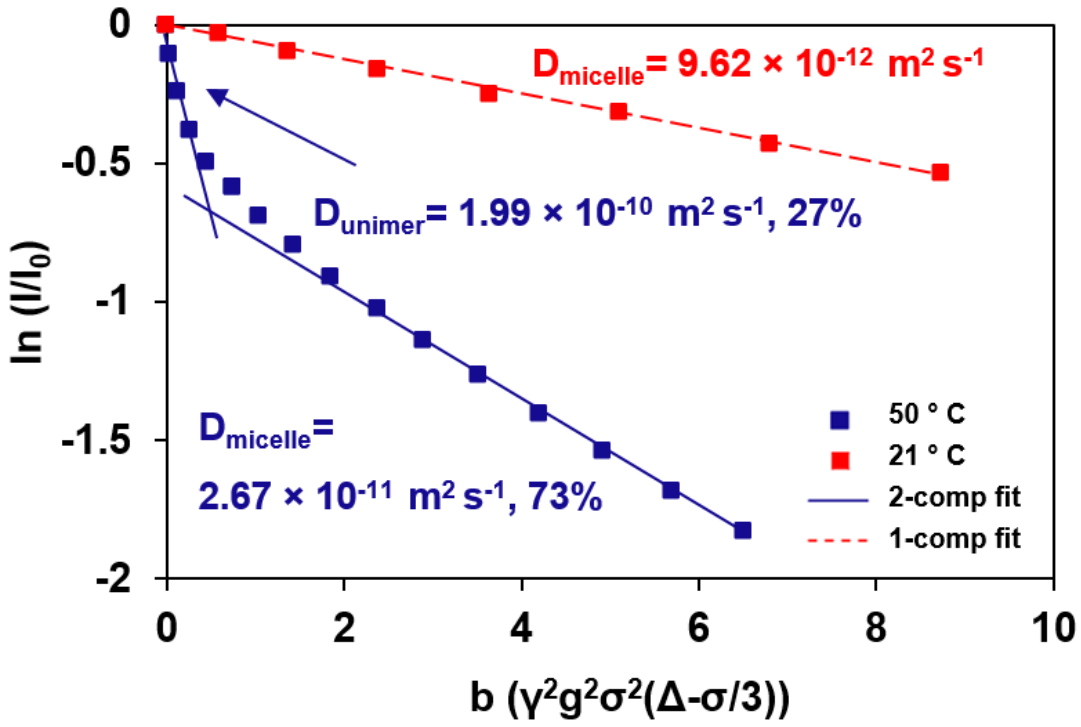

Figure 3.5. NMR diffusometry signal attenuation plots for 5k-10% PEO-PCL solutions at 21 and 50 ℃. At 21 ℃ we only detect one diffusing component that represents micelles. At 50 ℃ we observe two diffusing components: The fast component represents free unimers in solution, and the slow component represents micelles.

Importantly, for this investigation we are also able to quantify the populations of these two species by fitting the NMR diffusometry signal decay (Stejskal−Tanner) curves.[37] In this way, for the 5k-10% solution for example, we see that the unimer population increases from 10 to 27% as we increase temperature from 35 to 50 ℃. We discuss mapping of free unimer population via systematic variation of both solvent composition and temperature in section 3.3.4 below. Currently, block copolymer micelles are under extensive study by electron microscopy, light scattering, fluorescence and simulations, but these methods provide essentially no information about free unimer concentration in micellar solution. NMR diffusometry offers efficient and reliable access

to the free unimer concentration in micellar solution, which can deliver crucial information including the critical micelle concentration.

Currently, the predominant mechanisms identified for unimer chain exchange in micelles are insertion/expulsion and fusion/fission.[54-56] The insertion/expulsion mechanism is thought to dominate at a low polymer concentration, and the fusion/fission mechanism is expected to contribute more at high polymer concentration due to the higher possibility of micelle collision.[57] The free unimer population at equilibrium has also been shown to relate to micelle exchange kinetics.[58-59] In the present study, our observation of the relatively high population of free unimers coexisting with micelles (**Figure 3.6** and section 3.3.4 below) agrees with the scenario of polymer chain insertion/expulsion in relatively dilute solution (1% wt/vol). The insertion/expulsion process is governed by an entropic free energy barrier,[60] and the internal free energy landscape of a micelle gives rise to collective activation energy barriers that govern micelle assembly and disassembly. However, sudden discontinuities in either concentration or temperature, such as dilution or temperature elevation, can also result in increased micelle disintegration into free unimers, by disturbing the system far from equilibrium.

Zinn et al.[61] have performed TR-SANS and DSC experiments in combination with quantitative modeling on a systematic series of n-alkyl-PEOs to unravel the mechanism and thermodynamic contributions to the chain expulsion process. We are utilizing NMR spectroscopy and diffusometry to complement existing characterization tools (e.g. SANS, fluorescence) to explore the size and relative concentration of free unimers, which provides distinct information about the unimer exchange process.

3.3.4 Mapping Micelle-Unimer Coexistence Phase Diagrams as a Function of Temperature and Solvent Composition

Previously, we quantified the dependence of unimer population on solvent composition at room temperature.[16] Herein, we also investigate the evolution of free unimer population as a function of both solvent composition (vol % THF-d_8) and temperature. By varying these two separate thermodynamic variables, we can generate phase diagrams to depict regions in which either micelles or free unimers exist, or they coexist. Strikingly, for these systems we observe broad regions of coexistence of micelles and free unimers, and with strongly varying free unimer populations. For the 2k series (**Figure 3.6a**), we observe *coexistence of micelles and free unimers* (green squares) from 10 to 50 vol % THF-d_8 and from 21 to 50 ℃. The population of free unimers grows with either increasing temperature or vol % THF-d_8 (see below). At 60 vol % THF-d_8, coexistence remains at 21 ℃, but when we increase temperature further to a transition point at 39 ℃ we identify a *free unimer only* region (red diamonds) in the phase diagram. This *free unimer only* region continues to dominate at higher THF-d_8 vol % (≥ 70%) where no micelles exist regardless of temperature. The black dashed line is a guide to the eye between micelle-unimer coexistence and unimer-only regions.

For the 5k series (**Figure 3.6b**), we observe a region of *micelles only* (blue triangles) at both low temperature and THF-d_8 vol % THF-d_8, and this transforms to a *micelle-unimer coexistence* region when the temperature exceeds a critical value that depends on solvent composition, and finally we observe a fully solvated *unimer only* region at higher *T* and vol % THF-d_8. The transition temperatures from micelles only to micelle-unimer coexistence decrease from 35 to 30 ℃ as vol % THF-d_8 increases from 10 to 50%, which reiterates the strong influence of solvent composition on free unimer population. Another transition occurs at 42 ℃ for 60 vol %

THF-d_8, above which only free unimers exist. We depict two dashed lines as guides to the eye for the micelle only, coexistence and free unimer only regions. The presence of the micelle only region in the 5k series but not the 2k series must originate from the longer chain length in the 5k series, which should provide for stronger intra- and intermolecular interactions between polymer chains. Therefore, the 5k series micelles are more likely to remain stable when varying solution conditions (e.g., temperature or solvent composition) compared to the 2k series. Note that the micelle only region is where free unimers at low concentration (a few percent of the total unimer concentration in micelles) may be present but are not readily discernable by this method. Both BCM series exhibit an unexpectedly large coexistence region of micelles and unimers. Indeed, this realization and detailed investigation of free unimer and micelle phase maps will provide key information for understanding molecular interactions and dynamics of unimer exchange in BCM systems, including the behaviors of encapsulated cargo molecules such as therapeutic drugs.

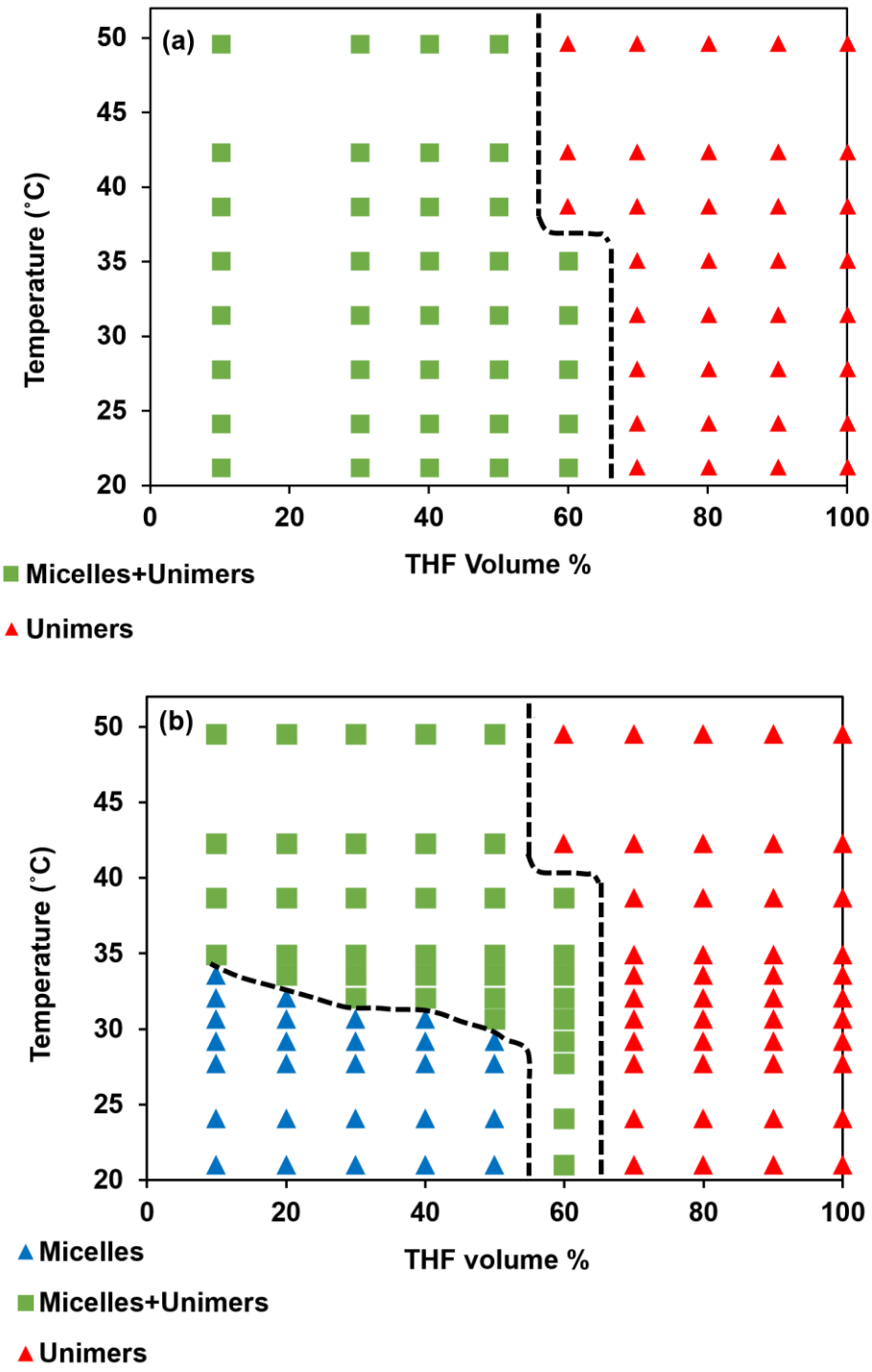

Figure 3.6. Micelle-unimer phase diagrams as function of temperature and solvent composition for the 2k series (PEO_{2k}-PCL_{3k}) (a) and 5k series (PEO_{5k}-PCL_{8k}), (b) Dashed lines are guides to the eye for phase boundaries. Both series exhibit surprisingly broad regions of micelle-unimer coexistence.

To expose more details of micellar solution behavior, we have extracted quantitative free unimer populations in solution. **Figure 3.7a** shows the gradual increase in relative percentage of free unimers (to the total polymer chain population) of 2k series BCMs within the 10 − 60 vol % THF-d_8 range from 21 to 50 ℃. At 24 ℃, the percentage of free unimers increases from 10 to 56% as a function of vol % THF-d_8, as in our previous study. At increased temperatures, higher vol % THF-d_8 also led to the growth of free unimer population. At fixed vol % THF-d_8, we generally observe higher concentration of free unimers in solution with increasing temperature to our estimated error of ± 10% in population. For example, at 30, 40 and 50 vol % THF-d_8, the free unimer percentages in the temperature range of 21 to 50 ℃ increased from 15 to 45%, 15 to 47% and 28 to 45%, respectively. At 60 vol % THF-d_8, the unimer percentage increased from 53 to 63% from 21 to 35 ℃, then to 100% above 39 ℃. We did observe some non-monotonic dependencies of free unimer percentage (e.g., the 35 ℃ point at 10 vol % THF-d_8), which we attribute to potential variations in sample preparation. Overall, higher temperature and/or increasing vol % THF-d_8 result in continuously increasing percentage of free unimers in solution. Thus, we have investigated the structural or stability change of BCMs upon temperature and solvent composition using NMR diffusometry. Moreover, we can extend this method to study the impacts of other factors on micellar dynamics, such as pH or concentration, to understand how the internal and external variables affect the self-assembly of micelles.

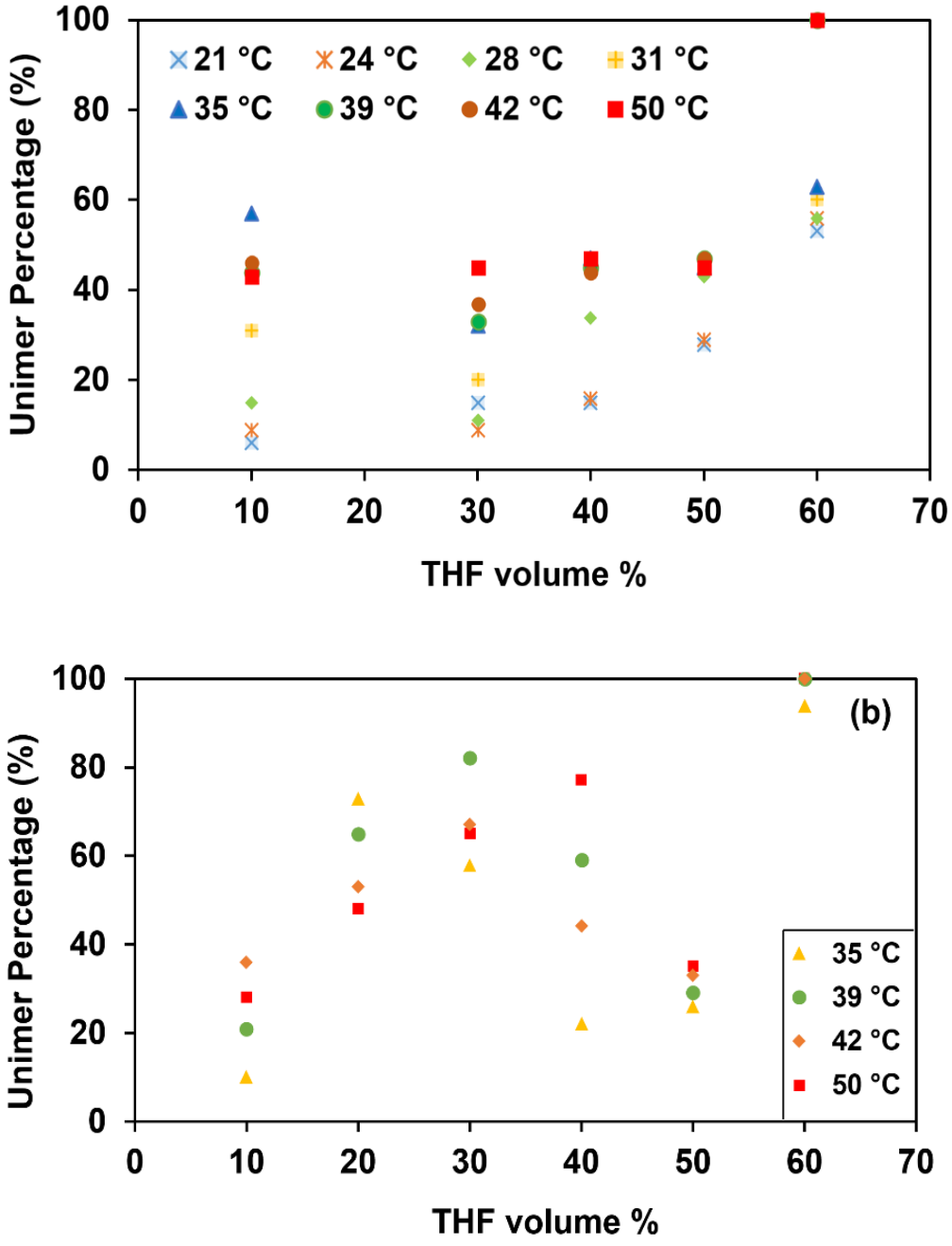

Figure 3.7. Relative unimer population for the PEO-PCL 2k series (a) and 5k series (b) as a function of vol % THF-d_8 at different temperatures. Generally, we observe higher concentration of unimers in solution with increased temperature at fixed vol % THF-d_8 or increased vol % THF-d_8 at fixed temperature. Error bars are ≈ ± 10% for unimer populations.

As indicated by the different phase behavior for the 2k and 5k series BCMs (**Figure 3.6**), we expect these two systems to exhibit different free unimer population distributions. While the 5k series shows correlations between free unimer population curves as we scan vol % THF-d_8 and temperature, as shown in **Figure 3.7b**, we notably observe non-monotonic growth of unimer population as a function of vol % THF-d_8 at fixed temperatures. While our error estimates of *ca.* +/- 10% in free unimer population can account for some of this, it is possible that the non-ideal mixing behavior of THF and water[62] may substantially modulate intermolecular interactions, therefore non-monotonically influencing molecular interactions in BCM solutions and thus free unimer populations. Our previous study has demonstrated evidence of variation of specific molecular interactions between THF and water, evident in diffusion coefficients with a complicated dependence on composition (mixed solvent fraction).[16] Related simulation and experimental studies have also suggested that THF / water mixtures can exhibit intricate complexation behavior,[63-65] such that THF and water molecules can nanoscopically phase separate and/or change their interactions significantly with, e.g., polymer chains.[65] Due to the chain length differences between 2k and 5k polymers, the 5k series (with 8k PCL block) may be more susceptible to specific solvent interactions with THF and thus experience variable solvent-PCL interactions at equilibrium as the THF-water fraction changes and thus the nanoscopic solvent separation behavior. In other words, these non-ideal solvent interactions, and associated effects on micellar self-assembly, could give rise to the observed non-monotonic behavior of unimer populations for the 5k series BCMs. Regardless of the free unimer fractions observed or potential non-ideal solvent interactions, in the end we are able to fit all data in the coexistence regions with two components from the signal decay curve (bi-linear curve) in NMR diffusometry and reliably delineate the overall boundaries of the phase diagrams. This study extends efforts to examine the

influence of polymer-solvent interactions on the unimer population in BCMs. More experiments are necessary to understand the nature of non-ideal solvent mixing by refining temperature and solvent composition, and this work will have guidance on further research into this uninvestigated area.

Overall, NMR diffusometry represents an impressive tool to noninvasively investigate the structure, solution composition, and molecular dynamics of BCM solutions. In mixed solvent BCM solutions, we determine the phase boundaries for the presence of micelles only, micelle and free unimer coexistence, and free unimers only, as well as the concentration of free unimers. Detailed exploration of non-ideal solvent structuring and solvent-chain interactions is beyond the scope of this paper, and the molecular interactions in these polymer-cosolvent-water mixtures are of importance in nanoscale assemblies and mesostructures and will form the basis of ongoing work.

3.4 Conclusions

In this study, we have used NMR spectroscopy and diffusometry to investigate the effects of temperature, solvent composition and polymer chain length (at constant block ratio) on structure and dynamics of block copolymer micelles. We have analyzed PEO_{2k}−PCL_{3k} and PEO_{5k}−PCL_{8k} block copolymer micelle systems in D_2O−THF-d_8 mixed solvents, including the measurement of diffusion coefficients, hydrodynamic radii, and populations of free unimers and micelles. By varying temperature and solvent composition, we are able to generate micelle-unimer coexistence phase diagrams to enable better understanding of how the compositional and thermodynamic environment affects dynamics and equilibria of micelles in solution.

For the 2k series, we observe the broad coexistence of micelles and free unimers in solution from 10 to 50 vol % THF-d_8 and over a range of temperatures, while at ≥ 39 °C at 60 vol % THF-d_8 we observe only free unimers. Compared to the 2k series, the 5k series exhibits a more complex

phase behavior, with regions representing micelles only, free unimer-micelle coexistence, and free unimers only. Notably, the 5k series also exhibits a broad range of micelle-unimer coexistence. Also surprisingly, both 2k and 5k series show substantial and continuously varying free unimer content in the micelle-unimer coexistence regions, in contrast to general expectations for sharp phase transitions and relatively fixed free unimer populations (at the CMC) in micellar solutions.

Collectively, our studies demonstrate that we can sensitively tune the micelle-unimer phase behavior with temperature (along with polymer structure and solvent composition), which is of importance for triggerable cargo delivery,[4] switchable nanoreactors[1] as well as for many other applications. Mapping these phase behaviors improves understanding of micellar dynamic and equilibrium behaviors and provides key feedback for design of block copolymer micelles. In further studies, we are currently exploring a range of NMR experiments to directly probe unimer and cargo dynamics in BCM systems, and correlate such dynamics with solution equilibrium properties such as the unimer-micelle phase diagrams presented here.

References

1. Gallou, F.; Isley, N. A.; Ganic, A.; Onken, U.; Parmentier, M., Surfactant technology applied toward an active pharmaceutical ingredient: more than a simple green chemistry advance. *Green Chem* **2016,** *18* (1), 14-19.
2. Chiappetta, D. A.; Sosnik, A., Poly(ethylene oxide)–poly(propylene oxide) block copolymer micelles as drug delivery agents: Improved hydrosolubility, stability and bioavailability of drugs. *Eur. J. Pharm. Biopharm.* **2007,** *66* (3), 303-317.
3. Ward, M. A.; Georgiou, T. K., Thermoresponsive polymers for biomedical applications. *Polymers* **2011,** *3* (3), 1215-1242.
4. Deng, C.; Jiang, Y.; Cheng, R.; Meng, F.; Zhong, Z., Biodegradable polymeric micelles for targeted and controlled anticancer drug delivery: Promises, progress and prospects. *Nano Today* **2012,** *7* (5), 467-480.
5. Ding, H.; Wang, X.; Zhang, S.; Liu, X., Applications of polymeric micelles with tumor targeted in chemotherapy. *J. Nanopart. Res.* **2012,** *14* (11), 1-13.
6. Tiwari, G.; Tiwari, R.; Sriwastawa, B.; Bhati, L.; Pandey, S.; Pandey, P.; Bannerjee, S. K., Drug delivery systems: An updated review. *Int. J. Pharm. Investig.* **2012,** *2* (1), 2-11.

7. Raoul, Z., Dynamics in Micellar Solutions of Surfactants. In *Dynamics of Surfactant Self-Assemblies*, CRC Press: 2005; pp 75-160.
8. Cabral, H.; Kataoka, K., Progress of drug-loaded polymeric micelles into clinical studies. *J. Controlled. Release.* **2014,** *190*, 465-476.
9. Tila, D.; Yazdani-Arazi, S. N.; Ghanbarzadeh, S.; Arami, S.; Pourmoazzen, Z., pH-sensitive, polymer modified, plasma stable niosomes: promising carriers for anti-cancer drugs. *EXCLI. J.* **2015,** *14*, 21-32.
10. Holder, S. J.; Sommerdijk, N. A. J. M., New micellar morphologies from amphiphilic block copolymers: disks, toroids and bicontinuous micelles. *Polym Chem* **2011,** *2* (5), 1018-1028.
11. Choucair, A.; Eisenberg, A., Control of amphiphilic block copolymer morphologies using solution conditions. *Eur. Phys. J. E.* **2003,** *10* (1), 37-44.
12. Shen, H.; Eisenberg, A., Block Length Dependence of Morphological Phase Diagrams of the Ternary System of PS-b-PAA/Dioxane/H2O. *Macromolecules* **2000,** *33* (7), 2561-2572.
13. Yu, Y. S.; Eisenberg, A., Control of morphology through polymer-solvent interactions in crew-cut aggregates of amphiphilic block copolymers. *J. Am. Chem. Soc* **1997,** *119* (35), 8383-8384.
14. Yuan, J.; Li, Y.; Li, X.; Cheng, S.; Jiang, L.; Feng, L.; Fan, Z., The "crew-cut" aggregates of polystyrene-b-poly(ethylene oxide)-b-polystyrene triblock copolymers in aqueous media. *Eur. Polym. J.* **2003,** *39* (4), 767-776.
15. Zhang, L.; Yu, K.; Eisenberg, A., Ion-Induced Morphological Changes in "Crew-Cut" Aggregates of Amphiphilic Block Copolymers. *Science* **1996,** *272* (5269), 1777-1779.
16. Kidd, B. E.; Li, X.; Piemonte, R. C.; Cooksey, T. J.; Singh, A.; Robertson, M. L.; Madsen, L. A., Tuning Biocompatible Block Copolymer Micelles by Varying Solvent Composition: Dynamics and Populations of Micelles and Unimers. *Macromolecules* **2017,** *50* (11), 4335-4343.
17. Cooksey, T. J.; Singh, A.; Le, K. M.; Wang, S.; Kelley, E. G.; He, L.; Vajjala Kesava, S.; Gomez, E. D.; Kidd, B. E.; Madsen, L. A.; Robertson, M. L., Tuning Biocompatible Block Copolymer Micelles by Varying Solvent Composition: Core/Corona Structure and Solvent Uptake. *Macromolecules* **2017,** *50* (11), 4322-4334.
18. Zhou, S.; Deng, X.; Yang, H., Biodegradable poly(ε-caprolactone)-poly(ethylene glycol) block copolymers: characterization and their use as drug carriers for a controlled delivery system. *Biomaterials* **2003,** *24* (20), 3563-3570.
19. Mansour, H. M.; Sohn, M.; Al-Ghananeem, A.; DeLuca, P. P., Materials for Pharmaceutical Dosage Forms: Molecular Pharmaceutics and Controlled Release Drug Delivery Aspects. *Int. J. Mol. Sci.* **2010,** *11* (9), 3298-3322.
20. Cho, H. K.; Cho, K. S.; Cho, J. H.; Choi, S. W.; Kim, J. H.; Cheong, I. W., Synthesis and characterization of PEO–PCL–PEO triblock copolymers: Effects of the PCL chain length on the

physical property of W1/O/W2 multiple emulsions. *Colloids. Surf. B. Biointerfaces.* **2008,** *65* (1), 61-68.
21. Schuetz, P.; Greenall, M. J.; Bent, J.; Furzeland, S.; Atkins, D.; Butler, M. F.; McLeish, T. C.; Buzza, D. M. A., Controlling the micellar morphology of binary PEO–PCL block copolymers in water–THF through controlled blending. *Soft Matter* **2011,** *7* (2), 749-759.
22. Kim, S. Y.; Shin, I. L. G.; Lee, Y. M.; Cho, C. S.; Sung, Y. K., Methoxy poly(ethylene glycol) and ϵ-caprolactone amphiphilic block copolymeric micelle containing indomethacin.: II. Micelle formation and drug release behaviours. *J. Controlled. Release.* **1998,** *51* (1), 13-22.
23. Oerlemans, C.; Bult, W.; Bos, M.; Storm, G.; Nijsen, J. F. W.; Hennink, W. E., Polymeric Micelles in Anticancer Therapy: Targeting, Imaging and Triggered Release. *Pharm. Res.* **2010,** *27* (12), 2569-2589.
24. Nakamura, K.; Endo, R.; Takeda, M., Surface properties of styrene–ethylene oxide block copolymers. *J. Polym. Sci. B. Polym. Phys.* **1976,** *14* (7), 1287-1295.
25. Minmin, T. A., Qin; Stephen E, Webber; Petr, Munk; Zdenek, Tuzar; Karel, Prochhka, Hybridization of Block Copolymer Micelles. *Langmuir* **1993,** *9* (7), 8.
26. Batrakova, E. V.; Kabanov, A. V., Pluronic block copolymers: Evolution of drug delivery concept from inert nanocarriers to biological response modifiers. *J. Controlled. Release.* **2008,** *130* (2), 98-106.
27. Batrakova, E. V.; Li, S.; Li, Y.; Alakhov, V. Y.; Elmquist, W. F.; Kabanov, A. V., Distribution kinetics of a micelle-forming block copolymer Pluronic P85. *J. Controlled. Release.* **2004,** *100* (3), 389-397.
28. Yan, N.; Zhang, Y.; He, Y.; Zhu, Y.; Jiang, W., Controllable Location of Inorganic Nanoparticles on Block Copolymer Self-Assembled Scaffolds by Tailoring the Entropy and Enthalpy Contributions. *Macromolecules* **2017,** *50* (17), 6771-6778.
29. Fan, H., Nanocrystal-micelle: synthesis, self-assembly and application. *Chem Comm* **2008,** (12), 1383-1394.
30. Callaghan, P. T., *Translational Dynamics and Magnetic Resonance: Principles of Pulsed Gradient Spin Echo NMR*. Oxford University Press: New York, 2011.
31. Price, W. S., *NMR studies of translational motion: principles and applications*. Cambridge University Press: 2009.
32. Kidd, B. E.; Forbey, S. J.; Steuber, F. W.; Moore, R. B.; Madsen, L. A., Multiscale Lithium and Counterion Transport in an Electrospun Polymer-Gel Electrolyte. *Macromolecules* **2015,** *48* (13), 4481-4490.
33. Wang, X.; Chen, Y.; Xue, L.; Pothayee, N.; Zhang, R.; Riffle, J. S.; Reineke, T. M.; Madsen, L. A., Diffusion of Drug Delivery Nanoparticles into Biogels Using Time-Resolved MicroMRI. *J. Phys. Chem. Lett.* **2014,** *5* (21), 3825-3830.

34. Alvares, R.; Gupta, S.; Macdonald, P. M.; Prosser, R. S., Temperature and Pressure Based NMR Studies of Detergent Micelle Phase Equilibria. *J. Phys. Chem. B.* **2014,** *118* (21), 5698-5706.
35. Hou, J.; Li, J.; Mountz, D.; Hull, M.; Madsen, L. A., Correlating morphology, proton conductivity, and water transport in polyelectrolyte-fluoropolymer blend membranes. *J. Memb. Sci.* **2013,** *448*, 292-299.
36. Kidd, B. E.; Lingwood, M. D.; Lee, M.; Gibson, H. W.; Madsen, L. A., Cation and anion transport in a dicationic imidazolium-based plastic crystal ion conductor. *J. Phys. Chem. B.* **2014,** *118* (8), 2176-85.
37. Cohen, Y.; Avram, L.; Frish, L., Diffusion NMR Spectroscopy in Supramolecular and Combinatorial Chemistry: An Old Parameter—New Insights. *Angew. Chem. Int. Ed.* **2005,** *44* (4), 520-554.
38. Bryskhe, K.; Jansson, J.; Topgaard, D.; Schillén, K.; Olsson, U., Spontaneous Vesicle Formation in a Block Copolymer System. *J. Phys. Chem. B.* **2004,** *108* (28), 9710-9719.
39. Knöös, P.; Wahlgren, M.; Topgaard, D.; Ulvenlund, S.; Piculell, L., Effects of Added Surfactant on Swelling and Molecular Transport in Drug-Loaded Tablets Based on Hydrophobically Modified Poly(acrylic acid). *J. Phys. Chem. B.* **2014,** *118* (32), 9757-9767.
40. Wong, T. C., Micellar Systems: Nuclear Magnetic Resonance Spectroscopy. In *Encyclopedia of Surface and Colloid Science, Second Edition*, 2006; pp 3738-3756.
41. Wilmsmeyer, K. G.; Li, X.; Madsen, L. A., Anisotropic viscoelasticity and molecular diffusion in nematic wormlike micelles. *Liq. Cryst.* **2018,** *45* (6), 844-856.
42. Stejskal, E.; Tanner, J., Spin diffusion measurements: spin echoes in the presence of a time-dependent field gradient. *J. Chem. Phys.* **1965,** *42* (1), 288-292.
43. Price, W. S., Pulsed-field gradient nuclear magnetic resonance as a tool for studying translational diffusion: Part 1. Basic theory. *Concepts. Magn. Reson.* **1997,** *9* (5), 299-336.
44. Wang, L. Q.; Exarhos, G. J.; Liu, J., Nuclear Magnetic Resonance—Characterization of Self-Assembled Nanostructured Materials. *Adv Mater* **1999,** *11* (16), 1331-1341.
45. Fleischer, G., Micellization in aqueous solution of a poly(ethylene oxide)/poly(propylene oxide)/poly(ethylene oxide) triblock copolymer investigated with pulsed field gradient NMR. *J. Phys. Chem.* **1993,** *97* (2), 517-521.
46. Hou, J.; Zhang, Z.; Madsen, L. A., Cation/anion associations in ionic liquids modulated by hydration and ionic medium. *J. Phys. Chem. B.* **2011,** *115* (16), 4576-82.
47. Edward, J. T., Molecular volumes and the Stokes-Einstein equation. *J. Chem. Educ.* **1970,** *47* (4), 261.
48. Goldmints, I.; Yu, G.-e.; Booth, C.; Smith, K. A.; Hatton, T. A., Structure of (Deuterated PEO)−(PPO)−(Deuterated PEO) Block Copolymer Micelles As Determined by Small Angle Neutron Scattering. *Langmuir* **1999,** *15* (5), 1651-1656.

49. Su, Y.-l.; Wang, J.; Liu, H.-z., FTIR Spectroscopic Study on Effects of Temperature and Polymer Composition on the Structural Properties of PEO−PPO−PEO Block Copolymer Micelles. *Langmuir* **2002,** *18* (14), 5370-5374.
50. Nilsson, M.; Håkansson, B.; Söderman, O.; Topgaard, D., Influence of Polydispersity on the Micellization of Triblock Copolymers Investigated by Pulsed Field Gradient Nuclear Magnetic Resonance. *Macromolecules* **2007,** *40* (23), 8250-8258.
51. Walderhaug, H.; Söderman, O.; Topgaard, D., Self-diffusion in polymer systems studied by magnetic field-gradient spin-echo NMR methods. *Prog. Nucl. Magn. Reson. Spectrosc.* **2010,** *56* (4), 406-425.
52. Stilbs, P., Micellar breakdown by short-chain alcohols. A multicomponent FT-PGSE-NMR self-diffusion study. *J. Colloid. Inter. Sci.* **1982,** *89* (2), 547-554.
53. Gille, K.; Knoll, H.; Rittig, F.; Fleischer, G.; Kärger, J., Study of Structure Formation in Aqueous Solutions of Poly(ethylene oxide)−Poly(propylene oxide)−Poly(ethylene oxide) Block Copolymers by Measuring Rate Constants of the Thermal Cis−Trans Isomerization of an Azobenzene Dye and Self-Diffusion of Copolymer Molecules. *Langmuir* **1999,** *15* (4), 1059-1066.
54. Kelley, E. G.; Murphy, R. P.; Seppala, J. E.; Smart, T. P.; Hann, S. D.; Sullivan, M. O.; Epps, T. H., Size evolution of highly amphiphilic macromolecular solution assemblies via a distinct bimodal pathway. *Nat Commun* **2014,** *5*.
55. Halperin, A.; Alexander, S., Polymeric micelles: their relaxation kinetics. *Macromolecules* **1989,** *22* (5), 2403-2412.
56. Kim, T. H.; Huh, J.; Hwang, J.; Kim, H.-C.; Kim, S. H.; Sohn, B.-H.; Park, C., Ordered Arrays of PS-b-P4VP Micelles by Fusion and Fission Process upon Solvent Annealing. *Macromolecules* **2009,** *42* (17), 6688-6697.
57. Li, Z.; Dormidontova, E. E., Equilibrium chain exchange kinetics in block copolymer micelle solutions by dissipative particle dynamics simulations. *Soft Matter* **2011,** *7* (9), 4179-4188.
58. Schönhoff, M.; Söderman, O., PFG-NMR Diffusion as a Method To Investigate the Equilibrium Adsorption Dynamics of Surfactants at the Solid/Liquid Interface. *J. Phys. Chem. B.* **1997,** *101* (41), 8237-8242.
59. Mok, M. M.; Thiagarajan, R.; Flores, M.; Morse, D. C.; Lodge, T. P., Apparent Critical Micelle Concentrations in Block Copolymer/Ionic Liquid Solutions: Remarkably Weak Dependence on Solvophobic Block Molecular Weight. *Macromolecules* **2012,** *45* (11), 4818-4829.
60. Narang, A. S.; Mahato, R. I., *Targeted delivery of small and macromolecular drugs*. CRC press: 2010.
61. Zinn, T.; Willner, L.; Lund, R.; Pipich, V.; Richter, D., Equilibrium exchange kinetics in n-alkyl–PEO polymeric micelles: Single exponential relaxation and chain length dependence. *Soft Matter* **2012,** *8* (3), 623-626.

62. Shultz, M. J.; Vu, T. H., Hydrogen Bonding between Water and Tetrahydrofuran Relevant to Clathrate Formation. *J. Phys. Chem. B.* **2015,** *119* (29), 9167-9172.
63. Smith, M. D.; Mostofian, B.; Petridis, L.; Cheng, X.; Smith, J. C., Molecular Driving Forces behind the Tetrahydrofuran–Water Miscibility Gap. *J. Phys. Chem. B.* **2016,** *120* (4), 740-747.
64. Mostofian, B.; Cai, C. M.; Smith, M. D.; Petridis, L.; Cheng, X.; Wyman, C. E.; Smith, J. C., Local Phase Separation of Co-solvents Enhances Pretreatment of Biomass for Bioenergy Applications. *J. Am. Chem. Soc* **2016,** *138* (34), 10869-10878.
65. Donaldson, S. H.; Jahnke, J. P.; Messinger, R. J.; Östlund, Å.; Uhrig, D.; Israelachvili, J. N.; Chmelka, B. F., Correlated Diffusivities, Solubilities, and Hydrophobic Interactions in Ternary Polydimethylsiloxane–Water–Tetrahydrofuran Mixtures. *Macromolecules* **2016,** *49* (18), 6910-6917.

Chapter 4: Probing Unimer Exchange Kinetics of Block Copolymer Micelles by Using Time-resolved (TR) NMR Relaxation

This chapter is in preparation and will be submitted for publication with the following co-authors: Xiuli Li, Bryce E. Kidd, Tyler J. Cooksey, Veera Venkata Shravan Uppala, Megan L. Robertson, Louis A. Madsen*

*Department of Chemistry and Macromolecules Innovation Institute, Virginia Tech, Blacksburg, 24061, USA

Abstract

Here we present a novel method to study the exchange kinetics of unimer chains between block copolymer micelles. By measuring the time-resolved NMR spin-relaxation time (T_1) constants for mixed PEO-b-PCL micelles solutions labeled with ^{1}H- and ^{2}H-cores, we can monitor the T_1 change in ^{1}H cores that is enhanced by intermolecular dipole-dipole interactions. The gyromagnetic ratio of ^{2}H is about 1/7 of ^{1}H, therefore ^{2}H is less effective to influence nearby ^{1}H and render a longer spin relaxation time for ^{1}H. The T_1 times of protonated chain cores in the mixtures are expected to increase with the increased number of surrounding deuterated polymer chains due to unimer chain exchange. Our TR-NMR showed barely any change over hours at 25 ℃ and 40 ℃, which indicates extremely slow chain exchange kinetics. As the temperature is increased to 55 ℃ and 62 ℃, the average exponential time constants for unimer exchange are 130 min and 60 min, respectively. Those trends are also in agreement with time-resolved small-angle neutron scattering (TR-SANS) results. This NMR method is simpler, more practical, less expensive, and could serve as a complementary or even future substitute for the neutron scattering or fluorescence methods. Multimodal NMR can complement and expand dynamics studies for polymeric micelles, gels and nanoparticles.

4.1 Introduction

Compared with traditional surfactants, the exchange rate of chains between block copolymer self-assemblies is substantially slower due to additional thermodynamic constraints in long polymer chains, such as entanglement, crystallinity or vitrification.[1] The slow kinetics result in limited application of block polymer micelles for selective solvent absorption onto surfaces, which requires a fast polymer chain (or unimer) release to stabilize the solid dispersion. On the other hand, slower exchange kinetics may open new opportunities, e.g. drug delivery and nanoparticle preparation.[2] Therefore, it is of great importance to understand the exchange kinetics of polymer aggregates for practical reasons, such as long-term performance (aggregation number and stability)

Currently, the predominant mechanisms identified for the unimer exchange in micelles include insertion / expulsion, fusion / fission and spanning.[3-5] The insertion / expulsion mechanism was described by Aniansson and Wall[6] and dominates at a relatively low polymer concentration, and the fusion / fission mechanism contributes more at a high concentration due to the higher possibility of micelle collision.[7] Halperin and Alexander[4] also showed the domination of insertion/expulsion when the micelles were at equilibrium due to unfavorable interactions between micelle coronas. In Chapter 3, we have observed the emergence of free unimers (> 35 °C), which agrees with the scenario of polymer chain insertion / expulsion in dilute solutions (1% wt/vol). To probe more deeply into this process, **Figure 4.1** illustrates how a unimer escapes out of a micelle, which involves the following steps: (1) extraction of a hydrophobic block from the core, (2) formation of an interface with the solvent, (3) diffusion through the corona, and (4) liberation from the micelle.[8] The chain insertion is expected to follow a reversed process of these steps.

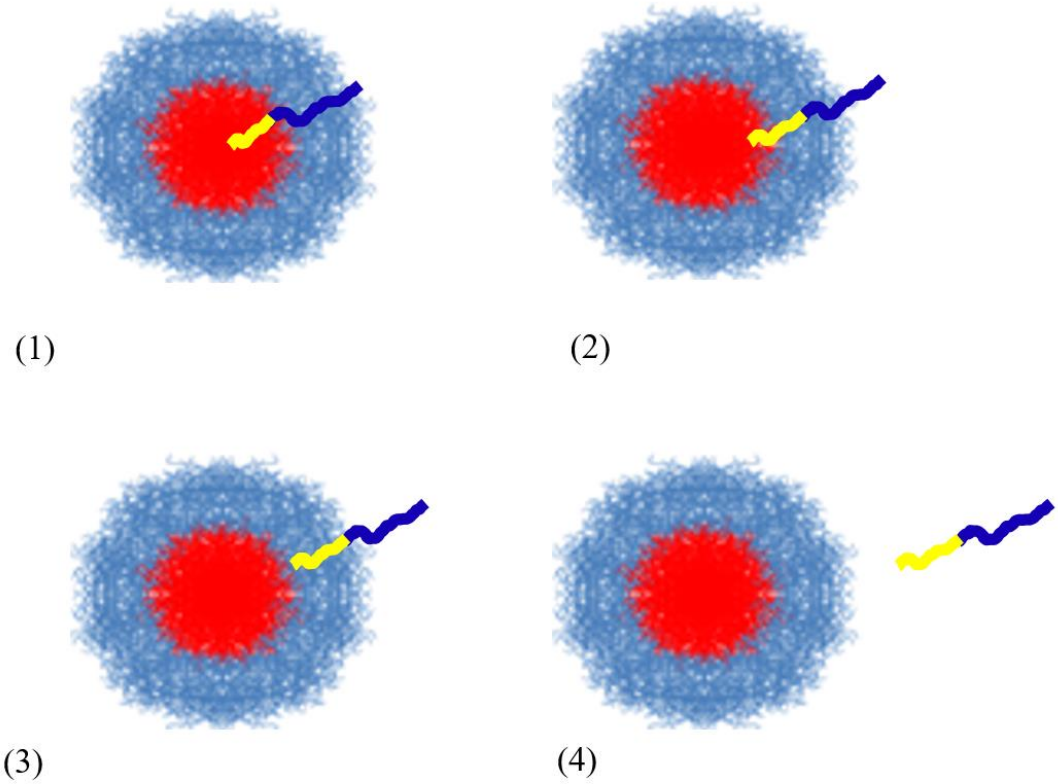

Figure 4.1. Schematic representation of the escape process of a unimer from a BCM as follows: (1) extraction of a hydrophobic block from the core, (2) formation of an interface with the solvent, (3) diffusion through the corona, (4) liberation from the micelle. The size and color were modified on purpose to display a specific chain being expelled from the micellar core.

The insertion / expulsion process is governed by the entropic free energy barrier.[9] The internal free energy of micellization can explain that both micelle assembly and disassembly are an activated processes that involve collective energy barriers. The internal free energy of micellization suppresses aggregation of unimers in a micelle (F_a) and disassociation of unimers from a micelle (F_d). As for F_a, the thermodynamic equilibrium of micellization requires a practically long time, therefore the micelles are loosely aggregated. F_d tends to hinder micelle disintegration.[10] However, sudden discontinuities in either concentration or temperature, such as

dilution or elevated temperature, can result in increased micelle disintegration / unimer population, by perturbing the system far away from equilibrium.

4.1.1 Small-angle Neutron Scattering

Small-angle neutron scattering (SANS) is an extensively used and developed method to investigate micelle kinetics quantitatively. SANS studies the structural changes in matter over time, including phase transitions, morphological transitions and transport / diffusive processes.[11-12] Compared to small-angle X-ray scattering, SANS is another powerful tool in soft matter, polymer and materials study. The differences between neutrons and X-rays are mainly their energy and interactions with matter. X-ray interacts strongly with electrons in an atom and the scattering comes from electromagnetic interactions. Neutrons from a reactor source can penetrate the core of an atom and the scattering comes from short-range nuclear interactions. The typical energy for "cold" neutrons is on the order of *m*eV while that for X-rays is *k*eV (a factor of $\approx 10^6$).[11] As a consequence of the relatively weak interaction with matter, the neutrons detect matter (e.g. isotopes and light elements) in a more sensitive way.

To investigate micelle chain exchange kinetics by SANS, the typical strategy is to mix two micellar solutions with differently isotope-labeled polymers (^{1}H / ^{2}H) and observe time-dependent variation in scattered neutron intensity.[13] **Figure 4.2** shows how the SANS experiment determines the exchange kinetics in micelles and the scattering curves of micellar solutions. Reservoirs with protonated (white) and deuterated (black) micelles are prepared in an isotopic solvent mixture that has the same scattering length density as the average scattering length density (grey) of the two polymers. After mixing certain amounts of isotope-labeled micelle solutions, the following time-dependent signals can be detected: 1) $t = 0$, the contrast is at maximum, 2) $t = t_x$, the intensity

decreases as the unimer chain exchange and the contrast becomes smaller, and 3) $t \rightarrow \infty$, the intensity decreases more and the contrast is at minimum.

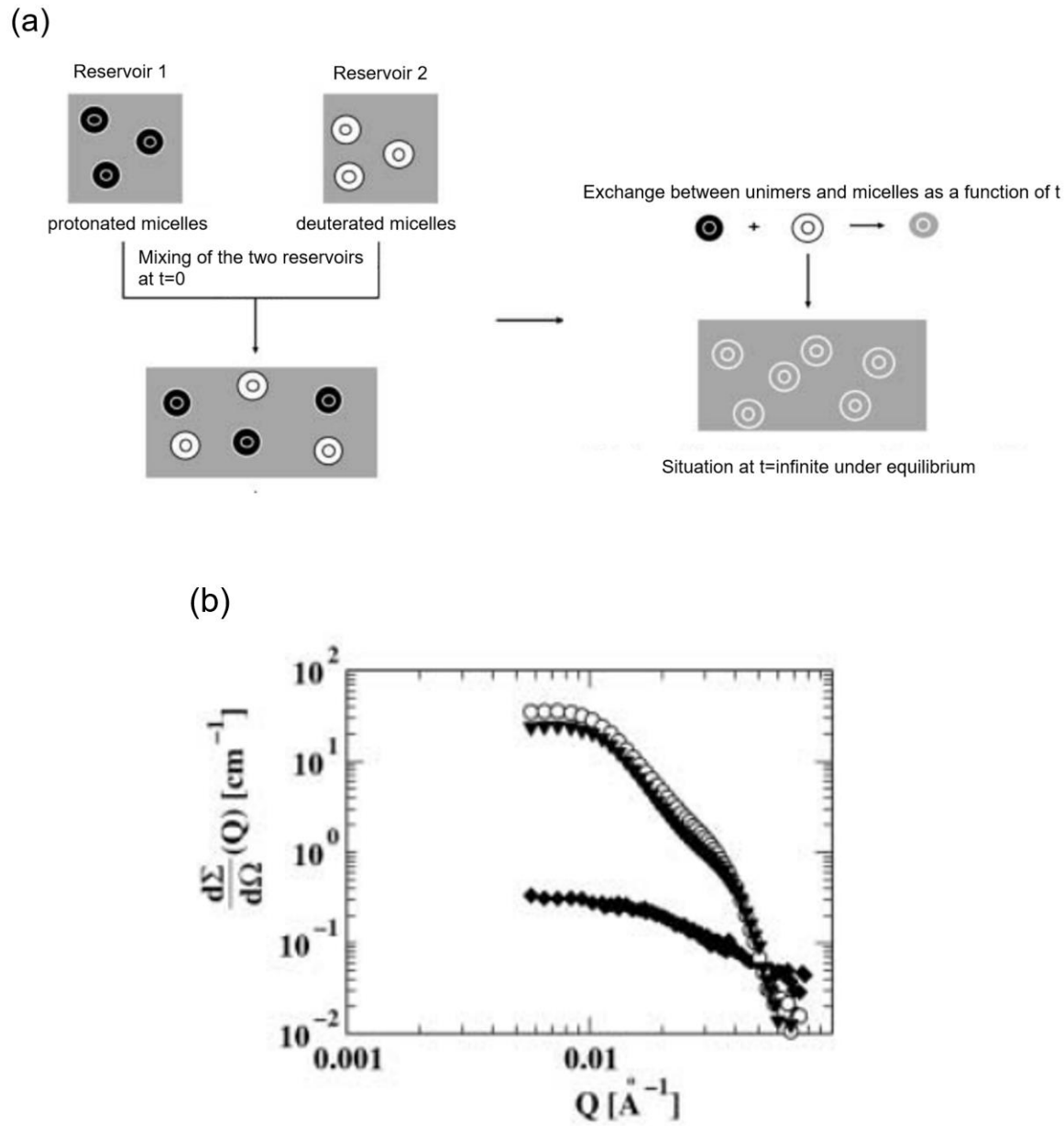

Figure 4.2. a) Schematics of the TR-SANS experimental method to determine the exchange kinetics of unimer exchange in micelles. b) Corresponding scattering curves of ^{1}H (circles) and ^{2}H (triangles) micellar solutions and 50 / 50 mixture (diamonds) of both at $t \rightarrow \infty$. Reproduced from Reference 13.

4.1.2 NMR Spin-Lattice Relaxation

TR-SANS can probe the chain exchange kinetics in micelles by monitoring the systematic scattering signal variations by mixing isotope-labeled visible. However, the usage of this technique has been hindered by the limited resource of facilities in the world and high cost of the instrument (upwards of $1 billion). Alternatively, NMR offers chemical specificity and the ability to study soft matter on multi-time and length scales. Development of a NMR method to characterize chain exchange kinetics would expand the research capabilities of block copolymer micelles.

In NMR, spin-lattice relaxation (T_1) describes the evolution of the spin system by changing magnetization along the z-axis.[14-15] Nuclei change their orientations after a 90˚ radiofrequency pulse, some up-sided spins will be flipped to down-sided spins, as shown in **Figure 4.3**. When the pulse is stopped, the higher energy spins (spin-down) will tumble due to the *Brownian* motion, and dissipate thermal energy to the surrounding molecular matrix (which is also known as the "lattice" for physicists), to return to the lower energy states (spin-up), thereby restoring a net magnetization along the primary magnetization field B_0.

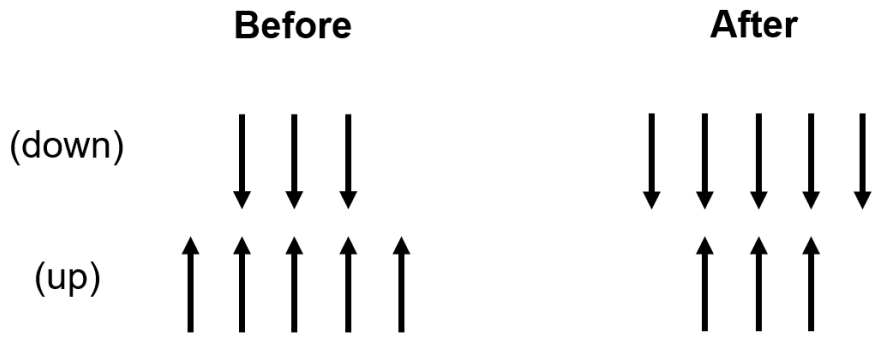

Figure 4.3. Spin orientation exchange between nuclei before and after the radiofrequency pulse in NMR.

Another important concept in T_1 relaxation is correlation time (τ_c), which describes the average time of interactions between nuclear spins and the external magnetic field induced by the

radiofrequency pulse.[16] The probability of energy transitions is relevant to the frequency of interactions with other nuclei in close proximity (≤ 12 Å). If the interaction frequency ($1/\tau_c$) is close to ω_0 (nuclear *Larmor* frequency), then the probability of energy transitions is enhanced. In liquids, the average molecular motion rates are usually several orders of magnitude larger than ω_0, which results in only a tiny proportion of the interactions having appropriate frequency and leads to inefficient relaxation.[17] For instance, the water-water interaction has τ_c around 10^{-12} s, so $1/\tau_c$ is far greater than ω_0. Therefore, water has a long T_1 time (~ 5 s) because of inefficient energy transitions. In the PEO-b-PCL BCM system we are using, the T_1 is 300 – 500 ms for PCL, ~ 1 s for PEO, and ~ 4 s for water (solvent) at room temperature. Their T_1 variations result from the drastic difference in the dynamic properties.

There have been multiple mechanisms to explain spin-lattice relaxation, among which the primary two are the intermolecular and intramolecular mechanisms. The intramolecular mechanism involves relaxations induced by quadrupolar,[18] dipole-dipole coupling,[19] J-coupling, [20] chemical shift anisotropy and spin rotation.[21] The intermolecular mechanism involves relaxation induced by unpaired electrons and extramolecular nuclei. Generally, the spin-lattice relaxation is derived from a combination of interactions listed above. The factors that affect τ_c (which thereby also affects T_1) are temperature, viscosity, state of sample and the addition of ions. According to *Bloembergen-Purcell-Pound* theory (BPP), as the size of molecule, viscosity or temperature increases, the molecular motions become slower and presents a longer correlation time (a longer τ_c), therefore $1/\tau_c$ gets closer to ω_0 and induces a more efficient relaxation (shorter T_1). At some viscosity, there is a most efficient relaxation (the shortest T_1), after that T_1 starts to increase, as is shown in **Figure 4.4**.

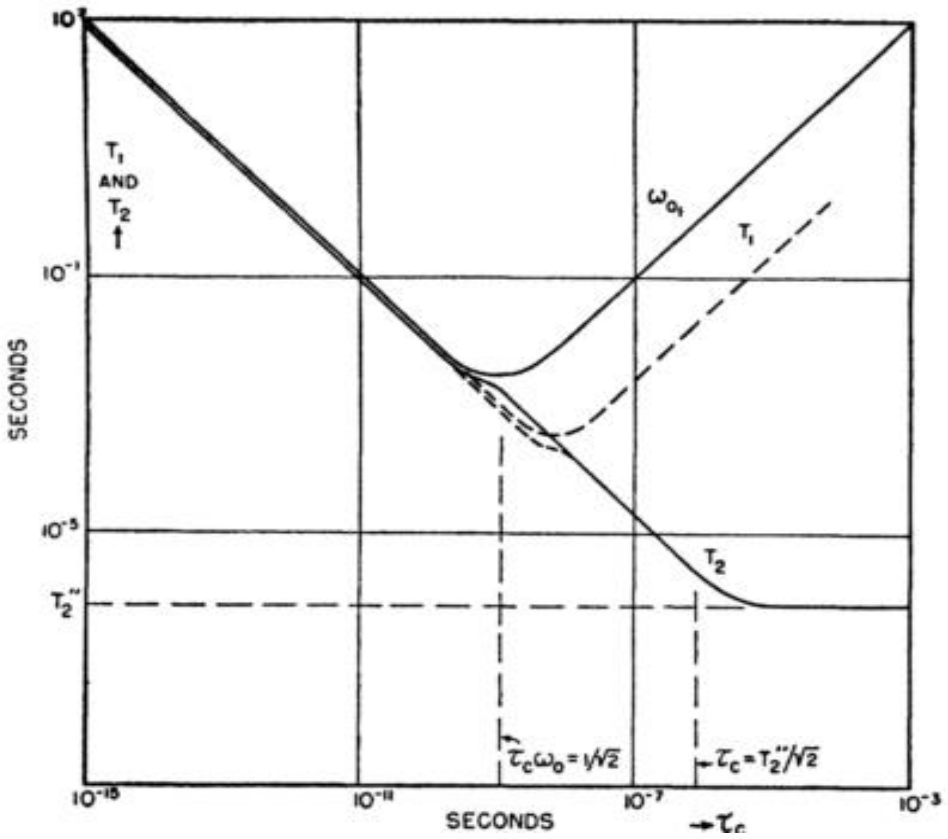

Figure 4.4. Spin-lattice (T_1) and spin-spin (T_2) relaxation times versus viscosity and molecular size (τ_c).[22] Reproduced from Reference 22.

According to previous study of the ^1H relaxation times in H_2O-D_2O mixtures,[23] dipole-dipole interaction influences the spin-lattice relaxation process to a large extent. Gyromagnetic ratio (γ) is a ratio of the magnetic moment of a rotating charged particle to its angular momentum. Since the γ of ^2H is about 1/7 of ^1H (See **Table 4.1**), ^2H is much less effective for the surrounding ^1H compared to ^1H themselves. Therefore, the spin-lattice relaxation times (T_1) of H_2O in mixtures are expected to increase with the increasing concentration of deuterated solute based on this intermolecular dipole-dipole interaction model.

Table 4.1. Gyromagnetic ratios of common NMR-responsive nucleus

Nucleus	**Gyromagnetic ratio** ($\gamma/(2\pi)$) (MHz $\cdot T^{-1}$)
^{1}H	42.577
^{2}H	6.536
^{13}C	10.708
^{7}Li	16.546

Spin-lattice relaxation is sensitive to changes in the local nuclear environment. Analogous to contrast-matching mixing experiments in TR-SANS, we propose a time-resolved (TR) NMR spin-lattice relaxation time (T_1) experiment that uses the same isotope-labeled micelle solutions in SANS to probe BCM chain exchange kinetics. The spin-lattice relaxation time (T_1) of protonated polymer chains are expected to increase with the increasing concentration of deuterated polymer chains.

4.2 Experimental Section

4.2.1 Sample Preparation

See Chapter 3 (section 3.2) for protonated and deuterated block copolymer preparation and characterization.[24-25]

4.2.2 Spin-lattice Relaxation

Spin-lattice relaxation time (T_1) measurements were conducted at 25 ℃ and elevated temperatures using a 400 MHz Bruker Avance III WB NMR spectrometer, equipped with a MIC probe and 5 mm ^{1}H RF coil. The inversion-recovery pulse sequence $(180_x - \tau - 90_x - \text{acquire})_n$ with 90 ° and 180 ° pulse lengths of 4.5 μs and 9 μs, respectively, allowed measurement of signal intensity *I* as a function of relaxation delay time in 16 steps and those data were fit with Equation

4.1, wherein I_0 is the initial intensity at t = 0, t_d is the relaxation delay time and T_1 is the spin-relaxation time measured.

$$I = I_0(1-2e^{-\frac{td}{T_1}}) \quad (4.1)$$

4.3 Results and Discussion

4.3.1 Spin-lattice Relaxation Times for ^{1}H Micelles

As discussed in Chapter 3, the PEO-b-PCL (with molecular weights 5000 g/mol and 8000 g/mol for PEO and PCL blocks, respectively) can self-assemble into spherical micelles at 1% wt/vol in mixed co-solvents (THF-d_8/D_2O). Here we use 10 – 20 vol% of THF-d_8 and 90 – 80 vol% of D_2O as a solvent for both protonated and deuterated BCM solutions.

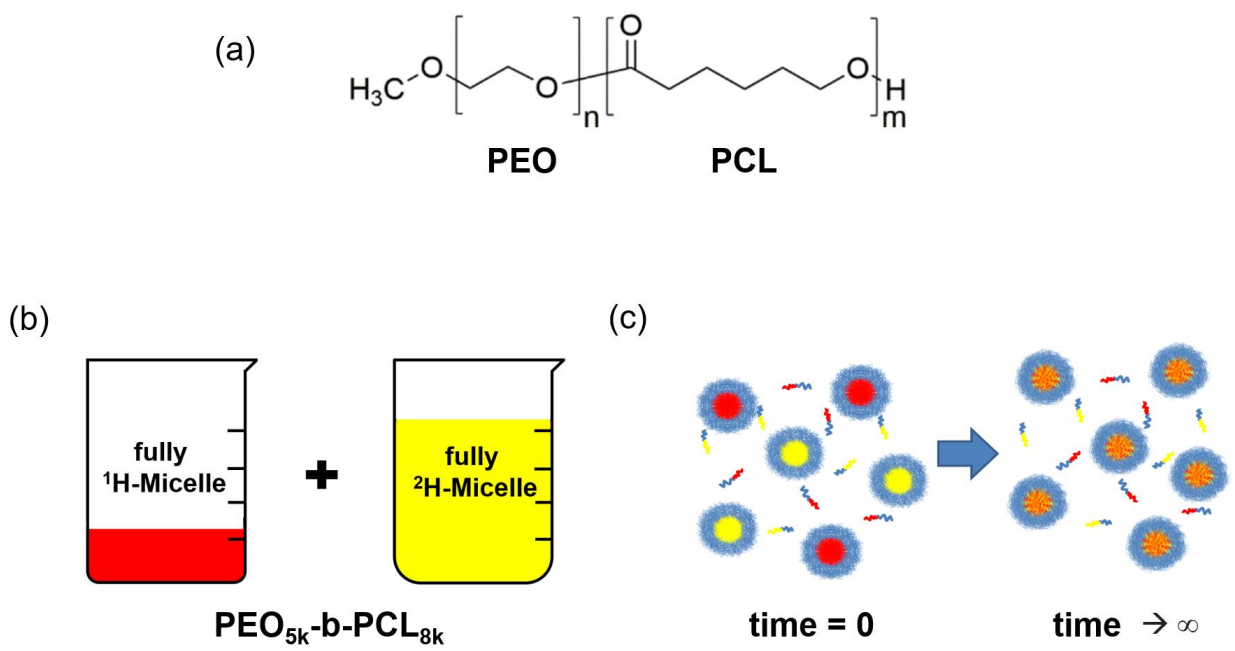

Figure 4.5. a) Molecular structures of PEO-b-PCL with the labeling of protons. Positions of 2, 3, 4, 5, 6 of PCL blocks are fully deuterated for the ^{2}H BCMs, b) Proposed mixing of differently isotope-labeled (10 vol % protonated-red and 90 vol % deuterated-yellow) BCMs, and c) Schematic of micelle distribution at mixing time t = 0 and $t \rightarrow \infty$.

For the mixed volume percentages of isotope-labeled micelles, we use 10 vol % of micelles with fully protonated core chains and 90 vol % of micelles with fully deuterated core chains. On one hand, using 90 vol% of ^{2}H micelles introduces a large fraction of ^{2}H-labeled core chains into the mixed micelles to guarantee maximal change in T_1 after mixing. On the other hand, using 10 vol% of ^{1}H micelles can enable ^{1}H NMR detection with sufficient S/N ratio from ^{1}H-labeled chains (**Figure 4.5**). In other words, using > 90 vol % of ^{2}H-labeled core chains will not generate a substantially larger change in T_1 on mixing, and using < 10 vol% of protonated core chains will cause NMR experiment time to greatly increase due to fewer protons present and thus low SNR.

Before mixing of the ^{1}H and ^{2}H BCM samples, we firstly evaluated the T_1 times for PCL sites of fully ^{1}H micelles at varied temperatures and solvent compositions, and summarized these results in **Table 4.2**. As the temperature increased from 25 to 60 °C (at a fixed solvent, 20 vol % THF-d_8:80 vol % D_2O) or THF-d_8 vol% increased from 10 to 20% (at a fixed temperature, 21 °C), the T_1 time for each PCL site increased, which agrees with the "fast motion limit" described by the BPP theory in Figure 4.4. As the THF-d_8 vol% increased from 10% to 20% at 25 °C, the T_1 time for PCL sites also increased steadily due to the more mobile environment generated by the increased amount of THF-d_8 in the system.

Table 4.2. a) T_1 relaxation time constants for the ^{1}H-sites on PCL for 100 vol % ^{1}H micelles composed of 20 vol % THF-d_8:80 % D_2O at varied temperatures, b) T_1 relaxation time constants for the ^{1}H-sites on PCL for 100 vol % ^{1}H micelles at 21 °C with varied THF compositions. The NMR T_1 measurement has an error bar < 1%.

a) **Temperature (°C)**	**PCL 6 T_1 time (ms)**	**PCL 2 T_1 time (ms)**	**PCL 3,5 T_1 time (ms)**	**PCL 4 T_1 time (ms)**
25	458	472	421	430
40	670	718	638	659
50	892	932	832	864
60	1072	1041	1006	1031

b) **Vol% THF-d_8**	**PCL 6 T_1 time (ms)**	**PCL 2 T_1 time (ms)**	**PCL 3,5 T_1 time (ms)**	**PCL 4 T_1 time (ms)**
10	399	404	373	379
15	426	423	383	387
20	444	451	401	411

4.3.2 Spin-lattice Relaxation Times for ^{1}H and ^{2}H Mixed Micelles

All the mixtures were prepared at room temperature by mixing ^{1}H micelles with ^{2}H micelles together. When the temperature reaches the desired set temperature, then the first T_1 experiment is conducted and the time is recorded as t_{mix} = 0 min. Here we expect to observe a significant increase of T_1 for the mixed samples at a certain solvent composition and temperature, so we are able to fit into an exponential function and extract the unimer exchange rate in the micelle

system. As mentioned in the previous schematic, we combined two BCM solutions (10 vol % ^{1}H: 90 vol % ^{2}H) and measured T_1 values as a function of time (t_{mix}) for all PCL signals at different temperatures (in **Figure 4.6**). Figure 4.6 a) or d) are difficult to determine if there is a plateau or increase due to scattered data points. However, in Figure 4.6 b) we observed a decrease in T_1 over time, and we will discuss the possible reason in a later session. Figure 4.6 c) suggested less scattered points at 20 vol % THF-d_8: 80 vol % D_2O. Therefore, more studies were done at this solvent composition.

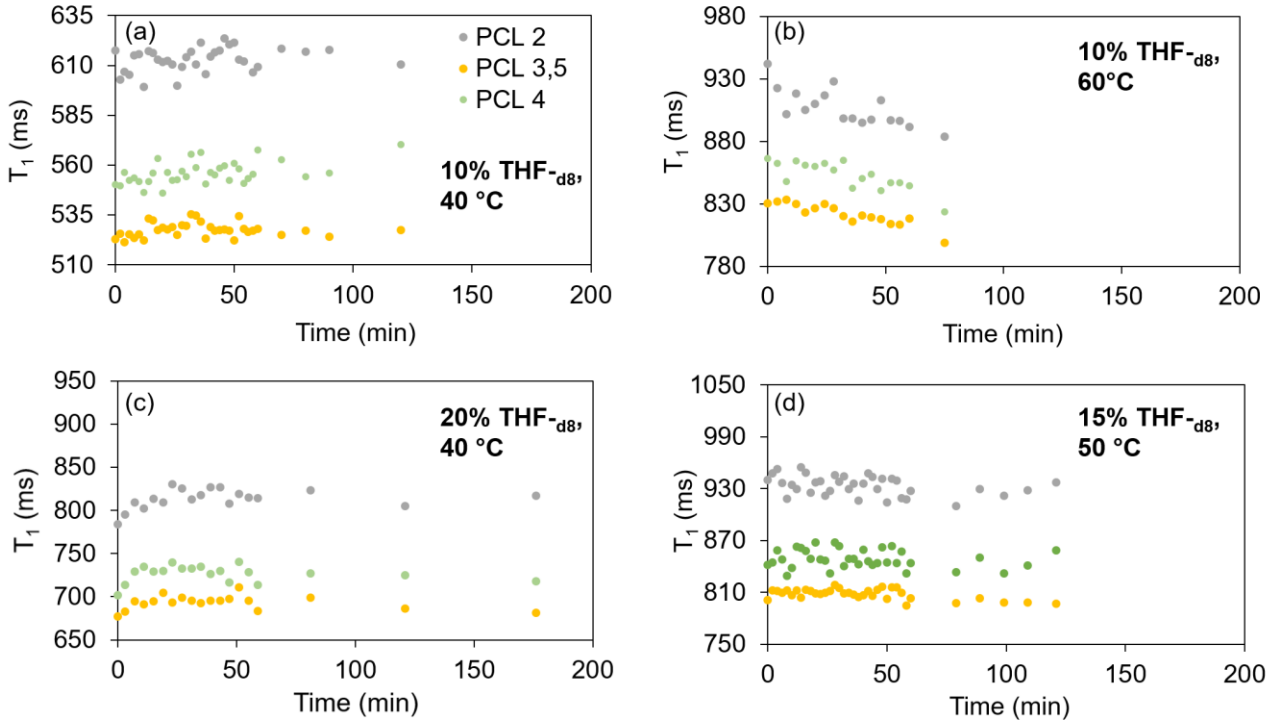

Figure 4.6. Evolution of T_1 as a function of time (t_{mix}) after mixing ^{1}H and ^{2}H micelle samples. The legend labels (upper left of graph (a)) indicate the sites for PCL 2, 3, 4, 5. PCL 6 is not included due to overlap with PEO in ^{1}H NMR spectrum. Solvent composition and mixing temperature are also labeled on the right corner of each graph, which are a) 10 vol % THF-d_8: 90 vol % D_2O at 40 °C, b) 10 vol % THF-d_8: 90 vol % D_2O at 60 °C, c) 20 vol % THF-d_8: 80 vol % D_2O at 40 °C, d) 15 vol % THF-d_8: 85 vol % D_2O at 50 °C.

4.3.3 TR-NMR Techniques for Unimer Exchange Kinetics

On the basis of previous NMR T_1 experiments, we selected ^{1}H and ^{2}H micelle samples at 20 vol % THF-d_8: 80 vol % D_2O and 40 °C. Our collaborators in Prof. Megan Robertson's group, Department of Chemical and Biomolecular Engineering, University of Houston conducted the TR-SANS studies. SANS experiments were performed with a SANS instrument at the High Flux Isotope Reactor (HFIR) facility of the Oak Ridge National Laboratory (ORNL) or at the Center for Neutron Research (NCNR) of the National Institute of Standards and Technology (NIST). From their SANS results, it is concluded that the micelle system did not fully mix over a 5-hour time scale at 40 °C. In both TR-SANS and TR-NMR, we define the post-mixed samples as the BCMs mixed from separate reservoirs of ^{1}H and ^{2}H BCMs (as shown in **Figure 4.5c**) and pre-mixed samples as BCMs that are formulated directly from a mixture of ^{1}H and ^{2}H block copolymer chains during preparation. By comparing the SANS intensity or T_1 time of pre-mixed and post-mixed BCMs, we are able to determine whether the chains are fully exchanged or not.

TR-NMR experiments were then conducted under the same conditions to further study the exchange process in the micelle system. We did a careful repeat experiment over the mixed 10 vol % ^{1}H and 90 vol % ^{2}H BCMs in 20 vol % THF-d_8: 80 vol % D_2O at 40 °C for ~ 20 hours. The T_1 time did not increase and unexpectedly, it decreased in the long term. As we propose that by introducing more moieties of ^{2}H polymer chains in the micelle system, the T_1 time will increase as a result of intermolecular dipole-dipole interaction (^{1}H – ^{2}H). Otherwise, this interaction is too negligible to be detected in NMR T_1 measurements and we shall see no change in T_1 times. Therefore, the only possible reason for the T_1 decrease would be the composition change in the micelle system upon heating. THF is a volatile solvent and can evaporate rapidly even in a well-capped and Teflon sealed tube or cell. We also integrated the residual THF peak in the post-mixed

sample and observed an obvious decrease in the peak area at t_{mix} = 20 hours compared to t_{mix} = 0 min (spectra not included in this chapter). As discussed in 4.3.1, increasing THF-d_8 vol % renders more mobility for polymer chains and thus a longer T_1. However, a gradual loss of THF upon heating at the same time, lowers the T_1. Therefore, we observed slight / no change or even unexpected T_1 decrease TR-NMR measurements.

We then flame-sealed the NMR tubes to guarantee no solvent loss and also checked the mass of the sample tube before and after heating (~ 0.4 mg, which is negligible). Other sets of TR-NMR experiments were conducted at the same composition (10 vol % ^{1}H and 90 vol % ^{2}H micelles in 20 vol % THF-d_8: 80 vol % D_2O) and different temperatures. We also summarize T_1 values of pre-mixed micelles (10 vol % ^{1}H and 90 vol % ^{2}H) at different temperatures in **Table 4.3**, in order to compare with the T_1 of the final post-mixed ($t_{mix} \rightarrow \infty$) BCMs.

In this batch, we have a PEO overlap that affects T_1 fitting for PCL 6 and 2 peaks. Therefore, we did not include an analysis of those two peaks in the following studies.

Table 4.3. The T_1 relaxation times for the ^{1}H-sites on PCL 3,5 and 4 for 10 vol % ^{1}H and 90 vol % ^{2}H pre- mixed and post-mixed micelles in 20 vol % THF-d_8:80 vol % D_2O at different temperatures (40 ℃ and 55 ℃).

Compositions	**20% THF-d_8 at 40 °C**		**20% THF-d_8 at 55 °C**	
	Pre-mixed	Post-mixed	Pre-mixed	Post-mixed
PCL 3,5 (ms)	587	563	821	831
PCL 4 (ms)	598	580	847	854

At 40 °C, we observed the T_1 of the post-mixed micelle was lower than the pre-mixed sample, which was indicative that no or incomplete mixing. While at 55 °C the T_1 agreed with pre-mixed and post-mixed BCMs (< 1% error bar) and supported that the mixing was completed at a higher temperature over the mixing time scale (> 10 h).

To probe into the chain exchange kinetics, we carefully collected T_1 values of BCMs over 2 hours with an 8 min interval and then the next 8 hours with a 15 min interval for both 40 and 55 ℃, respectively. We observed little T_1 change at 40 ℃, which indicates no/incomplete chain exchange and agrees with results from Table 4.3 and SANS. Excitingly, we did observe an increase of ~ 30 ms in T_1 (> 3%) at 55 ℃, which is supportive of chain exchange over the mixing time scale.

Next, we targeted a higher temperature for BCM mixing is 62 °C, as the mixture of THF and H_2O has an azeotrope at 63 °C. Obviously, the BCM T_1 represents different changing rates at different temperatures. According to our previous experiments at 25 ℃ and 40 ℃, we were not able to see significant T_1 change after mixing after 6 hours. This indicates the exchange of unimers between micelles was slow compared to the experimental time scale or, to put it in another way, the chains were kinetically trapped in micelles. In micelle kinetic studies, we typically assume the theory of a single exponential process for chain exchange at a steady state.

To probe chain exchange kinetics from TR-NMR results, we plotted relaxivity ($1/T_1$) and over t_{mix}. In a dilute solution limit, the relaxivity is linearly dependent on the proton concentration, for example, the relaxivity is linearly dependent on the concentration of MRI contrast agents. We can use this assumption to probe the relation between concentration vs. mixing time by fitting them with a single exponential model in Equation 4.2 for preliminary studies. In future studies, we will work on controlled or standard samples to determine how relaxivity is related to composition.

$$y = y_0 + A_1(\exp(-x/t)) \tag{4.2}$$

Figure 4.7 shows the evolution of T_1 as a function of t_{mix} of ^{1}H and ^{2}H micelle samples (in 20% vol THF-d_8: 80 vol % D_2O at 62 °C and 55 °C, respectively.

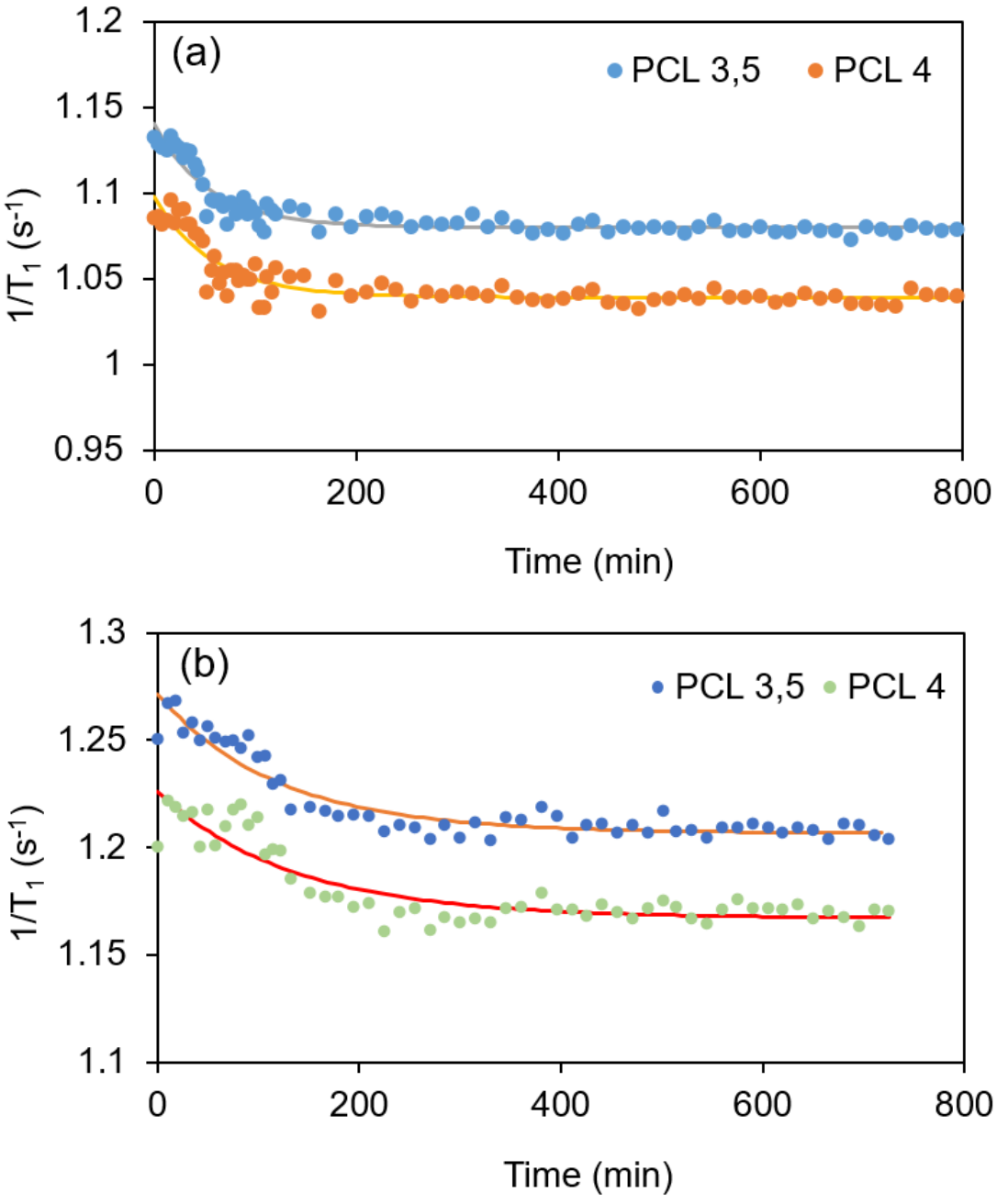

Figure 4.7. Evolution of T_1 as a function of t_{mix} of ^{1}H and ^{2}H micelle samples (in 20 vol % THF-d_8: 80 vol % D_2O) at a) 62 °C and b) 55 °C.

At 62 °C, the half-time ($t_{1/2}$) of T_1 much shorter than that of $t_{1/2}$ at 55 °C. **Table 4.4** shows the fitting results, time constants and exchange rates of chain exchange using a simple exponential model. At a higher temperature 62 ℃, unimer chains fully exchanged within 1 h and at a slightly lower temperature 55 ℃, chains did not fully exchange until ~ 2 h. Notably, there is existence of free unimers (~ 40%) in solution under these temperatures based on our previous studies in Chapter 3. Those free ^{2}H-chains in solution will not affect the overall T_1 of ^{1}H-chains we measure, due to their dilute concentration compared to the large quantity of ^{2}H solvent surrounded.

Table 4.4. Fitting time constants and exchange rates in an exponential decay model at 55 ℃ and 62 ℃, using PCL 3,5 and PCL 4 series data.

	62 °C				**55 °C**			
Peak	y_0	A_1	t(min)	$k_{ex}(min^{-1})$	y_0	A_1	t(min)	$k_{ex}(min^{-1})$
PCL 3,5	926.0	-49.1	57	0.0175	828.7	-42.3	123	0.0081
PCL 4	962.3	-51.7	60	0.0167	856.8	-41.3	138	0.0072

Besides single exponential decay process, most studies that observe exchange kinetics cannot be simply described by single relaxation time and are often fitted into double exponential decay.[26-27] Lund et al.[28-31] studied the polymeric systems by neutron scattering and described chain kinetics by a logarithmic decay model. For BCM unimer exchange kinetics, the exchange rates are determined by a combination of molecular interactions, including the interfacial tension between hydrophobic groups and solvents, hydrophilic groups and solvents or the steric hindrance between the chains in core and corona. Unimer kinetics in BCMs are commonly studied by starting with a non-equilibrium system, e.g., two micelle samples with different compositions or isotopic labels, and monitoring its relaxation to a new equilibrium (e.g., after mixing the two samples). The BCM

system is usually disturbed by a *T*-jump (temperature jump) or stopped-flow method.[32] Researchers have reported several BCM systems that exhibit chain exchange and their activation energies are in the range of 30 – 100 kJ/mol.[33] The dependence of chain kinetics on temperature very likely depends on the chain mobility in micellar cores.

Van Stam et al.[2] have tuned the chain exchange kinetics in BCMs by changing the temperature, cosolvents, and cosurfactants and investigated by steady-state fluorescence spectroscopy. Similarly, they did not detect any exchange at room temperature over several hours until the temperature was raised to 60 ℃. They proposed the chain exchange rate was probably related to the glass transition temperature (T_g) of the hydrophobic core-forming polymer. When the temperature is above its T_g, the internal core is possibly more mobile and accelerates the chain exchange. More investigations will be included in Chapter 6 to understand how core-forming polymeric block mobility impacts overall micelle dynamics. Furthermore, other parameters such as the core packing, interactions between building blocks and solvent can all together contribute to determining the exchange kinetics in micelles.[34]

TR-SANS monitors the systematic scattering signal reduction by mixing isotope-labeled visible species at elevated temperatures. Similarly, we utilize NMR and the difference in the gyromagnetic ratio of isotopes (^{1}H / ^{2}H) to probe BCM kinetics. In summary, we have obtained important chain kinetic information in BCMs by using this TR-NMR method, providing another fundamental approach to control and design nanostructures such as BCMs, whose growth mechanism is still challenging to fully understand.

4.4 Conclusions

By mixing of fully protonated and deuterated PEO-b-PCL micelles solutions, we have successfully created a weakening in magnetic environment. Because the gyromagnetic ratio (γ) for

^{1}H is larger than ^{2}H. When the ^{1}H chains are gradually surrounded by ^{2}H-unimers as it reaches equilibrium, we successfully observed an increase in spin-lattice relaxation time (T_1) with mixing time at higher temperatures 55 ℃ and 62 ℃, which is further supported by our previous studies that the existence of both micelles and free unimers. By fitting the relaxivity ($1/T_1$) value vs the mixing time, we can extract exchange time constants of 60 min at 62 ℃ and 130 min at 55 ℃ from an exponential decay model. Our initial results are comparable to our collaborator's from TR-SANS and other literature values.

This TR-NMR method can be useful to probe molecular exchange in predefined BCMs or other nanostructures, and devise controlled release of drug cargos in drug delivery application. It works on any solution-state NMR spectrometer with minimal perturbation to chemical structure, opening up a new possibility to conveniently characterize the BCM system. There are only a handful of SANS instruments worldwide, but at least one NMR spectrometer exists in most industrial lab or universities, and thus NMR is a more accessible and cost-effective analysis as a possible alternative to TR-SANS. We also believe that NMR spectroscopy and relaxation method will prove to be promising techniques for more general characterization of micelle dynamics and can extend to more complex systems to study soft matter kinetic behaviors.

References

1. Lu, J.; Bates, F. S.; Lodge, T. P., Chain Exchange in Binary Copolymer Micelles at Equilibrium: Confirmation of the Independent Chain Hypothesis. *ACS Macro Lett* **2013,** *2* (5), 451-455.

2. van Stam, J.; Creutz, S.; De Schryver, F. C.; Jérôme, R., Tuning of the Exchange Dynamics of Unimers between Block Copolymer Micelles with Temperature, Cosolvents, and Cosurfactants. *Macromolecules* **2000,** *33* (17), 6388-6395.

3. Kelley, E. G.; Murphy, R. P.; Seppala, J. E.; Smart, T. P.; Hann, S. D.; Sullivan, M. O.; Epps, T. H., Size evolution of highly amphiphilic macromolecular solution assemblies via a distinct bimodal pathway. *Nat Commun* **2014,** *5*.

4. Halperin, A.; Alexander, S., Polymeric micelles: their relaxation kinetics. *Macromolecules* **1989,** *22* (5), 2403-2412.
5. Kim, T. H.; Huh, J.; Hwang, J.; Kim, H.-C.; Kim, S. H.; Sohn, B.-H.; Park, C., Ordered Arrays of PS-b-P4VP Micelles by Fusion and Fission Process upon Solvent Annealing. *Macromolecules* **2009,** *42* (17), 6688-6697.
6. Aniansson, E. A. G.; Wall, S. N., Kinetics of step-wise micelle association. *J. Phys. Chem.* **1974,** *78* (10), 1024-1030.
7. Li, Z.; Dormidontova, E. E., Equilibrium chain exchange kinetics in block copolymer micelle solutions by dissipative particle dynamics simulations. *Soft Matter* **2011,** *7* (9), 4179-4188.
8. Nicolai, T.; Colombani, O.; Chassenieux, C., Dynamic polymeric micelles versus frozen nanoparticles formed by block copolymers. *Soft Matter* **2010,** *6* (14), 3111-3118.
9. Narang, A. S.; Mahato, R. I., *Targeted delivery of small and macromolecular drugs*. CRC press: **2010**.
10. Nyrkova, I. A.; Semenov, A. N., On the Theory of Micellization Kinetics. *Marcomol. Theory Simul* **2005,** *14* (9), 569-585.
11. Lund, R.; Willner, L.; Richter, D., Kinetics of Block Copolymer Micelles Studied by Small-Angle Scattering Methods. In *Controlled Polymerization and Polymeric Structures*, Abe, A.; Lee, K.-S.; Leibler, L.; Kobayashi, S., Eds. Springer International Publishing: **2013**; Vol. 259, pp 51-158.
12. Mortensen, K.; Talmon, Y., Cryo-TEM and SANS Microstructural Study of Pluronic Polymer Solutions. *Macromolecules* **1995,** *28* (26), 8829-8834.
13. Willner, L.; Poppe, A.; Allgaier, J.; Monkenbusch, M.; Richter, D., Time-resolved SANS for the determination of unimer exchange kinetics in block copolymer micelles. *Europhys. Lett.* **2001,** *55* (5), 667-673.
14. Roberts, J. D., *ABCs of FT-NMR*. **1996**.
15. Goldman, M., ADVANCES IN MAGNETIC RESONANCE Formal Theory of Spin-Lattice Relaxation. *J. Magn. Reson.* **2001,** *149*, 160-187.
16. Bloembergen, N., Proton Relaxation Times in Paramagnetic Solutions. *J. Chem. Phys.* **1957,** *27* (2), 572-573.
17. Levitt, M. H., *Spin Dymamics Basics of Nulcear Magnetic Resonance*. John Wiley&Sons, Ltd: **2011**.
18. Gordon, M. I.; Hoch, M. J. R., Quadrupolar spin-lattice relaxation in solids. *J. Phys. C: Solid State Physics* **1978,** *11* (4), 783-795.
19. Campbell, I. D.; Freeman, R., Influence of cross-relaxation on NMR spin-lattice relaxation times. *J. Magn. Reson.* **1973,** *11* (2), 143-162.
20. Kay, L. E.; Scarsdale, J. N.; Hare, D. R.; Prestegard, J. H., Simulation of two-dimensional cross-relaxation spectra in strongly coupled spin systems. *J. Magn. Reson.* **1986,** *68* (3), 515-525.

21. Leipert, T. K.; Marquardt, D. W., Statistical analysis of NMR spin-lattice relaxation times. *J. Magn. Reson.* **1976,** *24* (2), 181-199.
22. Bloembergen, N.; Purcell, E. M.; Pound, R. V., Relaxation effects in nuclear magnetic resonance absorption. *Phys. Rev.* **1948,** *73* (7), 679.
23. Anderson, W. A.; Arnold, J. T., Proton Relaxation Times in H 2 O—D 2 O Mixtures. *Phys. Rev.* **1956,** *101* (2), 511.
24. Cooksey, T. J.; Singh, A.; Le, K. M.; Wang, S.; Kelley, E. G.; He, L.; Vajjala Kesava, S.; Gomez, E. D.; Kidd, B. E.; Madsen, L. A.; Robertson, M. L., Tuning Biocompatible Block Copolymer Micelles by Varying Solvent Composition: Core/Corona Structure and Solvent Uptake. *Macromolecules* **2017,** *50* (11), 4322-4334.
25. Kidd, B. E.; Li, X.; Piemonte, R. C.; Cooksey, T. J.; Singh, A.; Robertson, M. L.; Madsen, L. A., Tuning Biocompatible Block Copolymer Micelles by Varying Solvent Composition: Dynamics and Populations of Micelles and Unimers. *Macromolecules* **2017,** *50* (11), 4335-4343.
26. Zinn, T.; Willner, L.; Lund, R.; Pipich, V.; Richter, D., Equilibrium exchange kinetics in n-alkyl-PEO polymeric micelles: single exponential relaxation and chain length dependence. *Soft Matter* **2012,** *8* (3), 623-626.
27. Willner, L.; Poppe, A.; Allgaier, J.; Monkenbusch, M.; Richter, D., Time-resolved SANS for the determination of unimer exchange kinetics in block copolymer micelles. *EPL* **2001,** *55* (5), 667.
28. Lund, R.; Willner, L.; Stellbrink, J.; Radulescu, A.; Richter, D., Tuning of structure and kinetics of chain exchange in star-like PEP-PEO block copolymer micelles. *Physica B: Condensed Matter* **2004,** *350* (1, Supplement), E909-E912.
29. Lund, R.; Willner, L.; Stellbrink, J.; Radulescu, A.; Richter, D., Role of Interfacial Tension for the Structure of PEP−PEO Polymeric Micelles. A Combined SANS and Pendant Drop Tensiometry Investigation. *Macromolecules* **2004,** *37* (26), 9984-9993.
30. Lund, R.; Willner, L.; Stellbrink, J.; Lindner, P.; Richter, D., Logarithmic Chain-Exchange Kinetics of Diblock Copolymer Micelles. *Phys. Rev. Lett.* **2006,** *96* (6), 068302.
31. Lund, R.; Willner, L.; Monkenbusch, M.; Panine, P.; Narayanan, T.; Colmenero, J.; Richter, D., Structural observation and kinetic pathway in the formation of polymeric micelles. *Phys. Rev. Lett.* **2009,** *102* (18), 188301.
32. Denkova, A. G.; Mendes, E.; Coppens, M.-O., Non-equilibrium dynamics of block copolymer micelles in solution: recent insights and open questions. *Soft Matter* **2010,** *6* (11), 2351-2357.
33. Wang, Y.; Kausch, C. M.; Chun, M.; Quirk, R. P.; Mattice, W. L., Exchange of Chains between Micelles of Labeled Polystyrene-block-poly(oxyethylene) As Monitored by Nonradiative Singlet Energy Transfer. *Macromolecules* **1995,** *28* (4), 904-911.

34. Yu, Y.; Zhang, L.; Eisenberg, A., Multiple Morphologies of Crew-Cut Aggregates of Polybutadiene-b-poly(acrylic acid) Diblocks with Low Tg Cores. *Langmuir* **1997,** *13* (9), 2578-2581.

Chapter 5: Quantifying Drug Partitioning in Pluronic® Block Copolymer Micelle Solutions: Investigations of Structural Change and Intermolecular Interaction

(Manuscript in preparation for publication)

Xiuli Li, Tyler J. Cooksey, Veera Venkata Shravan Uppala, Megan L. Robertson, Louis A. Madsen*

*Department of Chemistry and Macromolecules Innovation Institute, Virginia Tech, Blacksburg, 24061, USA

Abstract

Understanding cargo partitioning are crucial in the design of micelle-based formulations for potential cargo delivery. In Chapter 5 we present a study of the self-assembly of a Pluronic® F127 ($PEO_{99}PPO_{69}PEO_{99}$) triblock copolymer in water and its solubilization of three hydrophobic drugs, hydrochlorothiazide (HCT), indomethacin (IND) and paclitaxel (PTX). Using NMR diffusometry, we have quantified diffusion coefficients of different species in aqueous solution, including the polymers, drug cargos and solvent. We investigate effects of polymer concentration as well as drug composition on micelle-drug interactions. As the F127 concentration increases from 1 to 5% wt/vol, the partition percentages of HCT and IND in micelles both demonstrate increase. The facile and non-invasive NMR method presented here allows an estimation of drug distribution in a micellar system and opens opportunities to understand the dynamic process of drug partitioning in micelles.

5.1 Introduction

Poly(ethylene oxide)-*b*-poly(propylene oxide)-*b*-poly(ethylene oxide) (PEO-PPO-PEO) triblock copolymers provide wide-ranging possibilities to build microenvironments for incorporation of various cargos because of their amphiphilicity. Therefore, PEO-PPO-PEO

triblock copolymers are used in a wide range of applications, such as pharmaceutical formulations, foaming agents and advanced coatings.[1] Commercially available PEO-PPO-PEO copolymers manufactured by BASF are named as Pluronic® polymers. They have been applied as the medium in drug delivery systems for the solubilization and low toxicity delivery of poorly water-soluble drugs.[2] Researchers have probed the micellization and gelation of Pluronic® polymers by neutron scattering,[3] rheology,[4] fluorescence,[5] and NMR spectroscopy.[6] Above the CMC, the entropy-driven micellization occurs by forming a less polar core of PPO blocks and a water-swollen corona of PEO blocks. At even higher concentration of polymer (above the critical gelation concentration, CGC), a thermo-reversible gel forms as a result of intermolecular associations between the polymer chains.[7]

The drug delivery polymeric materials can greatly affect the pharmacological properties of drugs, including pharmacokinetics, biodistribution and sustained release.[8] A widespread distribution of drugs can result in dose-limiting side effects and affect normal tissues. Using drug delivery carriers, such as PEO-PPO-PEO copolymers, can help to reduce those effects by encapsulating drugs in hydrophobic reservoirs.[9] Therefore, it is important to understand and quantify how drugs are distributed in the delivery carriers and surrounding aqueous environment. The partition coefficient (K) defines the distribution of drugs in different phases, which is critical to estimating the release rate and residence time in the organism, as well as other aspects of biological activity.[10] Knowledge of K also provides insight into the nature and strength of molecular interactions between drug molecules and micelles, for example, van der Waals forces, hydrophobic interactions and hydrogen bonding.[11] Several factors have been determined to affect the solubilization capacity of micelles, including compatibility between the core-forming polymers and the cargo, micellar size, aggregation number, interfacial tension between aqueous medium and

the cargo, and the molecular volume of cargo.[12-13] *K* can sometimes be obtained experimentally from UV-Vis,[14] high performance liquid chromatography,[15] differential scanning calorimetry[16] and fluorescence spectroscopy.[17] Those methods either require additional separation of two phases or probe labeling, which can cause possible drug loss and complicated preparation procedures. Detailed studies are introduced in the following sections.

5.1.1 UV-vis Spectroscopy

Choucair et al.[11] investigated the solubilization of a hydrophobic polar dye molecule, 2-nitrodiphenylamine in polystyrene-b-poly (acrylic acid) micelle solutions. They evaluated solubilization capacity of micelles and the micelle-water partition coefficients by UV-vis and fit the data to a Langmuir adsorption isotherm, which can be expressed as Equation 5.1:

$$\frac{x}{x_{\max}} = \frac{K_{ad}C}{1 + K_{ad}C} \tag{5.1}$$

where x, x_{max}, K_{ad}, and C are the solubilizate mole fraction in the micellar phase, the maximum of that mole fraction, the adsorption constant, and molar concentration of free, unbound dye molecules, respectively. Their results showed that solubilization was a binding process and was dependent on the interfacial area of the micelles, and on the affinity of the dye for the micellar interface. It is the first study that treats the solubilization as an adsorption-like phenomenon and reveals the mechanism of interfacial solubilization in block copolymer aggregates. By understanding this process and the intermolecular interactions, we can find a number of applications in drug delivery, separation or toxic waste removal.

Sabate et al.[14] also determined the micelle association constant K_A based on Equation 5.1 by studying the interaction of pinacyanol (PIN) with surfactant micelles *n*-dodecyltrimethylammonium bromide (DTAB) by UV-visible spectrophotometry. They showed

that the dye bound with micelles in the monomeric form and the interaction between PIN with micellar DTAB produced a bathochromic shift.

5.1.2 Differential Scanning Calorimetry (DSC)

Lasonder et al.[16] studied the interactions of a phospholipid vesicle (dipalmitoyl phosphatidylcholine) with a few anti-inflammatory agents (sulindac, sulfide, naproxen, phenylbutazone, and indomethacin) and some physiologically inactive compounds with similar structures. They measured transition temperatures and determined K based on the method of Hill and Shen (see **Figure 5.1**). The calculated the partition coefficient by aqueous-phase DSC indicated the partition of a guest compound between the vesicle and water (e.g. $K_{indomethacin} > K_{naproxen} > K_{sulindac}$). This method provides a pathway to develop K values and understand intermolecular interactions from thermal changes. In all, it sheds light on the how to study the interactions of physiologically active compounds with nanocarriers, such as biological membranes.

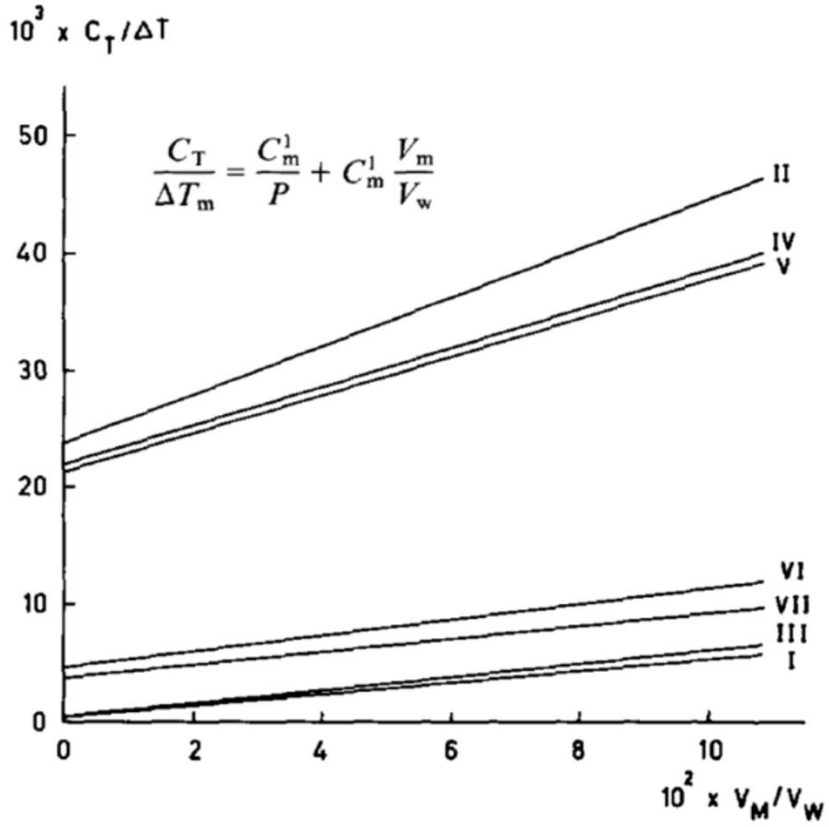

Figure 5.1. Plots for the determination of the partition coefficients for compounds I to VII. P is the defined partition coefficient. V_m and V_w are the volume of lipid bilayer and water, respectively, C^1_m is the concentration of drug needed to produce a l °depression, ΔT_m is the depression of the phase transition temperature compared to the pure surfactant, and C_T is the aqueous concentration of drug. According to the equation given in Figure 5.1, P could be determined from plots of $C_T/\Delta T$ versus V_m/V_w. Compounds I to VIII are molecules of: indomethacin (I), 5-methoxy-2-methyl-indole-3-acetic acid (II), sulindac sulfide (III), sulindac (IV), sulindac sulfone (V), naproxen (VI), phenylbutazone-d9 (VII), and lecithin (VIII). Reproduced from Reference 16.

5.1.3 Fluorescence Spectroscopy

Teng et al.[17] monitored the uptake and release kinetics of two hydrophobic fluorescent probes (pyrene and phenanthrene) in block copolymer micelles by fluorescence. They measured

the fraction of probe released at the earliest time, then the amount of probe present in the bulk solution of the stock solutions before dilution. By comparison they concluded that a certain fraction of the probe was solubilized in corona. They also measured diffusion constants and analyzed partition coefficients of the probes between the micelle and water. It provides insights to understand the solubilization of cargos in block copolymer carriers, also on the experimental design of drug-carrier dynamic / kinetic studies using fluorescence method.

Maity et al.[18] reported the binding interactions of a nonsteroidal anti-inflammatory drug (NSAID): indomethacin (IMC) in the presence of different micelles, e.g. SOS (anionic) and DTAB (cationic). By using the methods including steady state fluorescence, time-resolved (TR) fluorescence spectroscopy emission and isothermal titration calorimetry (ITC), they quantified the differences between IMC-loaded micelles and IMC in neat water. Moreover, the addition of KCl salt (20 mM) accelerated the release of IMC from micelles to aqueous solution. The IMC in micelles emitted higher fluorescence intensity and showed two life-time components. The thermodynamic and binding parameters between IMC and micelles has been estimated (**Table 5.1**), which is of significance in potential targeted drug design and its release in physiological systems.

Table 5.1. Photophysical parameters, partition coefficient and binding constant of IMC in different micelles. Reproduced from Reference 18.

Medium	CMC (in mM)	[Surfactant]	λ_{max}^{emi} (nm)	ϕ_f	Partition coefficient (K_{M-W})	Binding Constant (K) (M^{-1})
neat water			380	2×10^{-4}		
SOS	134	3 times of *CMC*	364	1.25×10^{-3}	250	$2.12\ (\pm 0.38) \times 10^3$
SDS	8.2	20 times of *CMC*	364	3.65×10^{-3}	1350	$24.35\ (\pm 1.64) \times 10^3$
DTAB	15.6		360	3.70×10^{-3}	165	$0.36\ (\pm 0.14) \times 10^3$
MTAB	4.2		360	4.10×10^{-3}	1180	$18.50\ (\pm 4.80) \times 10^3$
CTAB	0.92		365	7.60×10^{-3}	15825	$41.75(\pm 4.75) \times 10^3$

Here we present a simple and non-destructive NMR diffusometry approach to investigate the drug partitioning behavior in Pluronic® F127 block copolymer micelles (BCMs), along with SANS investigations of micelle size parameters, aggregation numbers, and micelle core swelling

with solvent. We define the BCMs as a micellar phase due to its encapsulation of hydrophobic cargos and the solvent as an aqueous phase. The activity coefficients of drug in both phases are assumed to be 1 (as in the case of a dilute system), thus a partition coefficient (K) is given by the ratio of model drug concentration in each phase with:

$$K = \frac{[M]_{drug,\ micelle}}{[M]_{drug,\ aqueous}} \tag{5.2}$$

where $[M]_{\text{drug, }micelle}$ is the concentration of model drug in the micellar phase, and $[M]_{\text{drug, }aqueous}$ is the concentration of model drug in the aqueous phase.

In this study, we apply model drugs with different solubilities – hydrochlorothiazide (HCT), indomethacin (IND) and paclitaxel (PTX), to investigate the hydrophobic drug solubilization and partitioning behavior in the Pluronic® F127 BCMs. Pluronic® F127 formulations have been widely applied to enhance the solubilization and prolonged release profiles for poorly water-soluble drugs.[19-20] HCT is a diuretic and anti-hypertensive drug for the treatment of diabetes. HCT is also used to treat edema (excess fluid held in body tissues) caused by certain medical problems, such as heart, kidney and liver diseases or estrogen and corticosteroids.[21] IND is an anti-inflammatory drug that reduces fever, pain and inflammation and relieves symptoms of arthritis or gout.[22] PTX is a chemotherapy medication to treat cancers, including lung, breast, prostate and other types of solid tumor cancers.[23] The water solubility of three drugs follows the order: PTX < IND < HCT (**Figure 5.2a**). Common incorporations of insoluble drugs into micelles are chemical conjugation and physical entrapment.[24] Model drugs are encapsulated in BCMs to ensure minimal premature leakage for delivery goals.[25] The drug loading process depends on the structures and interactions between the drug and the polymer, and also is influenced by polymer composition, hydrophobic ratio and molecular volume.[26] HCT- and IND-loaded micelles are prepared by a direct dissolution method (in **Figure 5.2b**). PTX-loaded micelles are prepared by a solid dispersion method.[27-28]

Using this NMR method, we are able to gain more insights into the molecular structures, dynamic, partitioning and distribution of drugs in polymeric carriers for potential drug delivery and therapy, thereby shedding light on understandings of molecular interactions and rational design of drug delivery formulations.

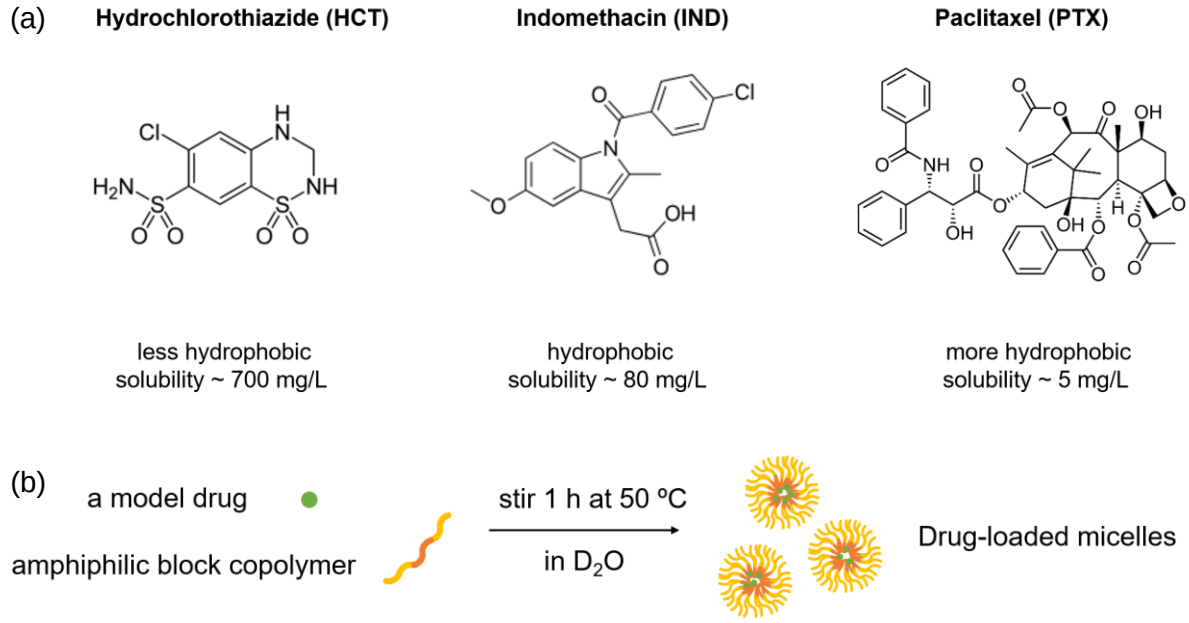

Figure 5.2. (a) Chemical structure and water solubility of model drugs: HCT, IND and PTX. (b) Direct dissolution method to prepare drug-loaded Pluronic® BCMs.

5.2 Experimental

5.2.1 Materials

The HCT, IND and Pluronic® F127 were purchased from Sigma-Aldrich. The HCT-loaded and IND-loaded BCMs solutions were prepared by mixing the drugs, triblock copolymer and deuterated water (for NMR detection) together at 50 °C for 1 h. The transparent solutions were transferred to either a 5 mm NMR tube after cooling for data acquisition to reduce possible micelle aggregation. Each sample tube was equilibrated at room temperature (25 °C) prior to running

diffusometry to ensure the sample is at thermal equilibrium. PTX-loaded BCMs were prepared by a solid dispersion method, where PTX and F127 polymer were dissolved separately in 2 mL DMF solvent to obtain transparent solutions, followed by fully mixing of two solutions and overnight vacuum dry to obtain homogenous solid dispersion. D_2O was then added to the solid dispersion at the same condition mentioned above to prepare PTX-loaded BCMs.

5.2.2 Pulsed-Field-Gradient (PFG) NMR Diffusometry

Our previous study has shown the utility of NMR in measurement of diffusion coefficients and relative populations of unimers and micelles.[29-31] NMR diffusometry typically applies the pulsed-field-gradient stimulated echo (PGSTE) sequence, which provides information on translational motion of various species in solution.[32-33] The self-diffusion coefficients of polymer, drug and solvent in solution were determined using a 400 MHz Bruker Avance III WB NMR spectrometer, equipped with a MIC probe coupled to a Diff60 single-axis (z-axis) gradient. The pulsed-gradient stimulated echo (PGSTE) sequence[34] was used with a 90 °RF pulse length of 4.5 μs. A half sinusoid gradient pulse length of δ = 3.14 ms (effective rectangular pulse length = 2 ms), diffusion time Δ = 25 ms, and post-gradient delay = 1 ms were used for ^{1}H diffusometry measurements. Maximum gradient strengths were adjusted in the range 5 – 600 G·cm^{-1} to achieve 90 – 99% signal attenuation in 16 – 32 steps. Sufficient signal-to-noise ratio (SNR) for each data point was achieved with 4 – 32 scans. Acquisition times and relaxation delay times were each 1 s, and 0.3 Hz line broadening was applied during data processing. All NMR measurements were performed at 25 ± 1 ℃.

5.2.3 Gel Permeation Chromatography (GPC)

The molecular weight and the dispersity of the Pluronic® F127 was characterized by a Viscotek GPCmax instrument using THF (OmniSolv, HPLC grade) as the mobile phase. The

injected volume was 100 μL of a 1 mg/mL solution, and the flow rate was 1 mL/min at 30 ℃. Universal analysis was employed for the characterization of the number-average molecular weight, M_n, and dispersity, $Đ$, utilizing the refractometer and viscometer.

5.2.4 Small-angle Neutron Scattering (SANS)

SANS measurements were conducted at the High Flux Isotope Reactor (HFIR), Oak Ridge National Laboratory (ORNL) on the CG-3 beamline. Data were collected from 2 mm thick samples using an incident neutron beam wavelength of 6 Å, at a sample-to-detector distance of 15.5 m, with an aperture width of 12 mm. The data were collected over a q-range of 0.0037 to 0.569 $Å^{-1}$. The data were reduced using Python routines in Mantid (developed by ORNL) and analyzed in SasView (developed by the DANSE project) using the Pedersen micelle model[35] and Percus-Yevick closure.[36]

5.3 Results and Discussion

In Pluronic® F127 micellar solutions, we observe a bimodal molecular weight distribution of F127 by multicomponent fitting in both SEC and NMR. We characterized the Pluronic® F127 solid sample used by GPC. In **Figure 5.3**, the molecular weight distribution was bimodal, which indicated the presence of diblock copolymer contaminants. The characteristics of the samples were: M_n = 14 kg/mol, $Đ$ = 1.25, and EO wt% = 72.2%. This corresponds to a composition of EO_{115}-PO_{67}-EO_{115} and this composition was used throughout the SANS analysis.

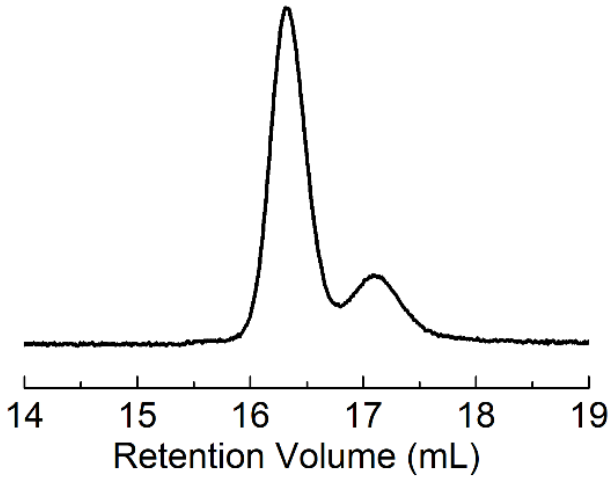

Figure 5.3. GPC data obtained from Pluronic® F127. A bimodal distribution indicates diblock contamination in the triblock copolymer. Data courtesy to Tyler Cooksey and Prof. Megan Robertson at Department of Chemical and Biological Engineering, University of Houston.

We also accessed the diffusion coefficients of polymer chain in micelle solutions (in forms of free unimers and micelles) by NMR diffusometry. By taking the natural log of normalized NMR signal intensity (I/I_0) and plotting vs. the b ($\gamma^2\delta^2g^2(\Delta-\delta/3)$) factor in the signal attenuation plots, any deviation from linear regression fitting (i.e., two straight slopes) represents more than one diffusion coefficient of the species of interests. **Figure 5.4a** shows an example of signal attenuation in 3% w/v BCM system, the fast diffusing species (i.e. small aggregate or short polymer chain) contributes to a rapid signal decay at lower gradient strengths, and the slow diffusing species (i.e. large aggregate or long polymer chain) contributes a slow signal decay at higher gradient strengths, which results in a change in the slope that indicates bimodal molecular distribution of polymers.

As a function of the Pluronic® F127 content, NMR diffusometry demonstrates a gradual decrease in self-diffusion coefficient (D), which arose from the growing diameters of the micelles

with increasing polymer concentration.[37-38] Sizes of these species (micelles and unimers) versus F127 concentration at 25 ℃ were calculated via the Stokes-Einstein equation (**Figure 5.4b)**. [39]

$$D = \frac{kT}{6\pi\eta r_H} \tag{5.3}$$

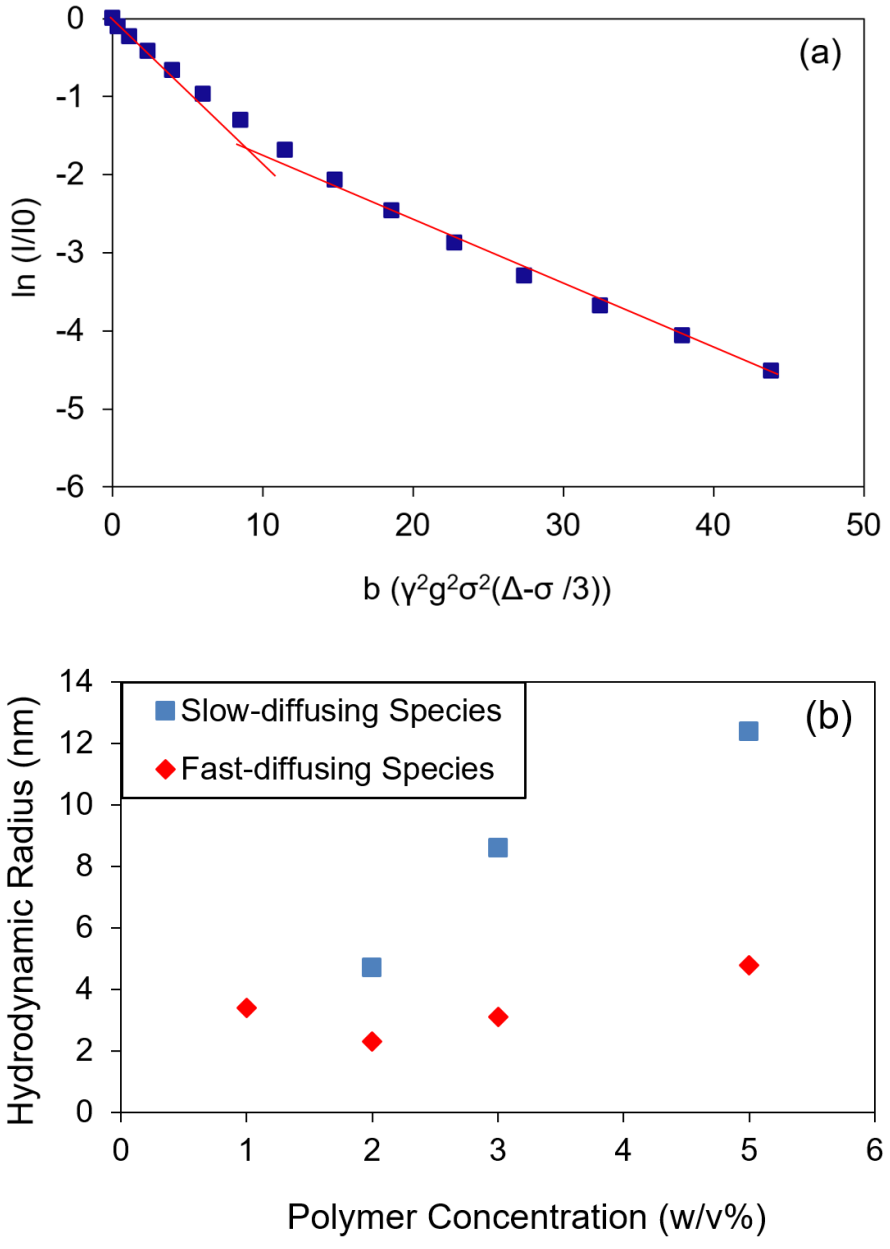

Figure 5.4. (a) Fitting in Stejskal−Tanner signal decay curve in 3% w/v F127 BCM, (b) Hydrodynamic radii of fast-diffusing and slow-diffusing species.

^{1}H NMR spectra with and without drug-loaded BCMs are provided in **Figure 5.5**. Peaks of polymer and solvent are enlarged for a better observation of drug peaks.

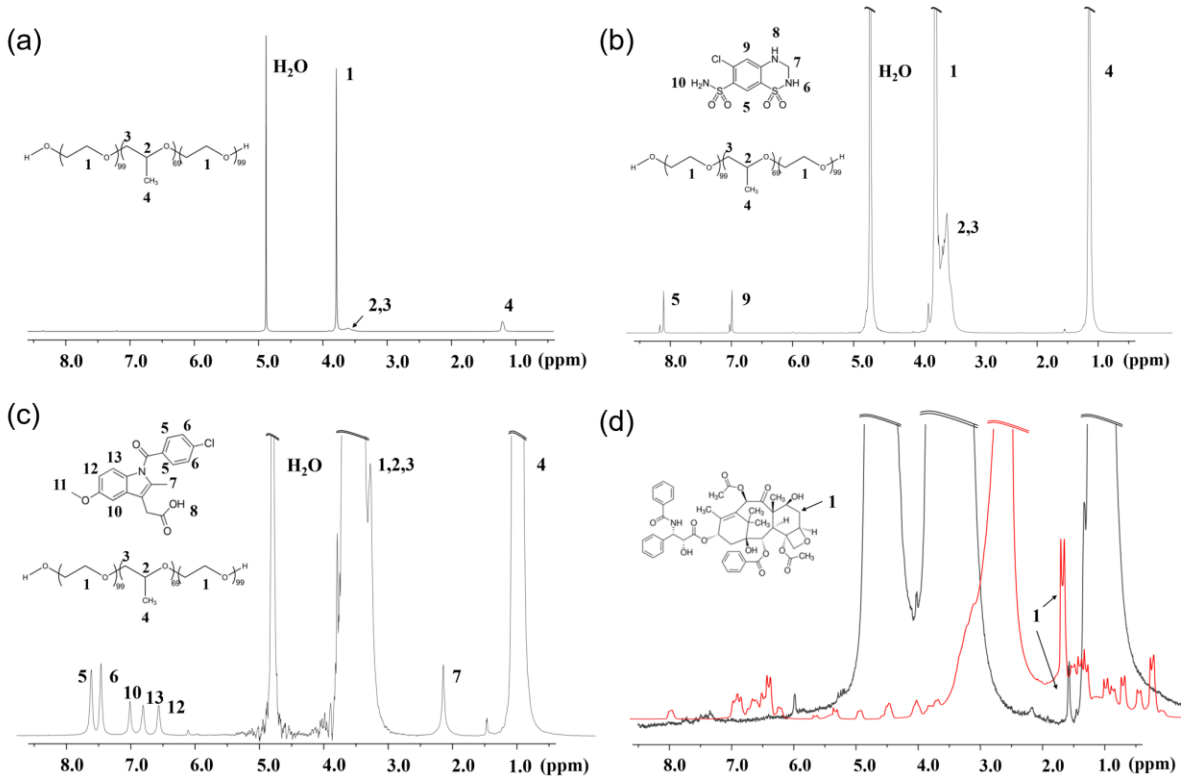

Figure 5.5. ^{1}H NMR spectra of BCMs without and with drug loaded. (a) 1% w/v F127 BCM. (b) 0.3% w/v HCT solubilized in 2% w/v F127 BCMs. Peak 7 overlaps with H_2O peak and we barely observe peak 6, 8, 10 due to deuterium exchange. (c) 0.3% w/v IND solubilized in 3% w/v F127 BCMs. Peak 9, 11 overlap with PEO peak and we barely observe peak 8 due to deuterium exchange. In b and c, we magnify signal intensities of peak 1,4 and water (off scale) to observe drug peaks. (d) 0.2% w/v PTX dissolved in DMSO-$_{d6}$ (red) and 0.06% w/v PTX solubilized in 5% w/v F127 BCMs (black). We have magnified signal intensities of polymer and solvents (off scale) in both spectra to observe drug peaks.

Notably, PTX is one of the most efficient and widely applied anticancer drugs with extremely low water solubility (~ 5 mg/L).[40-41] The aqueous solubility of PTX in BCMs (0.06%

w/v or 600 mg/L) increased more than two orders of magnitude over the intrinsic solubility of PTX, which strongly indicates that using polymeric micelles for solubilization is a promising approach to increase the hydrophobic drug solubility.

After the drug loading procedure, model drugs were dispersed in aqueous solutions as well as encapsulated in micelles, which can be modeled as a two-phase system: free drug and drug bound within micelles.[42] The time scale of exchange (τ_{ex}) is determined by the free cargo diffusion and binding with the bound sites. If solubilized drug molecules are in a "slow exchange" regime within the observable NMR time scale, which is the diffusion time (Δ) in a diffusometry experiment, i.e. $\tau_{ex} >> \Delta$, we are able to differentiate and quantify the drug concentrations in two phases from the Stejskal-Tanner signal attenuation plots: one for the free-diffusing drug molecules in aqueous solution and the other for those in the micellar cores. In fact, both HCT and IND exhibited only one diffusion coefficient when we vary the diffusion time, which means both drugs are exchanging rapidly between the aqueous and micellar phases, i.e. $\tau_{ex} << \Delta$ (in **Figure 5.6**).

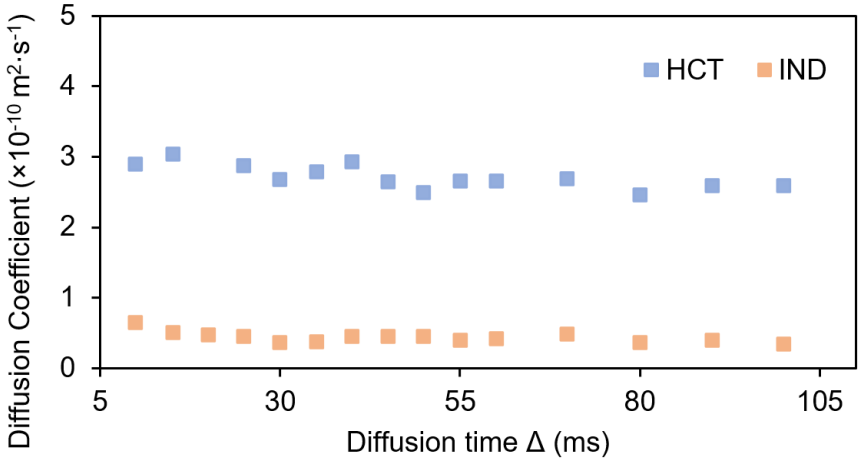

Figure 5.6. Diffusion coefficients of 1% wt/vol of HCT and 0.3% wt/vol IND solubilized in 3% wt/vol F127 micellar solution versus diffusion time. HCT and IND diffuse at an average rate of 2.7×10^{-10} $m^2\cdot s^{-1}$ and 1.1×10^{-10} $m^2\cdot s^{-1}$, respectively, when diffusion time (Δ) varies from 10 ms to 100 ms.

The lifetime of model drug residing in the hydrophobic region is shorter than the smallest observation time, which is 10 ms in our measurement. Therefore, we apply a single-component diffusion coefficient of drug molecules ($D_{drug,\,avg}$), which is a weighted average of contributions from drug solubilized in the micellar phase and drug dissolved in the aqueous phase in this "fast exchange" regime, with[43-45]

$$D_{drug,\,avg} = p_{drug,\,micelle} \cdot D_{drug,\,micelle} + p_{drug,\,aqueous} \cdot D_{drug,\,aqueous} \tag{5.4}$$

where $D_{drug,\,micelle}$ represents the diffusion coefficient of drug encapsulated by polymers in the micellar phase and $D_{drug,\,aqueous}$ represents that in the aqueous phase; $p_{drug,\,micelle}$ is the mole fraction of drug molecules trapped in micelles and $p_{drug,\,aqueous}$ is the mole fraction of drug molecules diffusing freely in solution. The total of $p_{drug,\,micelle}$ and $p_{drug,\,aqueous}$ equals to 1. The relative experimental error for NMR diffusion measurements was $\pm 3\%$.

In order to quantify populations of a model drug in those two phases, we made the assumptions that $D_{drug,\,micelle}$ is approximately the same as the diffusion coefficient of polymer in the micellar solution (D_{poly}), and $D_{drug,\,aqueous}$ is approximately the same as that of the drug dissolved in solvent without the presence of micelles ($D_{drug,\,soln}$). To authenticate this estimation, we validated two hypotheses. Firstly, the addition of model drugs would not affect the bulk viscosity dramatically. If so, an internal standard was added to calibrate viscosity and did not influence cargo encapsulation and release. Overall, our results were not distorted for small additions (< 1% wt/vol) of drugs. At 25 ℃, the diffusion coefficient of pure water is 1.9×10^{-9} $m^2\cdot s^{-1}$ and its viscosity is 1.0×10^{-3} Pa·s,[46] we assume the hydrodynamic radius of water remains unchanged because the thermal expansion coefficient of water barely varies with the temperature. Therefore, the viscosity of solution can be calculated from diffusion coefficients of water in micellar solution at variable polymer concentrations based on the Equation 5.3. Water diffusion coefficients were measured to

solve for the viscosities in solution. Therefore, the sizes of all diffusing species can be obtained in **Table 5.2**.

Table 5.2. Diffusion coefficients of residue water in pure F127 BCMs, HCT-loaded and IND-loaded BCMs.

	No drug loaded		HCT-loaded		IND-loaded	
F127 concentration (w/v %)	Diffusion coefficient (m^2 s^{-1})	Viscosity (Pa s)	Diffusion coefficient (m^2 s^{-1})	Viscosity (Pa s)	Diffusion coefficient (m^2 s^{-1})	Viscosity (Pa s)
5	1.90×10^{-9}	1.00×10^{-3}	1.70×10^{-9}	1.12×10^{-3}	1.80×10^{-9}	1.06×10^{-3}
3	2.08×10^{-9}	9.13×10^{-4}	1.88×10^{-9}	1.01×10^{-3}	1.81×10^{-9}	1.05×10^{-3}
2	2.08×10^{-9}	9.13×10^{-4}	2.08×10^{-9}	9.13×10^{-4}	1.81×10^{-9}	1.05×10^{-3}
1	2.07×10^{-9}	9.17×10^{-4}	2.02×10^{-9}	9.40×10^{-4}	N/A	N/A
0	2.00×10^{-9}	9.50×10^{-4}	2.12×10^{-9}	9.00×10^{-4}	2.01×10^{-9}	9.45×10^{-4}

Secondly, it should be reasonable to use the diffusion coefficient of the polymer (D_{poly}) to represent the diffusion coefficient of model drugs in the micellar phase ($D_{drug,\ micelle}$). This was supported by characterizing the diffusion of IND in F127 micelles. The pure IND in the aqueous solution (with no F127 present) diffused at a diffusion coefficient of 4.5×10^{-10} m^2 s^{-1}. However, IND molecules in the F127 solution diffused at a diffusion coefficient of 2.0×10^{-11} m^2 s^{-1}, which was close to that of the F127 BCMs with a diffusion coefficient of 1.8×10^{-11} m^2 s^{-1}. In **Figure 5.7**, the Stejskal-Tanner signal decay plots of IND and F127 indicate that drug encapsulated in micelles can diffuse at a similar rate with the polymer in solution.

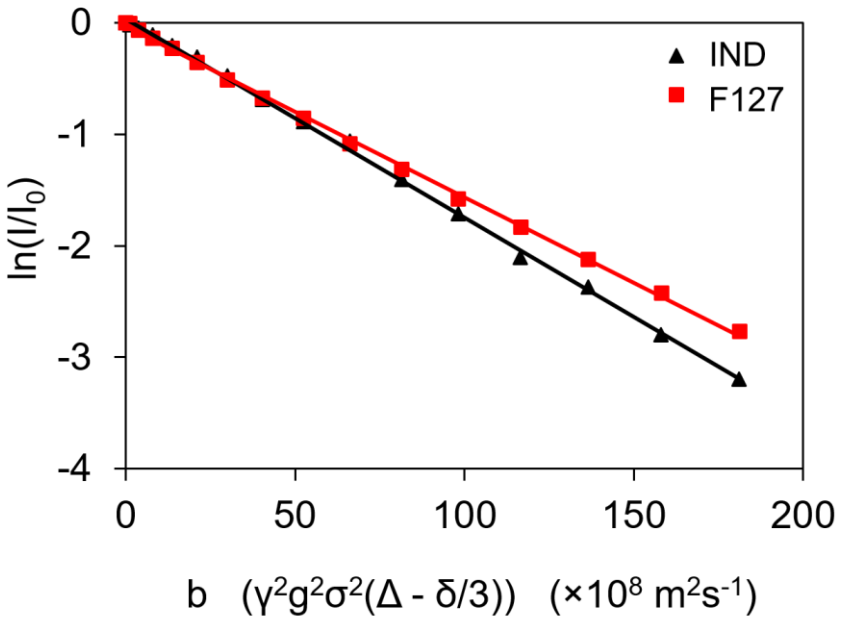

Figure 5.7. Stejskal-Tanner plots of NMR signal intensity for IND 0.3% wt/vol in 5% wt/vol F127 BCMs. Both IND and F127 (polymer) signals attenuate simultaneously with increased gradient strength. We fit with diffusion coefficients of 2.0×10^{-11} and 1.8×10^{-11} m^2 s^{-1} for the drug molecule and polymer, respectively.

This demonstrates that most of the drug molecules were successfully trapped in micelles thereby resulting in the diffusion coefficient of the drug that was comparable to the polymer chains. A small quantity of the drug molecules was dissolved in water, which contributes a slightly faster diffusion coefficient (~ 10%) of drug than that of polymers. Therefore, it is feasible to assume that fully-trapped drug molecules diffuse with micelle-forming polymers together at a same rate. In order to probe how drug hydrophobicity and polymer concentration affect partitioning and localization of drugs in micelles, we measured diffusion coefficients of HCT, IND and polymer (F127) in drug-loaded micellar solutions by NMR diffusometry and listed them in **Table 5.3**.

Table 5.3. Diffusion coefficients of drug (HCT / IND) and polymer (F127) in the drug-loaded BCMs at different polymer concentrations.

	HCT-loaded BCMs		IND-loaded BCMs	
F127 concentration /% w/v	$D_{poly}/m^2\ s^{-1}$	$D_{Drug}/\ m^2\ s^{-1}$	$D_{poly}/m^2\ s^{-1}$	$D_{Drug}/\ m^2\ s^{-1}$
5	3.01×10^{-11}	2.11×10^{-10}	1.79×10^{-11}	1.97×10^{-11}
3	3.28×10^{-11}	2.62×10^{-10}	1.54×10^{-11}	4.52×10^{-11}
2	4.20×10^{-11}	3.56×10^{-10}	2.38×10^{-11}	1.14×10^{-10}
1	5.27×10^{-11}	4.87×10^{-10}	3.58×10^{-11}	ǂ4.44×10^{-10}
0	N/A	7.26×10^{-10}	N/A	4.49×10^{-10}

Note: At 5, 3, 2, 1% w/v F127 concentrations, HCT additions are 0.2, 0.3, 0.3, 0.2% w/v and IND additions are 0.3% w/v. Added drug concentration of HCT is 1% w/v and IND is 0.05% w/v to make saturated solutions with no polymers. All diffusion measurements are taken at 25 ± 1 ℃ with an error within 3%. ǂ Precipitated sample.

Therefore, we are able to calculate the partition percentages of model drugs in F127 BCMs based on Equation 5.4 (in **Figure 5.8a**). For 1% w/v F127 IND-loaded BCM, drug partitioning percentage is low due to the poor solubilization of IND (precipitation). In **Figure 5.8b**, we have conceptually summarized conclusions of how micellar size as well as drug solubilization depends on polymer concentration based on NMR diffusometry.

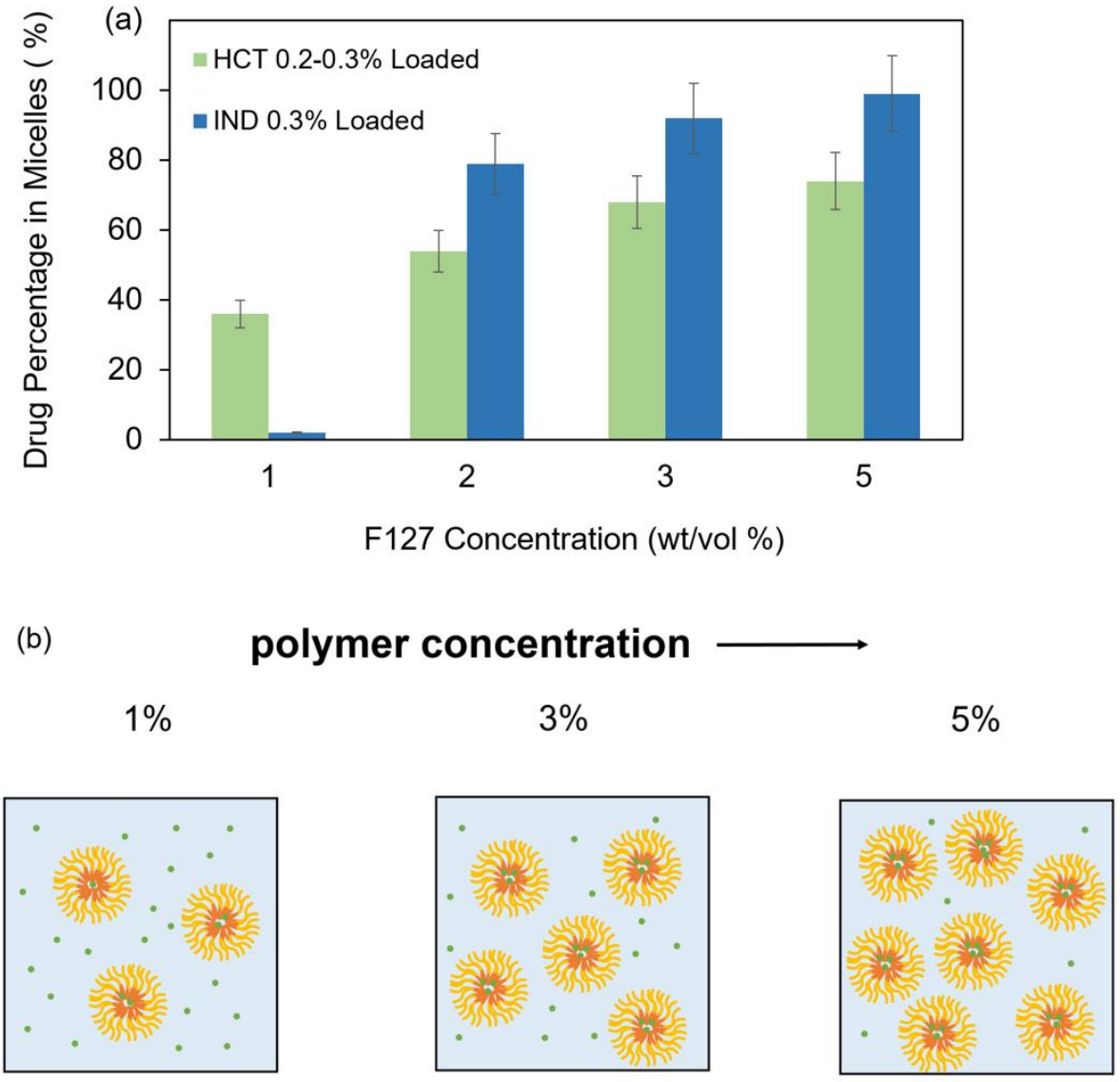

Figure 5.8. (a) Drug (HCT and IND) partition percentages in the F127 BCMs. Drug additions are mentioned in Table 1 in details. The increased amount of drugs solubilized is attributed to the increased number of total amphiphilic chains, which provides more reservoirs to trap hydrophobic drugs. (b) Schematic representation of micelle size evolution as well as distribution of HCT-loaded BCMs by varying the polymer concentration. The overall size of micelles expands as the drug are loaded in the micellar cores.

We also conducted SANS analysis to provide an in-depth understanding of how the drug loading and hydrophobicity impact the core and overall micelle radii, aggregation number, and water swelling of Pluronic® F127 BCMs. SANS data were fit with the Perderson form factor for spherical block copolymer micelles.[35] SANS signal collection from F127 micelles at 3% w/v. We observed a drastic increase in the low *q* plateau, which was caused by major changes in the micelle structural parameters occurred at 25 °C with the addition of 0.2% w/v HCT. However, at elevated temperatures (50 and 70 °C), the addition of HCT showed little effect on the self-assembled structures. This is probably due to unsuccessful encapsulation of HCT in micelles because HCT has an increased solubility in water at higher temperatures. SANS fitted results indicated that the aggregation number increased with drug addition, while the swelling of the micelle core with water was reduced. Moreover, the core radius and overall micelle radius both increased due to incorporation of HCT into BCMs. As discussed earlier, the structural parameters of the micelles indeed did not display significant changes upon addition of HCT at 50 and 70°C.

SANS is a powerful tool that probes structural and dynamical changes in soft matter. Those results support our NMR studies that HCT has partitioned into the Pluronic® BCM cores and changes the overall properties of self-assembly. Further NMR studies will be done to understand more on how temperature (e.g. 37 ℃) impacts the micelle structure as well as the drug partitioning percentages in Pluronic® BCM series.

5.4 Conclusions

The NMR diffusometry offers a quick and quantitative method to investigate the micellar dynamics of F127 at varied concentrations and its solubilization of different model drugs, i.e. HCT and IND. The effects of concentration and drug compositions on the micelle and drug diffusive behaviors were studied by NMR. The increased polymer concentration leads to an increased

micellar size, as well as the enhanced drug loading capacity. HCT and IND are two hydrophobic drugs with different solubility and display different solubilization in F127 BCMs. For example, at 2% wt/vol of F127, only 54% of HCT is in a micellar phase, while that is 79% for IND. The latter one has a lower solubility, which contributes a higher compatibility between the drug and core-forming blocks. Consequently, it demonstrates preference to reside in the phase of micelles. By increasing the F127 concentration to 5% wt/vol, both HCT and IND had an enhanced solubilization to 79% and 99%, respectively.

Overall, this study provides insights into the molecular interactions of polymer-drug, polymer-solvent, polymer-polymer, and drug-solvent in a Pluronic® F127 triblock copolymer micelle system. By understanding internal structures and properties of micelles and drugs, such as the molecular size and solubility, it offers new opportunities to prepare micellar formulations and predictions of in vitro release profiles of potential candidate drugs.

References

1. Escobar-Chávez, J. J.; López-Cervantes, M.; Naik, A.; Kalia, Y.; Quintanar-Guerrero, D.; Ganem-Quintanar, A., Applications of thermo-reversible pluronic F-127 gels in pharmaceutical formulations. *J. Pharm. Pharm. Sci.* **2006,** *9* (3), 339-58.
2. Pitto-Barry, A.; Barry, N. P., Pluronic® block-copolymers in medicine: from chemical and biological versatility to rationalisation and clinical advances. *Polym. Chem.* **2014,** *5* (10), 3291-3297.
3. Wu, C.; Liu, T.; Chu, B.; Schneider, D. K.; Graziano, V., Characterization of the PEO−PPO−PEO Triblock Copolymer and Its Application as a Separation Medium in Capillary Electrophoresis. *Macromolecules* **1997,** *30* (16), 4574-4583.
4. Hvidt, S.; Joergensen, E. B.; Brown, W.; Schillen, K., Micellization and gelation of aqueous solutions of a triblock copolymer studied by rheological techniques and scanning calorimetry. *J. Phys. Chem.* **1994,** *98* (47), 12320-12328.
5. Nivaggioli, T.; Alexandridis, P.; Hatton, T. A.; Yekta, A.; Winnik, M. A., Fluorescence Probe Studies of Pluronic Copolymer Solutions as a Function of Temperature. *Langmuir* **1995,** *11* (3), 730-737.

6. Ma, J.; Guo, C.; Tang, Y.; Xiang, J.; Chen, S.; Wang, J.; Liu, H., Micellization in aqueous solution of an ethylene oxide–propylene oxide triblock copolymer, investigated with 1H NMR spectroscopy, pulsed-field gradient NMR, and NMR relaxation. *J. Colloid. Inter. Sci.* **2007,** *312* (2), 390-396.
7. Walderhaug, H.; Söderman, O.; Topgaard, D., Self-diffusion in polymer systems studied by magnetic field-gradient spin-echo NMR methods. *Prog. Nucl. Magn. Reson. Spectrosc.* **2010,** *56* (4), 406-425.
8. Allen, T. M.; Cullis, P. R., Drug Delivery Systems: Entering the Mainstream. *Science* **2004,** *303* (5665), 1818.
9. Allen, T. M., Ligand-targeted therapeutics in anticancer therapy. *Nat. Rev. Cancer* **2002,** *2* (10), 750-763.
10. Sharma, P. K.; Bhatia, S. R., Effect of anti-inflammatories on Pluronic® F127: micellar assembly, gelation and partitioning. *Int. J. Pharm.* **2004,** *278* (2), 361-377.
11. Choucair, A.; Eisenberg, A., Interfacial Solubilization of Model Amphiphilic Molecules in Block Copolymer Micelles. *J. Am. Chem. Soc* **2003,** *125* (39), 11993-12000.
12. Letchford, K.; Liggins, R.; Burt, H., Solubilization of hydrophobic drugs by methoxy poly(ethylene glycol)-block-polycaprolactone diblock copolymer micelles: Theoretical and experimental data and correlations. *J. Pharm. Sci.* **2008,** *97* (3), 1179-1190.
13. Zhao, M.; Eghtesadi, S. A.; Dawadi, M. B.; Wang, C.; Huang, S.; Seymore, A. E.; Vogt, B. D.; Modarelli, D. A.; Liu, T.; Zacharia, N. S., Partitioning of Small Molecules in Hydrogen-Bonding Complex Coacervates of Poly(acrylic acid) and Poly(ethylene glycol) or Pluronic Block Copolymer. *Macromolecules* **2017,** *50* (10), 3818-3830.
14. Sabaté, R.; Gallardo, M.; de la Maza, A.; Estelrich, J., A Spectroscopy Study of the Interaction of Pinacyanol with n-dodecyltrimethylammonium Bromide Micelles. *Langmuir* **2001,** *17* (21), 6433-6437.
15. Barbato, F.; La Rotonda, M. I.; Quaglia, F., Interactions of Nonsteroidal Antiinflammatory Drugs with Phospholipids: Comparison between Octanol/Buffer Partition Coefficients and Chromatographic Indexes on Immobilized Artificial Membranes. *J. Pharm. Sci.* **1997,** *86* (2), 225-229.
16. Lasonder, E.; Weringa, W. D., An NMR and DSC study of the interaction of phospholipid vesicles with some anti-inflammatory agents. *J. Colloid. Inter. Sci.* **1990,** *139* (2), 469-478.
17. Teng, Y.; Morrison, M. E.; Munk, P.; Webber, S. E.; Procházka, K., Release Kinetics Studies of Aromatic Molecules into Water from Block Polymer Micelles. *Macromolecules* **1998,** *31* (11), 3578-3587.
18. Maity, B.; Chatterjee, A.; Ahmed, S. A.; Seth, D., Interaction of the Nonsteroidal Anti-inflammatory Drug Indomethacin with Micelles and Its Release. *J. Phys. Chem. B.* **2015,** *119* (9), 3776-3785.

19. Kabanov, A. V.; Batrakova, E. V.; Alakhov, V. Y., Pluronic® block copolymers as novel polymer therapeutics for drug and gene delivery. *J. Controlled. Release.* **2002,** *82* (2), 189-212.
20. Kabanov, A. V.; Lemieux, P.; Vinogradov, S.; Alakhov, V., Pluronic® block copolymers: novel functional molecules for gene therapy. *Adv. Drug Deliv. Rev* **2002,** *54* (2), 223-233.
21. Vogt, L.; Waanders, F.; Boomsma, F.; de Zeeuw, D.; Navis, G., Effects of dietary sodium and hydrochlorothiazide on the antiproteinuric efficacy of losartan. *J Am Soc Nephrol* **2008,** *19* (5), 999-1007.
22. Bhargava, K. P.; Gupta, M. B.; Tangri, K. K., Mechanism of ulcerogenic activity of indomethacin and oxyphenbutazone. *Eur. J. Pharmacol* **1973,** *22* (2), 191-195.
23. Singla, A. K.; Garg, A.; Aggarwal, D., Paclitaxel and it formulations. *Int. J. Pharm.* **2002,** *235*, 179-192.
24. Jones, M.-C.; Leroux, J.-C., Polymeric micelles – a new generation of colloidal drug carriers. *Eur. J. Pharm. Biopharm.* **1999,** *48* (2), 101-111.
25. Chacko, R. T.; Ventura, J.; Zhuang, J.; Thayumanavan, S., Polymer nanogels: A versatile nanoscopic drug delivery platform. *Adv. Drug Deliv. Rev* **2012,** *64* (9), 836-851.
26. Kadam, Y.; Yerramilli, U.; Bahadur, A.; Bahadur, P., Micelles from PEO–PPO–PEO block copolymers as nanocontainers for solubilization of a poorly water soluble drug. *Colloids. Surf. B. Biointerfaces.* **2011,** *83* (1), 49-57.
27. Shim, W. S.; Kim, S. W.; Choi, E.-K.; Park, H.-J.; Kim, J.-S.; Lee, D. S., Novel pH Sensitive Block Copolymer Micelles for Solvent Free Drug Loading. *Macromol. Biosci.* **2006,** *6* (2), 179-186.
28. Serajuddin, A. T. M., Solid dispersion of poorly water-soluble drugs: Early promises, subsequent problems, and recent breakthroughs. *J. Pharm. Sci.* **1999,** *88* (10), 1058-1066.
29. Kidd, B. E.; Li, X.; Piemonte, R. C.; Cooksey, T. J.; Singh, A.; Robertson, M. L.; Madsen, L. A., Tuning Biocompatible Block Copolymer Micelles by Varying Solvent Composition: Dynamics and Populations of Micelles and Unimers. *Macromolecules* **2017,** *50* (11), 4335-4343.
30. Wang, X.; Kelkar, S. S.; Hudson, A. G.; Moore, R. B.; Reineke, T. M.; Madsen, L. A., Quantitation of Complexed versus Free Polymers in Interpolyelectrolyte Polyplex Formulations. *ACS Macro Lett* **2013,** *2* (11), 1038-1041.
31. Li, X.; Cooksey, T. J.; Kidd, B. E.; Robertson, M. L.; Madsen, L. A., Mapping Coexistence Phase Diagrams of Block Copolymer Micelles and Free Unimer Chains. *Macromolecules* **2018,** *51* (20), 8127-8135.
32. Wilmsmeyer, K. G.; Li, X.; Madsen, L. A., Anisotropic viscoelasticity and molecular diffusion in nematic wormlike micelles. *Liq. Cryst.* **2018,** *45* (6), 844-856.
33. Chen, M.; Dugger, J. W.; Li, X.; Wang, Y.; Kumar, R.; Meek, K. M.; Uhrig, D. W.; Browning, J. F.; Madsen, L. A.; Long, T. E.; Lokitz, B. S., Polymerized ionic liquids: Effects of

counter-anions on ion conduction and polymerization kinetics. *J. Polym. Sci. A* **2018,** *56* (13), 1346-1357.

34. Callaghan, P. T., *Translational Dynamics and Magnetic Resonance: Principles of Pulsed Gradient Spin Echo NMR*. Oxford University Press: New York, 2011.

35. Pedersen, J. S.; Gerstenberg, M. C., The structure of P85 Pluronic block copolymer micelles determined by small-angle neutron scattering. *Collid Surf A Physicochem Eng Asp* **2003,** *213* (2), 175-187.

36. Cooksey, T. J.; Singh, A.; Le, K. M.; Wang, S.; Kelley, E. G.; He, L.; Vajjala Kesava, S.; Gomez, E. D.; Kidd, B. E.; Madsen, L. A.; Robertson, M. L., Tuning Biocompatible Block Copolymer Micelles by Varying Solvent Composition: Core/Corona Structure and Solvent Uptake. *Macromolecules* **2017,** *50* (11), 4322-4334.

37. Edward, J. T., Molecular volumes and the Stokes-Einstein equation. *J. Chem. Educ.* **1970,** *47* (4), 261.

38. Hou, J.; Zhang, Z.; Madsen, L. A., Cation/anion associations in ionic liquids modulated by hydration and ionic medium. *J. Phys. Chem. B.* **2011,** *115* (16), 4576-82.

39. Edward, J. T., Molecular volumes and the Stokes-Einstein equation. *J. Chem. Educ.* **1970,** *47* (4), 261.

40. Louage, B.; Nuhn, L.; Risseeuw, M. D.; Vanparijs, N.; De Coen, R.; Karalic, I.; Van Calenbergh, S.; De Geest, B. G., Well-Defined Polymer-Paclitaxel Prodrugs by a Grafting-from-Drug Approach. *Angew Chem Int Ed Engl* **2016,** *55* (39), 11791-6.

41. Paciotti, G. F.; Zhao, J.; Cao, S.; Brodie, P. J.; Tamarkin, L.; Huhta, M.; Myer, L. D.; Friedman, J.; Kingston, D. G. I., Synthesis and Evaluation of Paclitaxel-Loaded Gold Nanoparticles for Tumor-Targeted Drug Delivery. *Bioconjugate Chemistry* **2016,** *27* (11), 2646-2657.

42. J, K., Influence of 2-phase diffusion on spin-echo attenuation regarding relaxation in measurements using pulsed filed gradients. *Ann Phys* **1971,** *27* (1077), 9.

43. Krudopp, H.; Sönnichsen, F. D.; Steffen-Heins, A., Partitioning of nitroxides in dispersed systems investigated by ultrafiltration, EPR and NMR spectroscopy. *J. Colloid. Inter. Sci.* **2015,** *452*, 15-23.

44. Momot, K. I.; Kuchel, P. W., Pulsed field gradient nuclear magnetic resonance as a tool for studying drug delivery systems. *Concept. Magn. Reson. A* **2003,** *19A* (2), 51-64.

45. Nguyen-Kim, V.; Prévost, S.; Seidel, K.; Maier, W.; Marguerre, A.-K.; Oetter, G.; Tadros, T.; Gradzielski, M., Solubilization of active ingredients of different polarity in Pluronic® micellar solutions – Correlations between solubilizate polarity and solubilization site. *J. Colloid. Inter. Sci.* **2016,** *477*, 94-102.

46. Tanaka, K., Measurements of self-diffusion coefficients of water in pure water and in aqueous electrolyte solutions. *Journal of the Chemical Society, Faraday Transactions 1: Physical Chemistry in Condensed Phases* **1975,** *71* (0), 1127-1131.

Chapter 6: Investigation of Block Copolymer Micelles with Tuned Core Mobility by Varying Glass Transition Temperatures

This chapter is in preparation and will be submitted for publication with the following co-authors: Xiuli Li, Ryan J. Carrazzone, John B. Matson, and Louis A. Madsen*

Abstract

In Chapters 3–5, we have studied the block copolymer micelle (BCM) behavior, including the overall stability as a function of temperature or solvent content, cargo partitioning and chain exchange kinetics using multi-modal NMR methods. Therefore, we have a better understanding of the structure and dynamics of BCM systems. We expect to expand our knowledge on polymers and their molecular as well as macroscopic behavior using the NMR technique. Here we propose to design and synthesize a series of amphiphilic block copolymers, which contains the hydrophilic block polyethylene oxide (PEO) and the hydrophobic block poly- (tert-butyl acrylate-ran-n-butyl acrylate). The mole ratios of n-butyl acrylate are designed from 0% up to 100%. Based on the difference on the chemical structure/steric hindrance between n-butyl acrylate (*n*BA) and tert-butyl acrylate (*t*BA), they have glass transition temperatures (T_g) of - 46 ℃ and 25 ℃, respectively. By well tuning the chemical moieties of those two blocks in the polymers, we realized a wide range of T_g of micelles in solutions and thus controlled chain mobility/dynamics. We then use NMR diffusometry to measure the existing unimer concentrations in micellar solution to probe the dynamics, with a combination of other techniques. From our results, decreased T_g in core-forming blocks (25 ℃ to -46 ℃) for BCMs at room temperature or increased temperature (5 ℃ to 55 ℃) for 25% *n*BA BCMs both present an appearance of free unimers and further increased populations of unimers in micelle solution, which are resulted from enhanced mobility in micellar cores. Our

findings can be useful for inspiring future applications of BCMs in drug delivery and in heterogeneous phase "nanoreactor" synthesis.

6.1 Introduction

As is well known, amphiphilic block copolymers can self-assemble into a wide range of structures with various morphologies, such as micelles, lamellae or vesicles[1] both in bulk and in solution.[2] Important characteristics such as hydrophilic / hydrophobic ratio of polymer chain content,[3] hydrophobicity[4] and glass transition temperature (T_g) of the core-forming polymer blocks[5] can influence formation of self-assembly.[6-9] Also, the solution properties can have a dramatic impact on the self-assembly process.[8, 10-11] In Chapter 4, we have probed unimer (i.e. single block polymer chain) exchange kinetics in block copolymer micelles. However, many of the currently developed polymeric micelles contain a hydrophobic core with a high glass transition temperature (T_g), e.g.,100 °C for polystyrene. Those high T_g components in micelles constrains the kinetic process between unimers and micelles, thereby forming non-dynamic, or "frozen" micelles. Among applications of block copolymer micelles, many of them deal with drug delivery, and stabilization or removal of impurities,[12] thus the micelles are expected to be "dynamic", i.e. micelles and unimers are in equilibrium in solution.

Glass transition temperatures are affected by the configuration of polymer chains and the forces of interaction between chain segments.[13] By changing the polymer local structures, such as varying in the specific volume,[14] molecular weight,[15] cross-linking[16] or copolymerization, we are able to fine-tune the T_g of polymers for various purposes. Previous work has shown the significance using "soft" hydrophobic blocks for dynamic micelles. For example, Pergushov et al.[17] have developed micelles with a hydrophobic block polyisobutylene (PIB) of a short / medium length and a hydrophilic block poly(methacrylic acid) (PMAA) with a long length. These polymers are

soluble in water and form spherical micelles that are responsive to stimuli, including pH and ionic strengths. Colombani et al.[18] also synthesized poly(*n*-butyl acrylate)-b-poly(acrylic acid)(P*n*BA-PAA) polymeric micelles, followed by selective acidolysis of poly(*tert*-butyl acrylate) block, and demonstrated responses to stimuli as well as the structural changes of micelles (e.g. "apparent" critical micelle concentration).

Here we propose copolymerization of two monomers which have similar hydrophobicity in order to retain the micelle morphology as spheres. Accordingly, we use monomers of *n*-butyl acrylate (*n*BA) and *tert*-butyl acrylate (*t*BA) that have drastically different T_g.[19-20] To evaluate our hypothesis of tuning core mobility in dynamic micelles, we prepared a series of amphiphilic block copolymers utilizing poly (ethylene glycol) (PEO) as the hydrophilic blocks and random copolymers of poly (*n*-butyl acrylate) and poly (*tert*-butyl acrylate) as the hydrophobic blocks (**Scheme 6.1**).

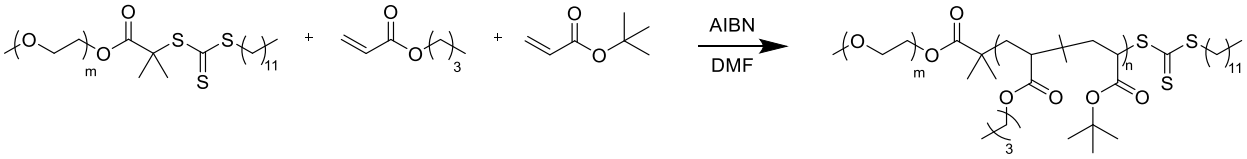

Scheme 6.1. Synthetic route of amphiphilic block copolymers containing poly (ethylene glycol) (PEO) as the hydrophilic blocks and random copolymers of poly (*n*-butyl acrylate) and poly (*tert*-butyl acrylate) as the hydrophobic blocks.

The series of poly(*t*BA -ran- *n*BA)-b-PEO polymers with varying T_g blocks was prepared in following two steps. Firstly, a PEGylated chain transfer agent was synthesized (Macro-CTA; PEG M_n = 4,000 g/mol). Next, *n*BA and *t*BA were polymerized in various ratios (0%, 10%, 25%, 40%, 50%, 60%, 75%, 90%, 100%, respectively) via reversible addition-fragmentation polymerization yielding polymers 1a-g. Amongst all the polymerizations the mole ratio of Macro-

CTA over total monomer was kept constant, while the molar ratio of *n*BA over *t*BA was changed systematically.

The polymer series was evaluated for chain mobility of the core-forming blocks. We employ differential scanning calorimetry (DSC) to determine the T_g of the hydrophobic blocks. As shown in **Figure 6.1**, the T_g for the hydrophobic blocks of the polymers exhibit a linear relationship with the molar ratio of *n*BA and *t*BA, which is in a range of - 46 to 25 ℃ with increasing *t*BA content. Interestingly, the 100% *t*BA -PEO block copolymer showed a substantially lower T_g than what is reported for pure *t*BA polymers,[13] which could be attributed to the relatively low molecular weight of the *t*BA block and the PEG tethered chain end.

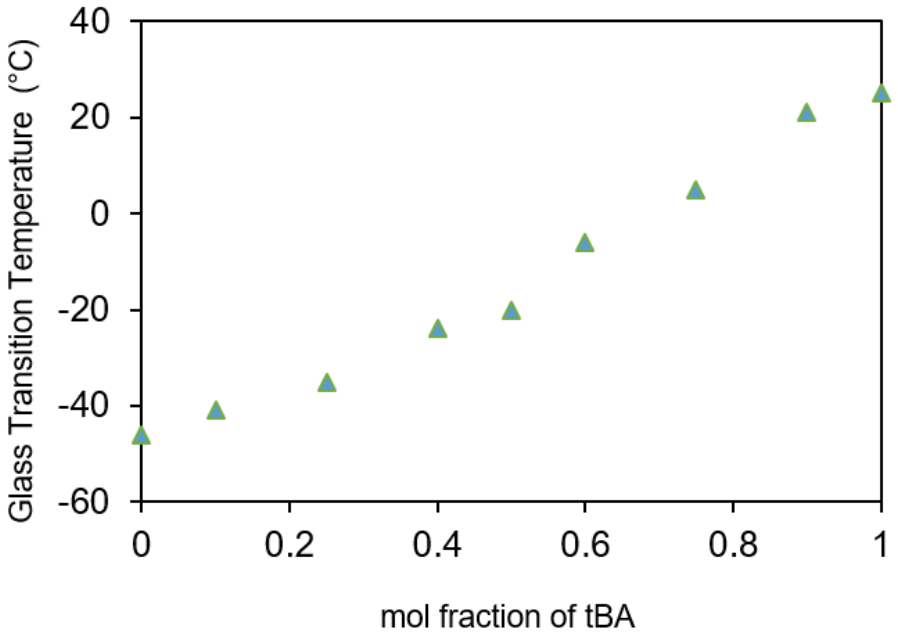

Figure 6.1. Glass transition temperatures (T_g) for the hydrophobic blocks of the polymers with the increase of molar ratio of *t*BA, which is in a range of - 46 to 25 ℃.

After establishing that T_g varies with the molar ratio of *n*BA vs. *t*BA for polymers named 1a-g, we measured initial contact angle of water droplets on films of polymers containing 100%,

50% and 0% *n*BA. Polymer films were created by spincoating polymer solutions (5 wt% in $CHCl_3$) at 5000 rpm onto cleaned glass slides, followed by drying at 30 ℃ overnight. Measurements were made in triplicate and the average results were taken as 95 ± 3 °, 100 ± 1 °, and 95 ± 2 ° for 100%, 50% and 0% *n*BA-containing polymers, respectively. Thus, the hydrophobicity of the core-forming blocks did not change, we sought to observe the change in free unimer chain equilibrium across the series using the NMR method. As described in previous chapters, NMR diffusometry have offered a wealth of information on the structure, dynamics, and molecular interaction in the micelle systems. Especially, NMR diffusometry is able to quantify the relative population (concentration) of same chemical species with different diffusive properties, such as free unimers and micelle aggregates in aqueous solution, which have deepened our understandings of the self-assembly behavior.

6.2 Experimental Section

6.2.1 Sample Preparation

The sections below on materials and synthesis was composed by our collaborator Ryan Carrazzone in Prof. John Matson's group, in the Macromolecule Innovation Institute at Virginia Tech.

Materials

All reagents were obtained from commercial vendors and used as received unless otherwise stated. 2,2′-Azobis(2-methylpropionitrile) (AIBN) was recrystallized from methanol prior to use. Monomers n-butyl acrylate (*n*BA) and tert-butyl acrylate (*t*BA) were purchased from Alfa Aesar and passed through a plug of basic alumina prior to use. Dry solvents were purified by passage through a solvent purification system (MBraun).

Synthesis of 2-methyl-2-(dodecylsulfanylthiocarbonyl)sulfanyl propanoic acid (CTA)

Dodecanethiol (5 mL, 20.9 mmol) was dissolved in acetone (30 mL) in a round bottom flask. To the flask was added tribasic potassium phosphate (8.86 g, 41.7 mmol). The reaction mixture was stirred at room temperature for 10 min. CS2 (3.78 mL, 62.6 mmol) was added dropwise, and the reaction mixture was stirred for an additional 1 h. To the flask was added a solution 2-bromo-2-methyl propanoic acid (3.91 g, 23.4 mmol) in 5 mL of acetone. The reaction mixture was stirred overnight at room temperature. The reaction mixture was diluted with DCM, transferred to a separatory funnel and washed consecutively with 1N HCl and brine. The organic layer was dried over Na_2SO_4 and concentrated via rotary evaporator. Silica gel was added to the solution and concentrated to dryness via a rotary evaporator. The silica was dry-loaded onto a column, eluting with DCM. The product containing fractions were combined and concentrated via rotary evaporator to yield a yellow solid. The crude product was recrystallized from hexanes to yield yellow crystals (4.88 g, 64% yield).

Synthesis of macroCTA

A round bottom flask was charged with CTA (0.91 g, 2.50 mmol), polyethylene glycol monomethyl ether (M_n = 4,000 g/mol, 5.0 g, 1.25 mmol), 4-dimethylamino pyridine (0.15 g, 1.25 mmol), and anhydrous CH2Cl2 (5.0 mL). N,N'-Dicyclohexylcarbodiimide (DCC) (0.52 g, 2.50 mmol) was dissolved in 5.0 mL of anhydrous CH_2Cl_2 in a vial. The DCC solution was added dropwise to the flask containing the other reagents, and the reaction mixture was stirred at rt overnight. The precipitated solids were removed by filtration. The desired product was isolated via precipitation from diethyl ether and was purified by repeated precipitations (2 – 4) from CH_2Cl_2 into diethyl ether to afford the product as a yellow solid.

*Synthesis of PEG-b-poly(n*BA-*stat- t*BA*) copolymers*

A typical polymerization procedure is as follows: To an oven-dried Schlenk tube equipped with a magnetic stir bar was added macroCTA (200 mg, 0.046 mmol), nBA (0.185 mL, 1.29 mmol), tBA (0.187 mL, 1.29 mmol), and 1.5 mL of anhydrous DMF. A solution of AIBN was prepared by dissolving 3.80 mg (0.023 mmol) in 1 mL of anhydrous DMF in a vial. 100 μL of this solution was added to the Schlenk tube. The tube was deoxygenated by subjecting the contents to three freeze−pump−thaw cycles. The Schlenk tube was then backfilled with N_2 and submerged in an oil bath maintained at 75 ℃. Samples were removed periodically by N_2-purged syringe to monitor molar mass evolution by SEC and conversion by ^{1}H NMR spectroscopy. The polymerization was quenched by submerging the tube into liquid N_2 and exposing the reaction mixture to air. The resulting PEG-b-poly(*n*BA-stat-*t*BA) was isolated via precipitation into a large excess of cold 1:1 hexane: ether. If necessary, further precipitations from CH2Cl2 into cold 1:1 hexane: ether were performed to remove residual monomer.

Micelle preparation

Block copolymer micelles were prepared via the solvent switch method. Each polymer was firstly dissolved in THF, followed by a dropwise addition of deionized H_2O. Next, the polymer solutions were transferred to dialysis tubing (MWCO 8 kDa) and dialyzed against DI H_2O for 18 h, changing the water after 2 h and 4 h. The resulting aqueous solution was diluted with distilled water to a final volume of 10.0 mL (5 mg/mL polymer concentration). Micelle solutions were analyzed by static and dynamic light scattering (SLS and DLS) to measure aggregate diameter, size distributions and aggregation numbers (N_{agg}) prior to NMR analysis.

6.2.2 Methods

Size exclusion chromatography (SEC) was carried out in THF at 1 mL/min at 30 ℃ on two Agilent PLgel 10 μm MIXED-B columns connected in series with a Wyatt Dawn Heleos 2

light scattering detector and a Wyatt Optilab Rex refractive index detector. No calibration standards were used, and dn/dc values were obtained by offline differential refractive index measurements. Dynamic light scattering (DLS) was conducted using a Malvern Zetasizer Nano operating at 25 ℃. A solution of micelles was prepared at 5 mg/mL and filtered with a 0.2 μm filter prior to scanning. The calculations of the particle size distributions and distribution averages were conducted using CONTIN particle size distribution analysis routines with number, volume, and intensity averages. Measurements were made in triplicate and errors reflect standard deviations. Static light scattering measurements were performed with a Wyatt Dawn Heleos 2 light scattering detector operating in batch mode. Micelle solutions were prepared at known concentrations and filtered with a 0.2 μm filter prior to scanning. Differential scanning calorimetry (DSC) studies were carried out on a Q-2000 DSC in aluminum pans operated with a dry nitrogen purge from -10 ℃ to 100 ℃ with a heating and cooling rate of 5 ℃/min modulated ± 3 ℃/min. Results are reported from the second heat cycle and figures are shown as exo down.

6.2.3 NMR Diffusometry

^{1}H PFG NMR diffusometry experiments were performed using a 400 MHz Bruker Avance III WB NMR spectrometer, equipped with a MIC probe and ^{1}H 5 mm coil coupled to a Diff60 single-axis (z-axis) gradient system. In an NMR diffusometry experiment, measured signal amplitude I as a function of gradient strength (g), was fit to the Stejskal-Tanner equation,[21-23]

$$I = I_0 \exp[-\gamma^2 \delta^2 g^2 (\Delta - \delta/3) D] \tag{6.1}$$

where I_0 is the signal amplitude at g = 0, γ is the gyromagnetic ratio, δ is the effective gradient pulse length, Δ is the diffusion time between gradient pulses, and D is the self-diffusion coefficient. The "b" factor, which represents all known NMR-specific parameters and is useful for qualifying diffusion behaviors and artifacts, is given by $b = -\gamma^2 g^2 \delta^2 (\Delta - \delta/3)$. The simple and robust pulsed-

gradient stimulated echo (PGSTE) sequence[21] was used with a 90 °RF pulse length of 4.5 μs. A half sinusoid gradient pulse length of δ = 3.14 ms (effective rectangular pulse length = 2.00 ms), a diffusion time of Δ = 25.00 ms and a post-gradient delay of 1.00 ms were used for ^{1}H diffusion measurements. Maximum gradient strengths were adjusted in the range 50 – 400 G cm^{-1} to achieve 90 – 99% signal attenuation in 32 steps. Sufficient signal-to-noise ratio (SNR) for each data point was achieved with 32 – 128 scans and acquisition times of 0.8 s for polymer signals with 1 Hz line broadening. Relaxation delay times of 0.8 s were used for both polymer and solvent signals.

6.3 Results and Discussion

^{1}H NMR spectra of Micelles

The linewidth of an NMR signal is related to the spin-spin relaxation time (T_2) of the nucleus of interest. Linewidths are influenced by T_2 and magnetic field inhomogeneity. They can be typically used to monitor changes in phase and aggregate semiquantitatively or quantitatively.[24] An example is the differential line-broadening,[25] where the interference between the dipolar and chemical shift anisotropy mechanisms result in the different linewidths in a multiplet. Difference in the linewidths reveals information on slow motions only as motions in the extreme narrowing regime contribute to the linewidths the same extent of all components of a multiplet.[26] Differential line-broadening has been applied to micellar as well as other soft matter systems.[25, 27-29]

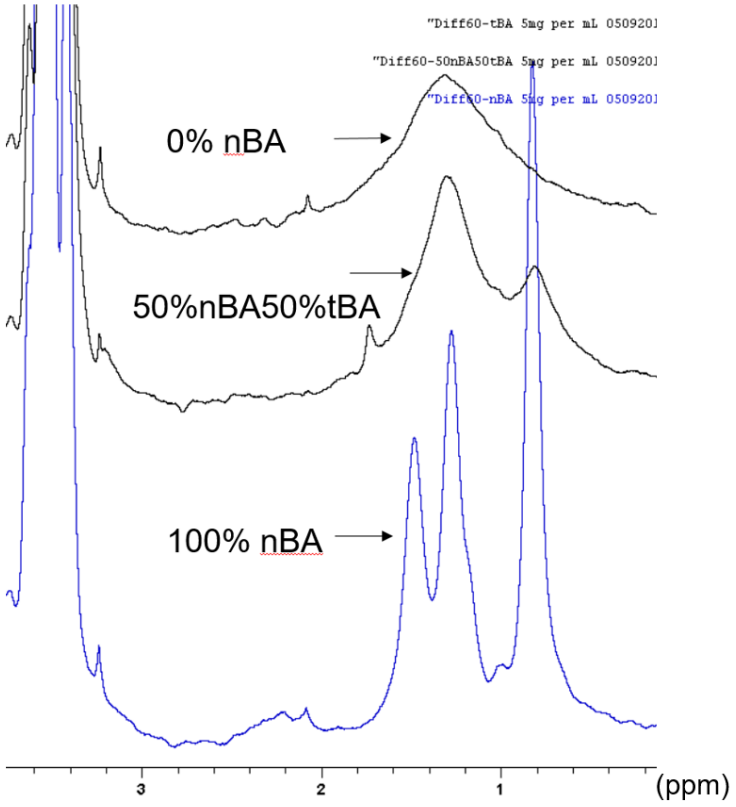

Figure 6.3. ^{1}H NMR spectra overlay of 0%, 50%, 100% *n*BA formed polymeric micelles solutions at 5 mg/mL, respectively.

As indicated in the **Figure 6.3**, *n*BA and *t*BA peaks appear at the range of 0.5 – 2 ppm. For 100% *t*BA -based micelles (i.e. 0% *n*BA), the peak is broadened up to ~ 240 Hz, while the peak width is only ~ 30 Hz for 100% *n*BA-based micelles. In NMR spectroscopy, the full width at half-maximum (FWHM) of peaks is determined by $1/\pi T_2$. The T_2 is the spin-spin relaxation time, which is related with the net magnetization in the transverse plane and indicates information on molecular mobility. Therefore, for the *t*BA polymer signals, a broader signal linewidth is due to a shorter T_2 value, indicating that *t*BA polymer chain environment is less mobile (or slower tumbling). This also agrees with the high T_g of the *t*BA block (25 °C), which to some extent inhibits the dynamic motion of polymer chains in micelles. In order to further investigate how a broad range of glass

transition temperatures influence the micelle dynamics in solutions and demonstrate a useful tool to probe micelle systems, we employ NMR diffusometry to quantify *t*BA/*n*BA-PEG formulated micelles.

Multicomponents Determination in Micelles via NMR Diffusometry

Here we use the NMR diffusometry (i.e. pulsed-field-gradient NMR) method to probe translational motion in polymeric micellar systems. If there are chemical species in distinct environments that do not exchange fast on the diffusion time scale (Δ = ~ 20 ms), we can observe multiple component diffusion coefficients in NMR diffusometry method. For example, some polymer chains reside in micelles and other polymer chains diffuse in solution, or molecules trap in highly cross-linked and others in coarsely cross-linked polymer systems (complexes, membranes or gels).[30-31] We access the diffusion coefficients as well as relative polymer chain (in forms of free unimers and micelles) populations from Stejskal−Tanner signal attenuation plots. By taking the natural log of normalized NMR signal intensity (I/I_0) and plotting vs. the b ($\gamma^2\delta^2g^2(\Delta-\delta/3)$) factor in the signal decay curve, it becomes straightforward as well as robust to determine the existence of multicomponents in the system. Similar to the PEO-PCL system we studied in Chapter 3, a single linear regression indicates a single component, and the slope corresponds to the diffusion coefficient (D) of the species of interests (associated with a distinct peak in spectrum). Any deviation from linear regression fitting (i.e., two straight lines) represents more than one diffusion coefficient of the species of interests. In the micellar system, the fast diffusing species (i.e. free unimers) contribute to a rapid signal decay at lower gradient strengths, and the slow diffusing species (i.e. micelles) contribute a slow signal decay at higher gradient strengths, which results in a change in the slope.

As shown in **Figure 6.4**, the 100% *n*BA and 100% *t*BA-formed block copolymer micelles display different dynamic behavior because of their differences in core glass transition temperatures (- 46 °C and 25 °C, respectively). For 100% *t*BA micelles, there is a single component fit where the slope corresponds to the diffusion coefficient (*D*) of polymer; while for 100% *n*BA micelles, there are two well-defined slopes (a deviation from linearity) that suggests more than one diffusion coefficient for a given polymer moiety, e.g. both free unimers and micelles coexist in solution.

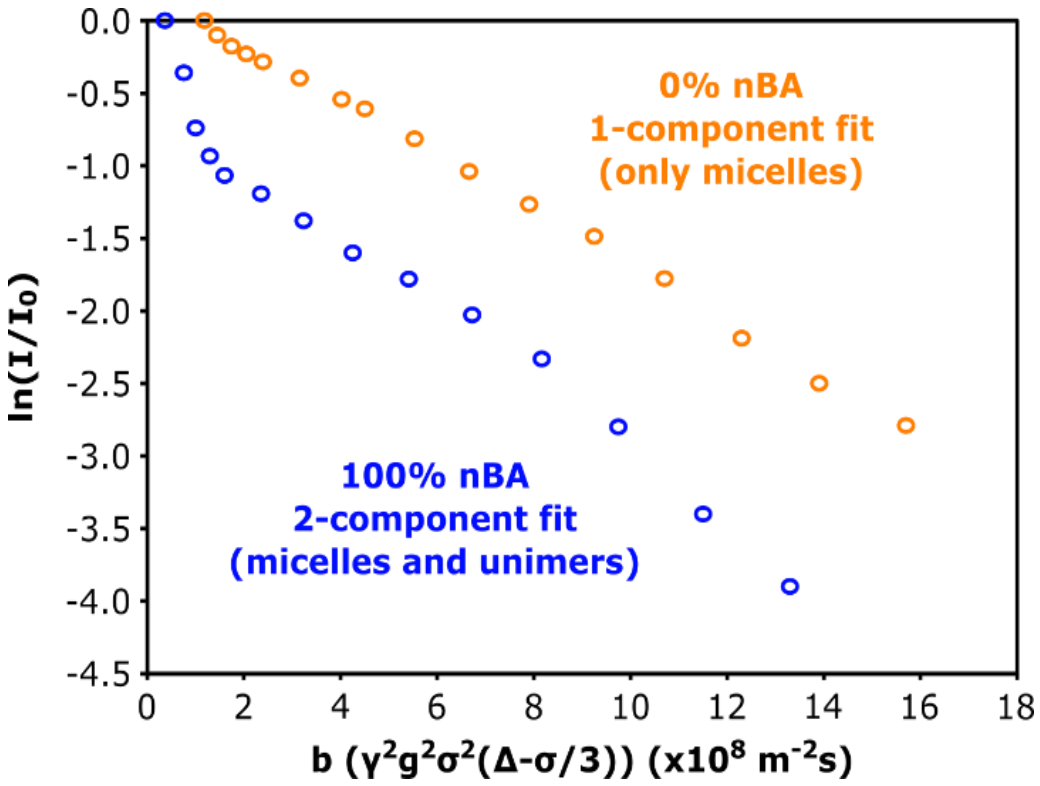

Figure 6.4. Stejskal−Tanner plots of micelles at varied *t*BA / *n*BA ratios. The 100% *t*BA micelles show a straight fitting curve, which implies only one component in solution – micelles. The 100% *n*BA micelles show a deviated fitting curve, which implies multiple components in solution. The slow-diffusing component (a steep line) represents micelles, and the fast-diffusing component (a shallow line) represents unimers in solution.

After scrutinizing a series of 1a-g polymers with designed *t*BA/*n*BA mole ratios, we further discuss unimer population gained by NMR diffusometry as a function of T_g. **Table 6.1** listed the basic properties in polymers 1a-g, including their chemical composition, molecular weight, polydispersity, hydrodynamic diameter, and aggregation number determined by GPC and DLS. Here we control the polydispersity ~ 1.10, therefore unimer distribution variance in solutions would be originated from the chemical structure differences (i.e. T_g).

Table 6.1. Glass transition temperature, molecular weight and polydispersity of polymers with varied *n*BA-*t*BA block ratios (determined by DSC/GPC); hydrodynamic diameter and aggregation number of *n*BA-*t*BA formulated micelles (determined by DLS). Data courtesy to Ryan Carrazzone and Prof. John Matson in the Department of Chemistry and Macromolecule Innovation Institute, Virginia Tech.

Polymer	Mol % nBA[a]	$M_{n\ GPC}$ (kg/mol)[b]	$M_{n\ NMR}$ (kg/mol)[c]	T_g (°C)[d]	$Đ$[b]	D_h (nm)[e]	N_{agg}[f]
		Polymer				Micelles	
1a	100	12.2	12.0	-46.0	1.07	25.1 ± 0.1	84
1b	75	12.6	11.3	-35.0	1.07	28.9 ± 0.1	110
1c	60	11.9	11.9	-24.0	1.12	27.9 ± 0.1	118
1d	50	13.3	12.1	-20.0	1.10	26.2 ± 0.2	86
1e	40	11.7	11.6	-6.0	1.11	27.1 ± 0.6	83
1f	25	12.9	12.6	5.0	1.08	27.0 ± 0.2	94
1g	0	11.8	11.6	25.0	1.05	24.5 ± 0.2	72

Note: [a] Calculated by *n*BA:*t*BA molar ratio via 1H NMR spectroscopy. [b] Absolute molecular weight measured by multi-angle light scattering. [c] Calculated by end-group analysis via ^{1}H NMR spectroscopy. [d] Glass transition temperature measured by DSC with a modulated heating rate (3 ℃/min, ± 2.5 ℃, 60 s); data reported from second heat cycle. [e] Hydrodynamic diameter measured by DLS at 5 mg/mL in DI H_2O. [f] Aggregation number derived from M_n of polymer and M_w of micelle at 5 mg/mL in DI H_2O; M_w of micelle determined by SLS.

In **Figure 6.5**, we observed the unimer % in micelle solutions gradually increased from 0% to ~ 55% as the *n*BA mole % increased from 0% to 100%. Specifically, in 0% *n*BA-formulated micelles, polymers are '*frozen*' at a relatively high T_g, thus we did not detect a measurable amount of unimer chains in solution. As we introduced more *n*BA (low T_g blocks) moieties in polymers, chains are more dynamic in mobility and prone to exchange unimers to reach an thermoequilibrium at the experimental timescale. Error bars in our NMR diffusometry measurement and sample preparation difference may rise in the range of 10 – 20%.

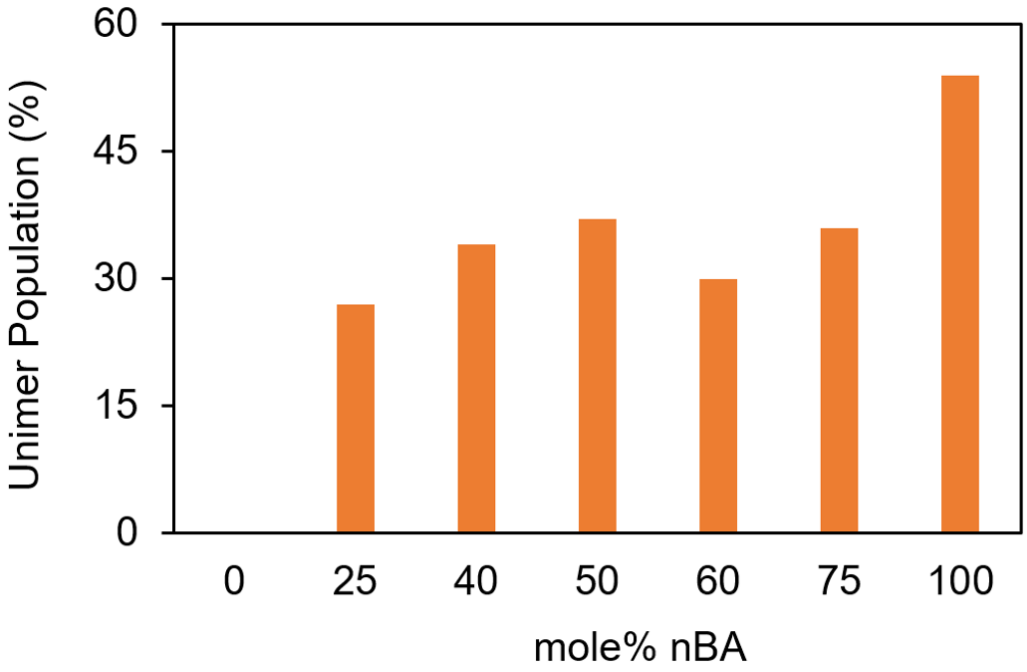

Figure 6.5. Unimer population percentages over mole% of *n*BA blocks in micelles. The unimer % increases from 0 to 55% as the mole% of *n*BA increase from 0 to 100%, indicating the mobility of polymer chains in block copolymer micelles are greatly influenced by the glass transition temperatures, i.e. chemical structures.

Besides the impacts of T_g on the unimer concentration at room temperature, we are also interested in how the temperature influences a single-composition micelle. Therefore, we further

varied the temperature from 5 ℃ to 25 ℃ and then 50 ℃ for 25% *n*BA-BCMs at 5 mg/mL. **Figure 6.6 (a)** displays the 1D ^{1}H NMR spectra overlay at different temperatures for the same composition of BCMs. The measured T_g for 25% *n*BA-75% *t*BA polymers is 5 ℃. At 5 ℃, we observed a broad butyl acrylate peak at 1.5 ppm with a linewidth of 300 Hz. As we increased the temperature to 25 ℃, the peak began to grow narrower to a linewidth of 120 Hz, and when the temperature raised to 50 ℃, the peak was the narrowest with a linewidth of only ~ 80 Hz. A shoulder peak of *t*BA at 50 ℃ was also found at 1.4 ppm. As we mentioned in earlier section, the linewidth is strong evidence of molecular dynamics. When the temperature is around the T_g of polymer, the micelle cores were immobilized and reflected slow dynamics in NMR spectrum (i.e. broadened linewidth). When the temperature raised, the micelles indicated faster dynamics (or motion) as expected. Furthermore, we can also further support this information as we conducted the NMR diffusometry measurements at those temperatures. **Figure 6.6 (b)** demonstrated the signal decay curves at those temperatures, and apparently, we start to observe the emergence of unimers in solution at higher temperatures. Further studies can be done to investigate more on how micelles behave at different temperatures or chemical structures.

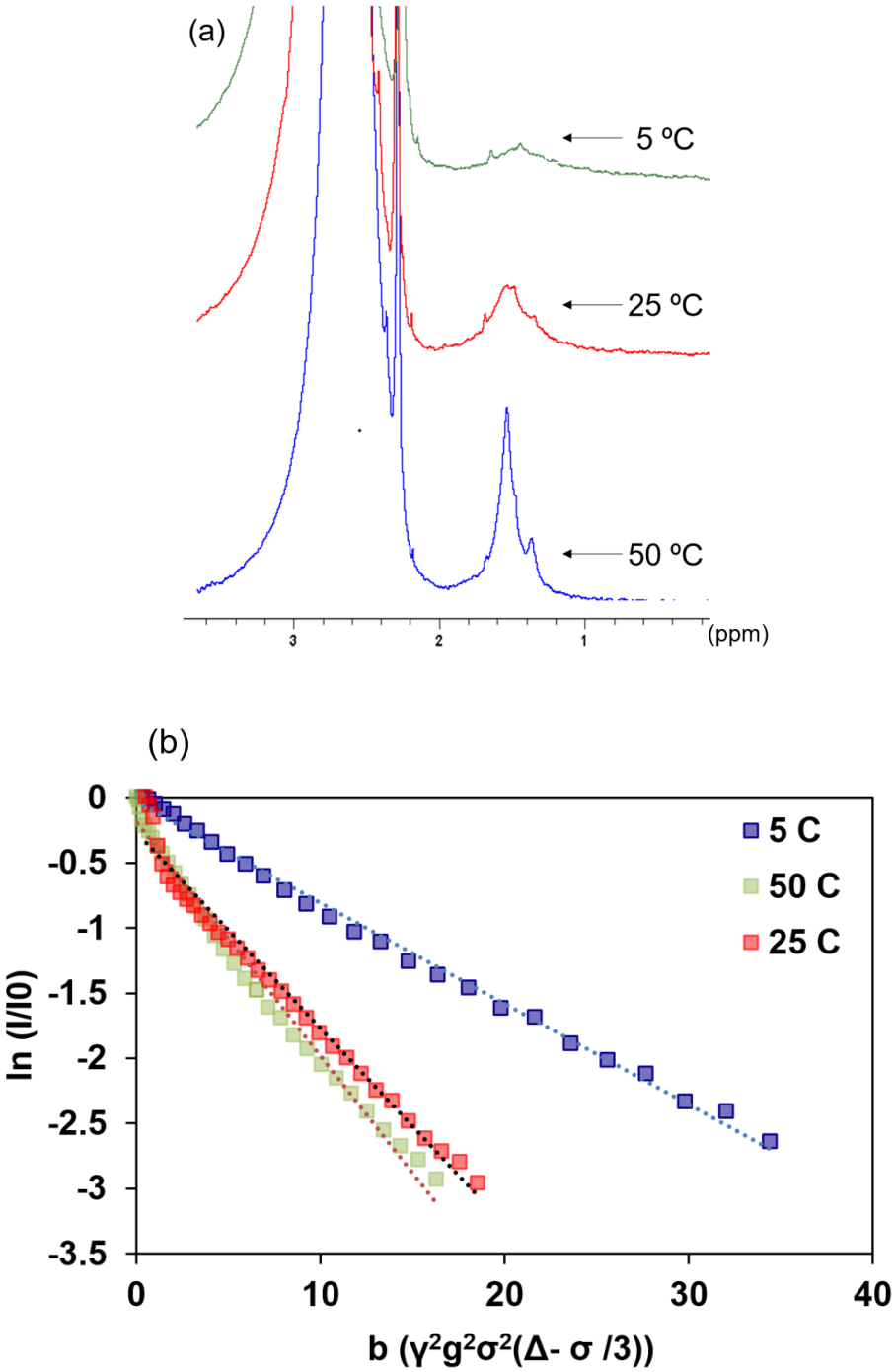

Figure 6.6. (a) ^{1}H NMR spectra overlay of 25% *n*BA formed polymeric micelles solutions at 5 ℃, 25 ℃ and 50 ℃ (5 mg/mL), respectively. (b) Stejskal−Tanner plots of 25% *n*BA formed micelles at different temperatures. At low temperature at T_g of 5 ℃, there is only one component (micelles)

in solution – micelles, while at higher temperatures of 25 ℃ and 50 ℃, we observe the existence of unimers in solutions.

6.4 Conclusions

Here we expand NMR spectroscopy and diffusometry methods to quantify how micelle dynamics is influenced by internal chemical structures / properties (i.e. T_g). As the mole fraction of n-butyl-acrylate (*n*BA) reduces in the PEO-conjugated polymers, their T_g decrease due to the increase in free volume between chains. We continue to utilize the NMR method to obtain the information of micelle structure and unimer content at equilibrium, providing more insights into micelle systems with designed structures/properties. From our results, decreased T_g or increased T can result in more mobility in micellar cores, thus presenting more free unimers in solutions. Our results show two regimes of unimer distribution in solution: one is a pure-micelle region (little unimer detected) when the temperature is near the T_g of the core-forming block, and the other is a coexistence region of micelles and free unimers in which the temperature is above the T_g of the core-forming block. This observation, that the core mobility shows a correlation with the free unimer content in solution, appears to be a new discovery in the area of polymeric micelles. This finding can potentially inform development and optimization of new block copolymer micelles for potential drug delivery and release, chemical separation and multifunctional delivery carriers with designed purposes.

References

1. Kamaly, N.; Yameen, B.; Wu, J.; Farokhzad, O. C., Degradable Controlled-Release Polymers and Polymeric Nanoparticles: Mechanisms of Controlling Drug Release. *Chem. Rev.* **2016,** *116* (4), 2602-2663.
2. Darling, S. B., Directing the self-assembly of block copolymers. *Prog. Polym. Sci.* **2007,** *32* (10), 1152-1204.

3. Shen, H.; Eisenberg, A., Block Length Dependence of Morphological Phase Diagrams of the Ternary System of PS-b-PAA/Dioxane/H2O. *Macromolecules* **2000,** *33* (7), 2561-2572.
4. Lee, J.; Cho, E. C.; Cho, K., Incorporation and release behavior of hydrophobic drug in functionalized poly(d,l-lactide)-block–poly(ethylene oxide) micelles. *J. Controlled. Release.* **2004,** *94* (2), 323-335.
5. Mok, M. M.; Lodge, T. P., Temperature-based fluorescence measurements of pyrene in block copolymer micelles: Probing micelle core glass transition breadths. *J. Polym. Sci. Poly. Phys* **2012,** *50* (7), 500-515.
6. Zhang, L.; Eisenberg, A., Multiple Morphologies and Characteristics of "Crew-Cut" Micelle-like Aggregates of Polystyrene-b-poly(acrylic acid) Diblock Copolymers in Aqueous Solutions. *J. Am. Chem. Soc.* **1996,** *118* (13), 3168-3181.
7. Mai, Y.; Eisenberg, A., Self-assembly of block copolymers. *Chem. Soc. Rev.* **2012,** *41* (18), 5969-5985.
8. Harada, A.; Kataoka, K., Supramolecular assemblies of block copolymers in aqueous media as nanocontainers relevant to biological applications. *Prog. Polym. Sci.* **2006,** *31* (11), 949-982.
9. Kataoka, K.; Harada, A.; Nagasaki, Y., Block copolymer micelles for drug delivery: design, characterization and biological significance. *Adv. Drug Deliv. Rev* **2001,** *47* (1), 113-131.
10. Owen, S. C.; Chan, D. P. Y.; Shoichet, M. S., Polymeric micelle stability. *Nano Today* **2012,** *7* (1), 53-65.
11. Bae, Y.; Fukushima, S.; Harada, A.; Kataoka, K., Design of Environment-Sensitive Supramolecular Assemblies for Intracellular Drug Delivery: Polymeric Micelles that are Responsive to Intracellular pH Change. *Angew. Chem. Int. Ed.* **2003,** *42* (38), 4640-4643.
12. Stuart, M. A. C.; Huck, W. T. S.; Genzer, J.; Müller, M.; Ober, C.; Stamm, M.; Sukhorukov, G. B.; Szleifer, I.; Tsukruk, V. V.; Urban, M.; Winnik, F.; Zauscher, S.; Luzinov, I.; Minko, S., Emerging applications of stimuli-responsive polymer materials. *Nature Materials* **2010,** *9*, 101.
13. Rogers, S.; Mandelkern, L., Glass Transitions of the Poly-(n-Alkyl Methacrylates). *J. Phys. Chem.* **1957,** *61* (7), 985-991.
14. Wood, L. A., Glass transition temperatures of copolymers. *J. Polym. Sci.* **1958,** *28* (117), 319-330.
15. Jr., T. G. F.; Flory, P. J., Second-Order Transition Temperatures and Related Properties of Polystyrene. I. Influence of Molecular Weight. *J. Appl. Phys* **1950,** *21* (6), 581-591.
16. Loshaek, S., Crosslinked polymers. II. Glass temperatures of copolymers of methyl methacrylate and glycol dimethacrylates. *J. Polym. Sci.* **1955,** *15* (80), 391-404.
17. Pergushov, D. V.; Remizova, E. V.; Feldthusen, J.; Zezin, A. B.; Müller, A. H. E.; Kabanov, V. A., Novel Water-Soluble Micellar Interpolyelectrolyte Complexes. *J. Phys. Chem. B.* **2003,** *107* (32), 8093-8096.

18. Colombani, O.; Ruppel, M.; Schubert, F.; Zettl, H.; Pergushov, D. V.; Müller, A. H. E., Synthesis of Poly(n-butyl acrylate)-block-poly(acrylic acid) Diblock Copolymers by ATRP and Their Micellization in Water. *Macromolecules* **2007,** *40* (12), 4338-4350.
19. Buback, M.; Junkers, T., Termination Kinetics of tert-Butyl Methacrylate and of n-Butyl Methacrylate Free-Radical Bulk Homopolymerizations. *Macromol. Chem. Phys.* **2006,** *207* (18), 1640-1650.
20. Tong, J. D.; Moineau, G.; Leclère, P.; Brédas; Lazzaroni, R.; Jérôme, R., Synthesis, Morphology, and Mechanical Properties of Poly(methyl methacrylate)-b-poly(n-butyl acrylate)-b-poly(methyl methacrylate) Triblocks. Ligated Anionic Polymerization vs Atom Transfer Radical Polymerization. *Macromolecules* **2000,** *33* (2), 470-479.
21. Callaghan, P. T., *Translational Dynamics and Magnetic Resonance: Principles of Pulsed Gradient Spin Echo NMR*. Oxford University Press: New York, 2011.
22. Stejskal, E.; Tanner, J., Spin diffusion measurements: spin echoes in the presence of a time-dependent field gradient. *J. Chem. Phys.* **1965,** *42* (1), 288-292.
23. Price, W. S., Pulsed-field gradient nuclear magnetic resonance as a tool for studying translational diffusion: Part 1. Basic theory. *Concepts. Magn. Reson.* **1997,** *9* (5), 299-336.
24. De Kruijff, B.; Cullis, P. R.; Radda, G. K., Differential scanning calorimetry and 31P NMR studies on sonicated and unsonicated phosphatidylcholine liposomes. *Biochimica et Biophysica Acta (BBA) - Biomembranes* **1975,** *406* (1), 6-20.
25. Kim, H. J.; Howell, S. C.; Van Horn, W. D.; Jeon, Y. H.; Sanders, C. R., Recent advances in the application of solution NMR spectroscopy to multi-span integral membrane proteins. *Prog. Nucl. Magn. Reson. Spectrosc.* **2009,** *55* (4), 335-360.
26. Chevelkov, V.; Faelber, K.; Schrey, A.; Rehbein, K.; Diehl, A.; Reif, B., Differential Line Broadening in MAS Solid-State NMR due to Dynamic Interference. *J. Am. Chem. Soc* **2007,** *129* (33), 10195-10200.
27. Dai, J.; Alaei, Z.; Plazzotta, B.; Pedersen, J. S.; Furó, I., Release of Solubilizate from Micelle upon Core Freezing. *J. Phys. Chem. B.* **2017,** *121* (45), 10353-10363.
28. Hartzell, C. J.; Stein, P. C.; Lynch, T. J.; Werbelow, L. G.; Earl, W. L., Differential line broadening in the NMR spectrum of methanol adsorbed on sol-gel silica. *J. Am. Chem. Soc* **1989,** *111* (14), 5114-5119.
29. Zoonens, M.; Catoire, L. J.; Giusti, F.; Popot, J.-L., NMR study of a membrane protein in detergent-free aqueous solution. *Proc. Natl. Acad. Sci.* **2005,** *102* (25), 8893-8898.
30. Gao, P.; Fagerness, P. E., Diffusion in HPMC Gels. I. Determination of Drug and Water Diffusivity by Pulsed-Field-Gradient Spin-Echo NMR. *Pharm. Res.* **1995,** *12* (7), 955-964.
31. Thieu, L. M.; Zhu, L.; Korovich, A. G.; Hickner, M. A.; Madsen, L. A., Multiscale Tortuous Diffusion in Anion and Cation Exchange Membranes. *Macromolecules* **2019,** *52* (1), 24-35.

Chapter 7: Ionic Polymers: Polymerization Kinetics in Poly(ionic liquid)s and Determination of Molecular Weight for Polyelectrolytes in the Semidilute Unentangled Regime

Section 7.2 is adapted from the NMR section of the following reference: Chen, M. , Dugger, J. W., Li, X. , Wang, Y. , Kumar, R. , Meek, K. M., Uhrig, D. W., Browning, J. F., Madsen, L. A., Long, T. E. and Lokitz, B. S. *J. Polym. Sci. Part A: Polym. Chem*., 56: 1346-1357 © (**2018**), American Chemical Society.

Abstract

In previous chapters, we have introduced how NMR serves as a sophisticated and powerful tool to investigate block copolymer micelle systems. Furthermore, it can also be useful to investigate the transport and orientational order in various polymers, including ionic polymers in the applications of batteries, water purification and functionalized membranes. Our goal is to gain more perspectives of soft materials regarding their structural and dynamical properties on length scales ranging from molecular to micron-scale. By detailed NMR diffusometry measurements, in combination with other advanced techniques, we are able to gain a better picture of soft matter behaviors and thus to guide synthesis and processing efforts. In Chapter 8, we will introduce the influence of counter-anions on ion conduction as well as polymerization kinetics. Also, we used NMR diffusometry, rheology and small angle X-ray scattering to innovatively explore the general number-averaged molecular weight for ionic polymers via terminal modulus, relaxation time, diffusion rate, correlation length, and viscosity measurements.

7.1 Poly(ionic liquid)s (PILs)

7.1.1 Introduction

Poly(ionic liquid)s (PILs), are a class of polyelectrolytes that have sparked great interests in recent years. PILs have combined merits of ionic liquids with polymeric materials, leading to improved mechanical stability, processability, durability, multifunctionality and spatial controllability.[1] Nowadays, the rapid development in chemistry and materials science have fostered a generation of novel and versatile poly(ionic liquid)s that are of great importance in fundamental research and practical applications (e.g. energy, environment and catalysis).[2] Typical synthesis of PILs includes two pathways: one is conventional free radical polymerization and the other is controlled radical polymerization.[3-5] The conventional free radical polymerization is commonly applied to synthesize crosslinked polymer matrices and the controlled radical polymerization synthesizes more defined block copolymer structures to have precise control over morphology.

In this section, we present a synthesized and polymerized imidazolium-containing monomer, 1-[ω-methacryloyloxydecyl]-3-(n-butyl)-imidazolium (1BDIMA), using free radical and controlled free radical polymerization and followed by post-polymerization ion exchange with bromide (Br), tetrafluoroborate (BF_4), hexafluorophosphate (PF_6), or bis(trifluoromethylsulfonyl)imide (Tf_2N). An interesting phenomenon that was noticed is that the solvent has a large impact on the conversion rates in the reversible addition-fragmentation chain-transfer polymerization (RAFT) for 1BDIMA with different counter-ions. To solve these puzzles, we use NMR diffusometry to investigate the kinetic differences by scrutinizing the diffusion coefficients for each monomer, counter-ion and solvents (MeCN and DMF). Our results indicate

that the reaction rates are not diffusion limited, and point to a need for deeper understanding of the role electrostatics plays in the kinetics of free radical polymerizations.

7.1.2 Materials and Methods

The self-diffusion coefficients of monomer and solvent in solutions were determined using a 400 MHz Bruker Advance III WB NMR spectrometer equipped with a MIC probe, a Micro5 triple-axis gradient, and a 5 mm $^{1}H/^{19}F$ detection coil. As mentioned previously, the signal amplitude *I* was measured as a function of gradient strength (*g*) and was fit according to the Stejskal-Tanner equation,[6-9] gradient delay of 1 ms were used for diffusometry measurements. Maximum gradient strengths were in the range 45 – 240 G cm^{-1}. Sufficient signal-to-noise ratio (SNR) for each data point was achieved with 4 – 8 scans. Acquisition times and relaxation delay times were each 1 s, and 0.3 Hz line broadening was applied during data processing. Deuterated solvents (MeCN-d_3 and DMF-d_7) were used to reduce ^{1}H solvent signal interference. All NMR tubes were flame sealed to prevent solvent evaporation. The NMR measurements were performed at 21 and 62 °C, where the samples were equilibrated at each temperature for more than 5 min. Four capillary tubes (1.2 mm in diameter) were added into the 5 mm tube to suppress thermal convection at a higher temperature. The diffusion coefficients reported were the average of x and y axes instead of z axis to minimize experimental errors caused by convective flow. The imidazolium proton peaks at 8.0 ppm for both 1BDIMA-Br and 1BIDMA-Tf_2N were used to determine the monomer diffusion coefficient.

7.1.3 Results and Discussion

Figure 7.1a shows that the solvent has a large impact on the conversion rates in the RAFT for 1BDIMA with different counter-ions. For instance, 1BDIMA-Tf_2N did not polymerize in acetonitrile (MeCN) at 65 ℃, while 1BDIMA-Tf_2N proceeded a high conversion in

dimethylformamide (DMF) under the same conditions. Similarly, 1BDIMA-Br also demonstrated a significantly faster polymerization in DMF than in MeCN.

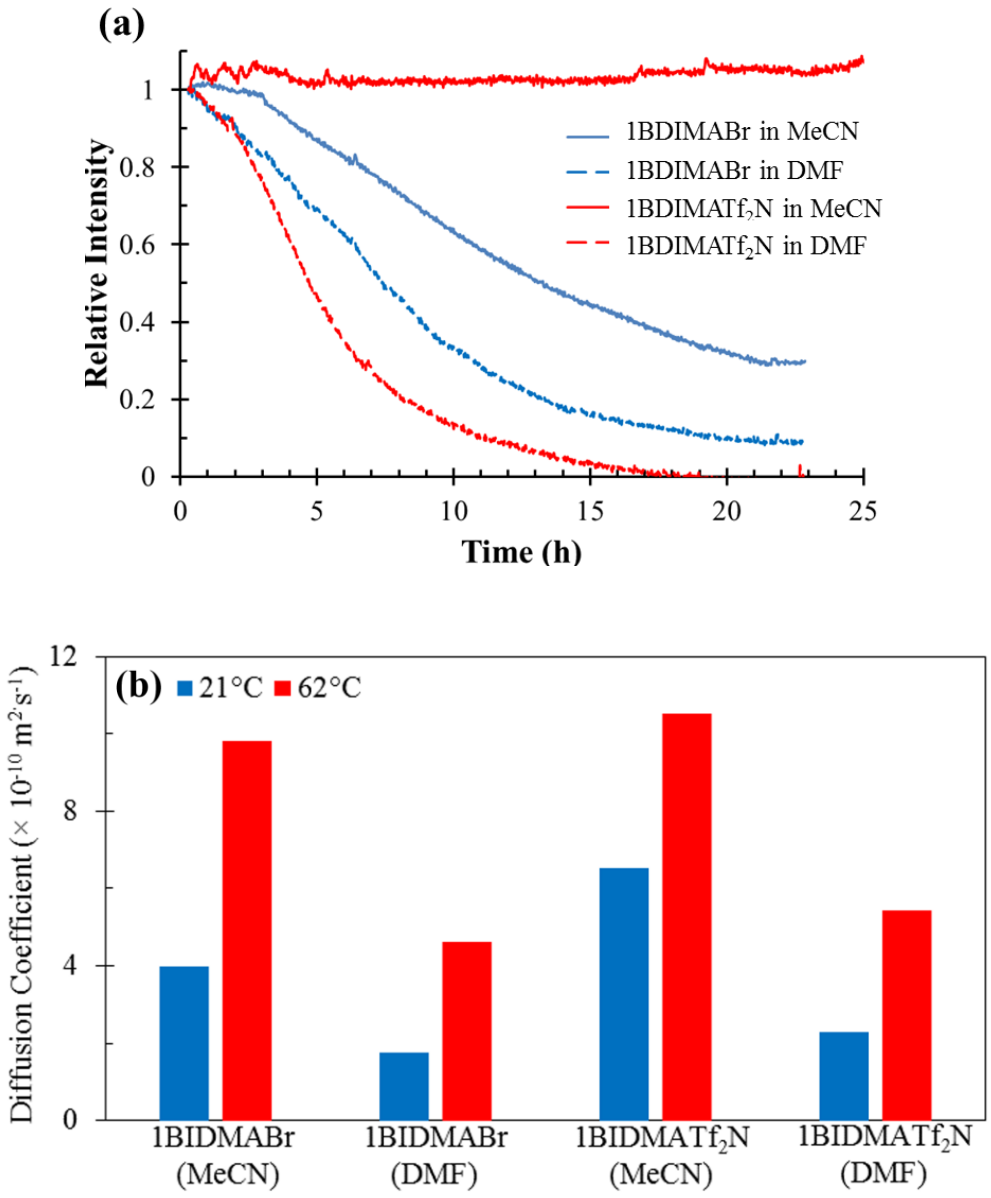

Figure 7.1. (a) RAFT polymerizations of 1BIDMA-Br and 1BIDMA-Tf_2N in solvents of DMF and MeCN. *In situ* FTIR: [M]=1 M, [CTA]/[I] = 3, T = 65 °C, 1289 – 1308 cm^{-1}. (b) Diffusion coefficients of IL monomers with different counter-anions and in different solvents. NMR diffusometry measurements were done at 21 ℃ and 62 ℃, respectively. Errors in D values are ± 5%.

Initially, it was suspected that the observed kinetic differences were related to Columbic interactions in the system impacting 1) the diffusion rate of monomers and/or 2) monomer aggregation hindering polymerization/propagation. ^{1}H NMR diffusometry was used to probe the solvent and counter-ion effects on the diffusive behavior of ionic-liquid monomers (**Figure 7.1b)** and to determine if monomer aggregation was occurring. To mimic the RAFT polymerization conditions, the monomer concentration and temperature were set to 1 M and 62 ℃. The monomer diffusion for both 1BDIMA-Br and 1BDIMA-Tf_2N in MeCN was more than twice as fast compared to DMF due to MeCN's lower viscosity (0.343 mPa s, 25 ℃ for MeCN, and 0.802 mPa s, 25 ℃ for DMF). Additionally, the monomers with Tf_2N counter-ions diffused faster than monomers with Br counter-ions in both solvents. The faster diffusion was attributed to the weak interactions between imidazolium and Tf_2N, resulting from the delocalization of negative charge on Tf_2N. Notably, the ionic monomers with Tf_2N in MeCN diffuse at the fastest rate; however, the *in situ* FTIR results showed no monomer conversion taking place, suggesting that the RAFT polymerization rate of ionic-liquid monomers is not simply diffusion-controlled. Eliminating differences in monomer diffusion as the underlying cause of the polymerization rate differences, we then investigated the monomer aggregation behavior in solution. The Stokes-Einstein equation was used to assess how counter-ion and solvent affected the relative sizes of the monomers. It is well known that the Stokes-Einstein equation shows nonideal behavior for charged species.[8, 10-13] However, the Stokes-Einstein equation was still employed to provide a qualitative comparison. A small difference in the effective R_h of the monomer as a function of counter-ion was observed, but no large self-assembled aggregates were detected under the measured conditions (**Table 7.1**). The calculated monomer sizes were all approximately 1 nm, which is roughly the hydrodynamic size of a typical monomer. This indicates a lack of monomer aggregation in the samples and excludes

aggregate formation as a major factor in the kinetic differences seen in the 1BDIMA monomer studies presented here. Future studies will include Raman spectroscopy and wide angle X-ray scattering (WAXS) to further substantiate the conclusions from NMR diffusometry. Additionally, *in situ* NMR diffusometry was used to elucidate size and diffusion coefficient changes in real time during polymerization.

Table 7.1. Diffusion coefficients of solvents and sizes of monomers in different solutions at 62 ℃.

	1BIDMABr (in MeCN)	**1BIDMABr (in DMF)**	**1BIDMATf$_2$N (in MeCN)**	**1BIDMATf$_2$N (in DMF)**
$D_{solvent}$ (m^2 s^{-1})	4.57×10^{-9}	1.94×10^{-9}	4.44×10^{-9}	1.87×10^{-9}
$2R_{h\ monomer}$ (nm)	1.15	1.18	1.05	0.97

7.1.4 Conclusions

In situ FTIR measurements showed faster polymerization rates in DMF compared to MeCN. NMR diffusometry ruled out monomer diffusion and/or aggregation as major contributors to the differences in polymerization kinetics. A possible explanation lies in Marcus theory, where the influence of solvent and counterions on the electron transfer process may be critical for polymerization, especially in a controlled process like RAFT. Future experiments are under development to better elucidate the differences in polymerization kinetics for these systems.

7.2 Polyelectrolytes

The molecular weight for ionic polymers is difficult to determine due to the strong electrostatic repulsions along the chains. Here we use NMR diffusometry, rheology as well as small angle X-ray scattering to explore the general molecular weight for ionic polymers via

terminal modulus, relaxation time, diffusion rate, correlation length, and viscosity measurements. Above the overlap concentration (c^*), polyelectrolytes are termed semidilute but unentangled. We use scaling models to derive different methods to calculate the number-average molecular weight (M_n), from the sodium or cesium sulfonated polystyrene (PSS) and cesium salt of poly (2-acrylamido-2-methyl-1-propanesulfonate, PAMS) polyelectrolytes (where M_n are known) in the semidilute unentangled concentration regime. We evaluate this method using NMR diffusometry to measure self-diffusion coefficient (D), rheology to measure shear rate dependence of viscosity (η_{sp}) and small-angle X-ray scattering to measure the correlation length (ξ). We then compare this method with other proposed models. Each method yields the number density of chains and we are able to access the number-averaged molecular weights that are insensitive to solvent quality as well as the presence of salts. In summary, this technique provides possible opportunities for molecular weight determination for general ionic polymers, and can be extended to neutral polymer systems.

7.2.1 Introduction

Polyelectrolytes are polymers with either positively or negatively charged ionizable groups. They can dissociate in polar solvents, leaving charges on polymer chains and releasing counter ions in solution.[14] The properties of polyelectrolytes in solutions depend on the polymer backbone, solvent quality, fraction of dissociated ionic groups, salt concentration and polymer–substrate interactions.[15-16] Polyelectrolytes include polystyrene sulfonate, polyacrylic and polymethacrylic acids and their salts, DNA and other polyacids and polybases.[17]

The balance between electrostatic repulsions along each chain in polyelectrolytes is complicated and has not been fully understood. The electrostatic interactions between ions in polyelectrolyte solutions result in different behaviors compared to those of uncharged polymers,[18]

including crossover from dilute to semidilute solution regime occurs at a lower polymer concentration;[19] the osmotic pressure of polyelectrolytes in salt-free solutions is higher than that of neutral polymers;[20] the viscosity of polyelectrolyte solutions is proportional to square root of polymer concentration and the chains of polyelectrolyte in semidilute regime follow unentangled dynamics over a wider concentration range.[14, 21]

Usually, we measure molar masses of polymers by a variety of dilute solution methods, including NMR end group analysis for M_n,[22] osmometry for M_n,[23] light scattering for M_w,[24] viscometry for M_η[25] and size exclusion chromatography[26] (SEC, a wide range of molecular weight).[27] A critical overlap concentration (c^*) is generally defined where the steric and frictional interactions of neighboring polymer coils are negligible.[28] When the polyelectrolyte concentration is below the overlap concentration ($c < c^*$), polymer solutions are termed as diluted. Dilute solutions of polyelectrolytes typically contain too little polymer to measure by SEC or light scattering, owing to the low c^* of high molecular weight polyelectrolytes. Conventional methods to determine molecular weight for charged polymers are inaccurate and are limited to the polymer type and molecular weight range. Thus, it is crucial for us to develop novel methods for molecular weight determination, especially those ionic polymers with high molecular weights.

When the polyelectrolyte concentration is above the overlap concentration ($c > c^*$), the solution is in the semidilute regime[14] (i.e. there are no much polymers present but chains overlap their pervaded volumes). In this regime, for polyelectrolytes with no added salt, the polyelectrolyte coils shrink rapidly as the solution is concentrated, and this renders concentrations that are semidilute but not entangled (when the chain entanglement occurs, the c is defined as entanglement concentration, c_e).[29] Dynamic properties of semidilute polymer solutions can be described by the

Rouse model.[30] Here we present work to exploit experiments on semidilute unentangled solutions ($c^* < c < c_e$) of ionic polymers to determine precisely their number-average molecular weight M_n.

Below we demonstrate step by step how we use currently existing models to deduce the proposed molecular weight determination method for ionic polymers. Polyelectrolyte chains in dilute solution (with no added salt) are highly extended. Semidilute solutions have a correlation length ξ that describes the average distance from one chain of monomer to the closest monomer on a different chain. Polyelectrolyte solutions with no added salt, the correlation length is:[31]

$$\xi \cong \left(\frac{\mathrm{B}}{cb}\right)^{1/2} \tag{7.1}$$

where b is the repeat unit (monomer) length, c is the number density (concentration) of monomers in solution and B is the dimensionless chain contraction factor.

Considering the effective electrostatic screening length and the electrostatic persistence length in semidilute polyelectrolyte solutions when salt is present. The corrected correlation length with added salt is:[14, 32]

$$\xi \cong \left(\frac{B}{bc}\right)^{1/2} (1+\frac{2c_s}{fc})^{1/4} \tag{7.2}$$

where c_s is the number density of monovalent salt ions (anions or cations) and f is the fraction of monomers bearing an effective charge.

The chain conformation leads to the root-mean-square chain end-to-end distance of:[14, 32]

$$\mathrm{R} \cong \left(\frac{b}{Bc}\right)^{1/4} N^{1/2} (1+\frac{2c_s}{fc})^{-1/8} \tag{7.3}$$

where N is the number of repeat units per chain.

The terminal relaxation time of polyelectrolyte chain is:[14, 32]

$$\tau \cong \frac{\eta_s b^3}{kT} B^{-3/2} N^2 (cb^3)^{-1/2} (1+\frac{2c_s}{fc})^{-3/4} \tag{7.4}$$

where η_s is solvent viscosity and T is temperature. Brownian motion drives the chain to move in a distance of order its own size during this relaxation time (τ). The diffusion coefficient is ratio of the mean-square coil size and the terminal relaxation time:

$$D \cong \frac{R^2}{\tau} \cong \frac{kTB}{\eta_s bN} (1+\frac{2c_s}{fc})^{1/2} \tag{7.5}$$

After a series of derivations, we find that the diffusion coefficient is independent of polyelectrolyte concentration in the low salt limit (where $c_s \approx 0$). Plugging in ξ to cancel out the c_s, B and f items, we have:

$$\frac{D}{\xi^2} \cong \frac{ckT}{\eta_s N} \tag{7.6}$$

This model measures directly the number density of chains (c/N) and indicates the number-average molecular weight (M_n), which is shown below.

The specific viscosity η_{sp} of semidilute unentangled polyelectrolyte solution is:[14, 21, 32]

$$\eta_{sp} \cong \frac{\eta - \eta_s}{\eta_s} \cong B^{-3/2} N^2 (cb^3)^{-1/2} (1+\frac{2c_s}{fc})^{-3/4} \cong \frac{N}{c\xi^3} \tag{7.7}$$

which can be simplified to another expression:

$$\frac{c}{N} \cong \frac{1}{\eta_{sp} \xi^3}$$

where η_s is the pure solvent viscosity and η is the viscosity of polymer solution. $\eta_{sp}\xi^3$ is reversely proportional to the number density of chains (c/N). The terminal modulus in the *Rouse* model is $G = (\eta-\eta_s)/\tau$, is always simply kT per chain and not dependent on correlation length.

$$G = \frac{ckT}{N} \tag{7.8}$$

Therefore, we summarize how to determine the number density of chains of polymers in solution using proposed parameters, which concludes as follows:

$$\frac{c}{N} = \frac{\mathrm{G}}{kT} \cong \frac{1}{\eta_{\mathrm{sp}}\xi^3} \cong \sqrt{\frac{\eta_s}{\tau\xi^3 kT}} \cong \frac{\eta_s D}{\xi^2 kT} \tag{7.9}$$

where the number density of repeat units $c = c_{\mathrm{m}}N_{\mathrm{AV}}/M_0$, where N_{AV} is Avogadro's number and M_0 is the molecular weight of repeat unit, the number of repeat units per chain $N = M_{\mathrm{n}}/M_0$, the number density of chains becomes:

$$\frac{\mathrm{c}}{N} = \frac{c_m N_{AV} / M_0}{M_n / M_0} = \frac{c_m N_{AV}}{M_n} \quad \text{or} \quad \mathrm{M_n} = \frac{c_m N_{AV}}{c / N} \tag{7.10}$$

This suggests the number-average molecular weight can be calculated from c_{m} (the original mass concentration in g/L) and the number density of chains c/N, derived from the NMR diffusometry, rheology and X-ray scattering methods. Practically, this model not only applies to ionic polymers but also neutral polymers in semidilute unentangled solutions of any solvent quality.

Here we investigate distinct measurements to determine number-average molecular weight (M_{n}), including the specific viscosity η_{sp} in solution, polymer chain diffusion D and correlation length ξ. (measured within the precision of ± 5 – 10%). Furthermore, we propose the other three methods that involve rheology experiments to measure terminal modulus G, terminal chain relaxation time τ and the shear rate dependence of viscosity (η_{sp}) to determine number-average molecular weights. In the end of this chapter we will summarize those methods and discuss precision briefly over the commercially reported molecular weight values for the polyelectrolytes.

In all, we would like to provide a significant and robust method to characterize polyelectrolyte molecular weight, thus facilitating the determination of molecular weight (M_{n}) for the polyelectrolytes, especially those with high molecular weights. **Figure 7.2** describes the overall goal to develop the fundamental methods for M_{n} determination of ionic polymers.

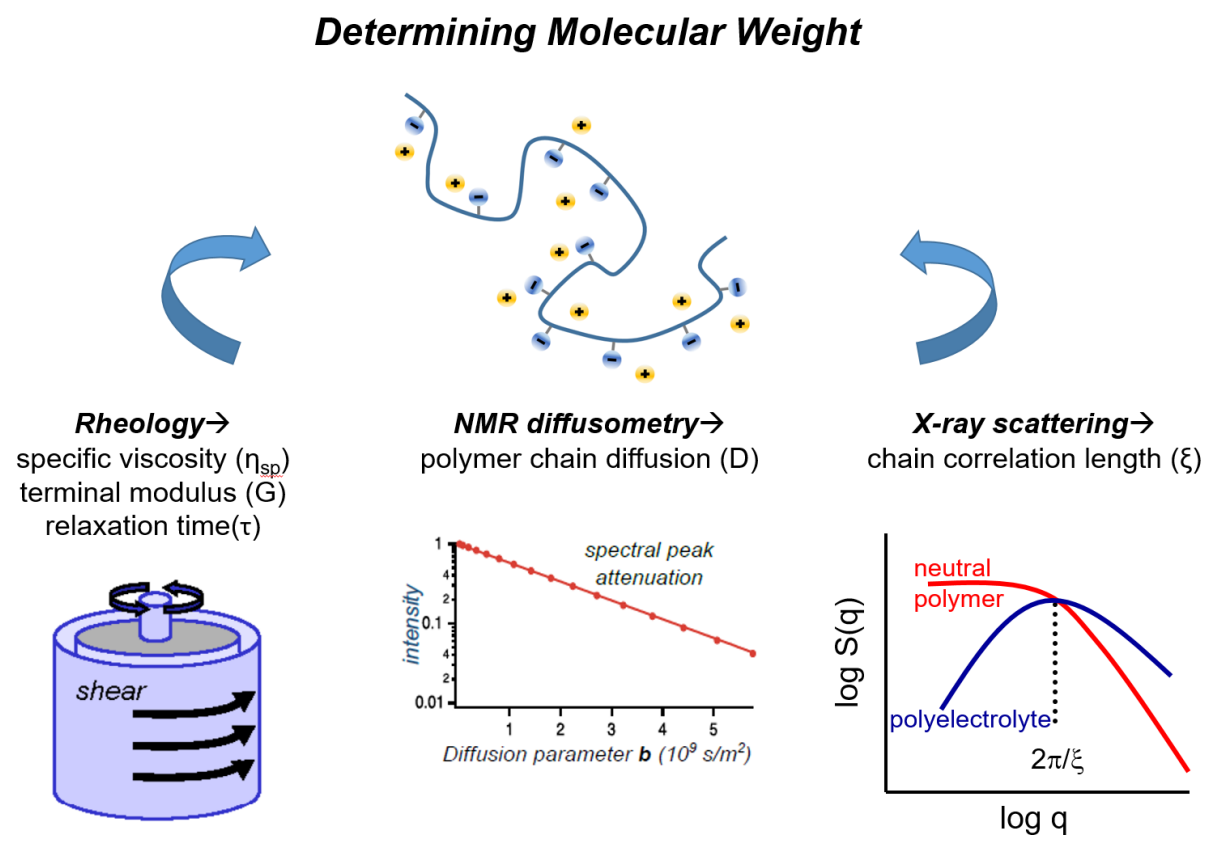

Figure 7.2. Summary strategies and methods for general molecular weight determination for ionic polymers. Our goal is to understand the chain configuration in ionic polymer solutions with no salt added (in the semidilute unentangled regime).

7.2.2 Materials and Methods

The self-diffusion coefficients of polyelectrolytes in solutions were determined using a 400 MHz Bruker Advance III WB NMR spectrometer equipped with a MIC probe, a Diff60 z-axis gradient, and a 5 mm ^{1}H detection coil. Gradient strengths were in the range 500 – 800 G ·cm^{-1}, Δ is in the range of 25 – 100 ms and δ is 5 ms due to the short spin-spin relaxation time from long polymer chains. 32 – 256 number of scans were set to gain sufficient signal for diffusion measurement for polymer peaks. Acquisition and relaxation delay times were each 0.8 s and 3 Hz line broadening was applied during data processing. All measurements were performed at 25 ℃

and temperature was equilibrated for more than 10 min. Two polyelectrolytes, caesium poly(styrene sulfonate) (CsPSS) and caesium poly(2-acrylamido-2-methyl-1-propanesulfonate) (CsPAMS), were both provided by the supplier Sigma-Aldrich. CsPAMS was titrated from HPAMS form. The molecular weight of CsPSS was 1534 kg/mol (PDI ~ 3.34) and CsPAMS was around 3300 kg/mol (bimodal distribution). The benzene peak at 7.5 ppm for PSS and methyl peaks at 1.5 ppm for PAMS were used to determine the ionic polymer diffusion coefficients in polyelectrolyte solutions.

7.2.3 Results and Discussion

The correlation between polymer molar mass and diffusion coefficients was originally proposed and used to measure the molecular weight of nonionic polymers in a dilute concentration regime.[33] For high molecular weight polyelectrolytes, the dilute regime has a very low c^* (< ~ 0.1 g/L) due to polymer chain conformation. Such a low polymer concentration results in a low signal-to-noise ratio for NMR data collection, thus requiring detailed and careful NMR diffusion measurements to scan over a range of c in the semidilute unentangled regime. To investigate semidilute polymer solutions, NMR usually requires samples of 0.1 to 10 mg of polymer in solutions per mL in volume, with corresponding data collection times around 1 minute to a few hours per sample. Our previous studies on self-assemblies and small molecules (solvents or hydrophobic cargos) would help us to develop methodology to access D for ion-containing polymers. Typically for NMR diffusometry, we are able to probe the movement of molecules from 10^{-8} – 10^{-15} m^2 s^{-1}, with error of ±2 – 10%.[34-38] Compared to viscosity measurements, NMR diffusometry has the advantages that the determination of M_n can be performed at equilibrium, and can be done in a completely closed (e.g., glass sealed) system with no solvent evaporation or exposure to air. The latter condition guarantees there is no possible change of the polymer solution

concentration during experiments. **Figure 7.3** shows chemical structures and 1st slices of diffusion measurements of CsPSS (0.0924 M) and CsPAMS (0.05 M) in aqueous solutions.

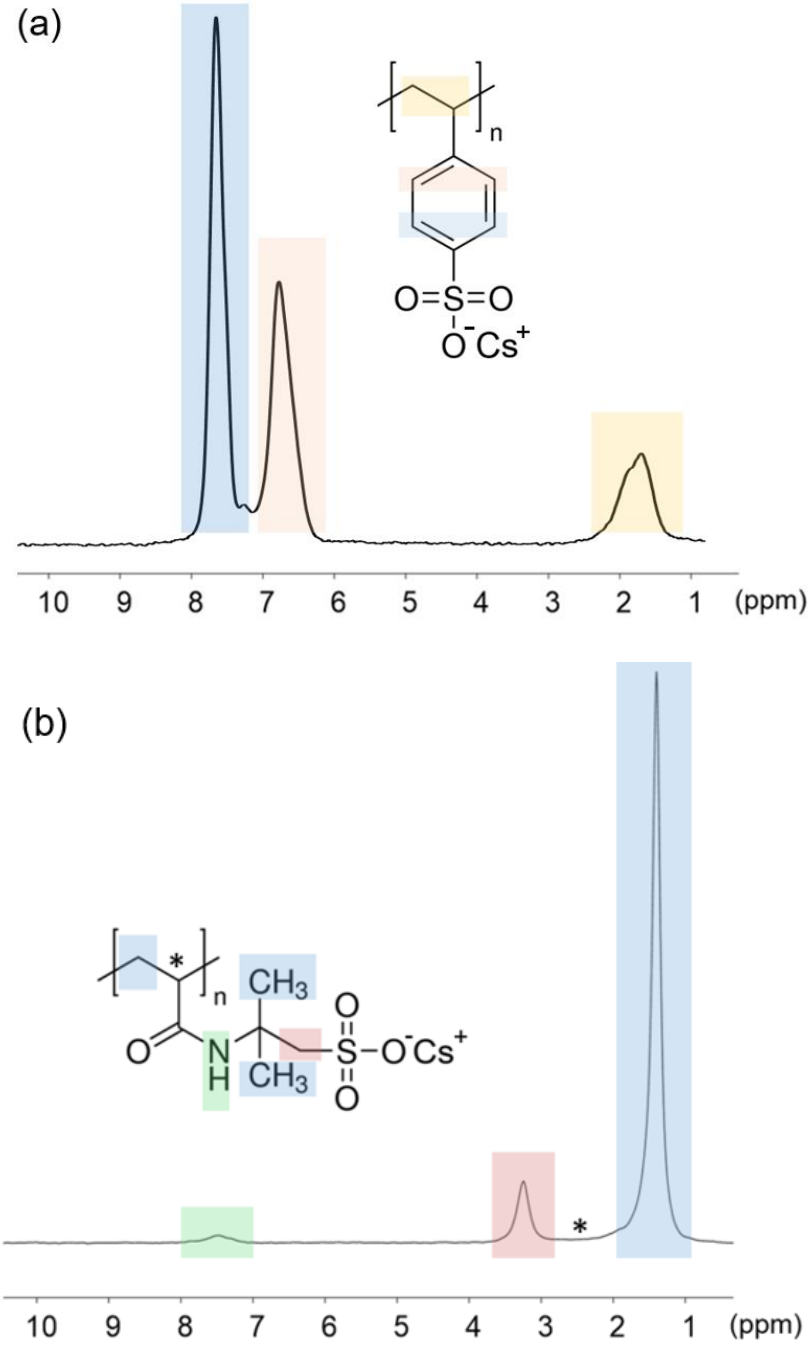

Figure 7.3. The 1st slice spectra in NMR diffusion measurements of (a) 1500 kg/mol CsPSS and (b) 3000 kg/mol CsPAMS polyelectrolyte solutions, respectively. Solvent peaks have decayed due to fast diffusion. Chemical structures as well as peak assignments are also indicated in both graphs.

In NMR diffusometry slices, the solvent peak was completely eliminated due to rapid signal decay and thus polymer peaks have remained so we are able to have a better examination over the polymer structures. Notably, all polymer peaks in CsPSS polyelectrolyte have broadened over 100 Hz, which may indicate the chain interaction (entanglement or overlap) weighting effects from large molecular weights (sizes).

In order to verify that polymer concentrations are in $c^* < c < c_e$, we scan a range of concentrations and expect them to be semidilute but not entangled. If that is the case, the solutions should give the same results for M_n for our method. Here we choose concentration ranges from 0.09 – 0.003 M and 0.05 – 0.005 M, for 1500 kg/mol CsPSS and 3000 kg/mol CsPAMS solutions, respectively. Those ranges have been determined by previous rheology tests and references by the Colby group at Penn State (details not covered), which we will discuss in an upcoming publication. In NMR diffusometry, we are able to determine the semidilute regime based on a previous study reported by Oostwal et al..[39] **Figure 7.4** shows ^{1}H NMR diffusion coefficients for NaPSS of 6 molecular weights (M_w from top to bottom: 16 k, 31k, 65 k, 88 k, 177 k, 354 k) in aqueous solutions with no added salt. The dashed line indicates the entanglement concentration c_e, and for those concentrations less than c_e, the solutions are semidilute and unentangled, where D is not dependent of concentration. In the semidilute unentangled regime, we are able to combine with correlation length (ξ) to determine the number-average molecular weight by Equation 7.6. We can expand this method to a wide variety of ionic polymer chemistries and ion densities using NMR diffusometry. In general, our measurement takes 2 – 4 hours for the most dilute polymer concentrations (~ 10^{-3} M).

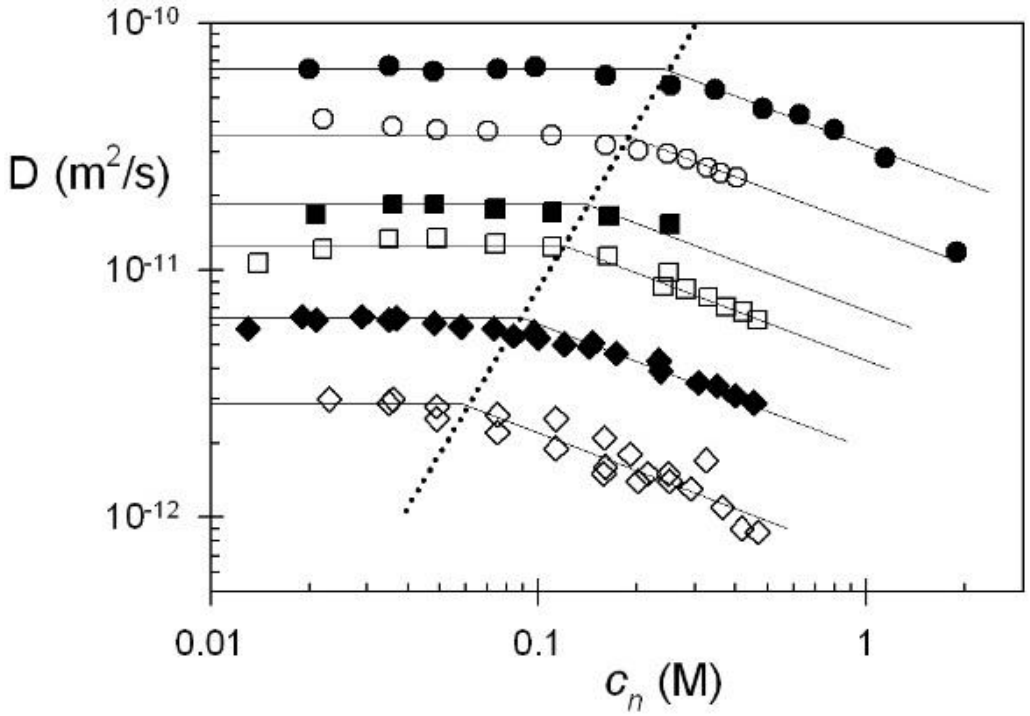

Figure 7.4. Classical diffusion coefficient data from ^{1}H PFG NMR measurements of Oostwal for six molecular weights (from top to bottom; 16 k, 31k, 65 k, 88 k, 177 k, 354 k) of NaPSS in water (with no added salt). Reproduced from Reference 39.

In order to determine the c_e for CsPSS and CsPAMS solutions. We measured diffusion coefficients of polyelectrolytes over a range of concentrations. **Figure 7.5** shows (a) the *D* of CsPSS in concentration range of 0.09 – 0.003 M and (b) CsPAMS in concentration range of 0.05 – 0.005 M. By extrapolating linear fits of *D* values for CsPSS we are able to estimate the c_e is ~ 0.03 M and this value is close what we obtain from SAXS method (not included in this chapter). The inconsistency in first a few *D* values may require more number of scans to increase the signal to noise ratio at semidilute regime. However, Figure 7.5 (b) shows much higher *D* than expected at two most diluted concentrations. We then further check the Stejskal-Tanner signal attenuation plots for all CsPAMS concentrations in **Figure 7.6**.

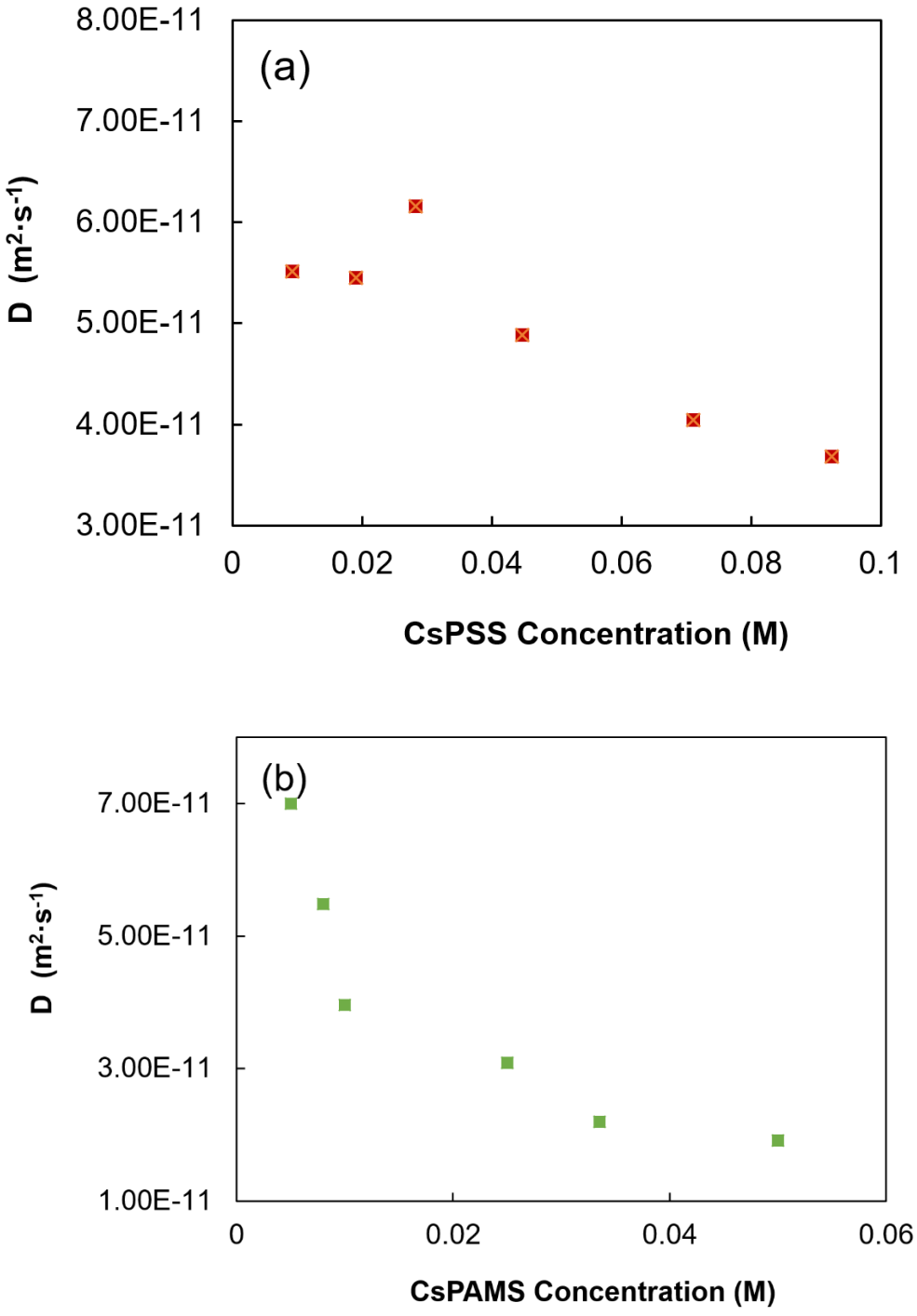

Figure 7.5. Diffusion coefficient data from ^{1}H NMR measurements of (a) CsPSS and (b) CsPAMS solutions.

By checking the NMR signal attenuation plots, we can see all 6 samples cannot be properly fit with a single diffusion coefficient (a straight fit line). We assume the scattering of data originated from the polydispersity of CsPAMS. The *D* values achieved are averages from fast diffusion of shorter polymer chains and slow diffusion of longer chains. Many studies have used NMR diffusometry (PFG or DOSY) to measure the polydispersity (PDI) of polymers.[40-41] Statistical analysis of NMR spectra allows the estimation of PDI in polymers. However, our theory is based on monodisperse polymer chains and polydispersity will open a totally new field in our methodology. Further studies will be taken for NMR as well as rheology measurements to account for polydispersity effects and we will not be discussed in this chapter.

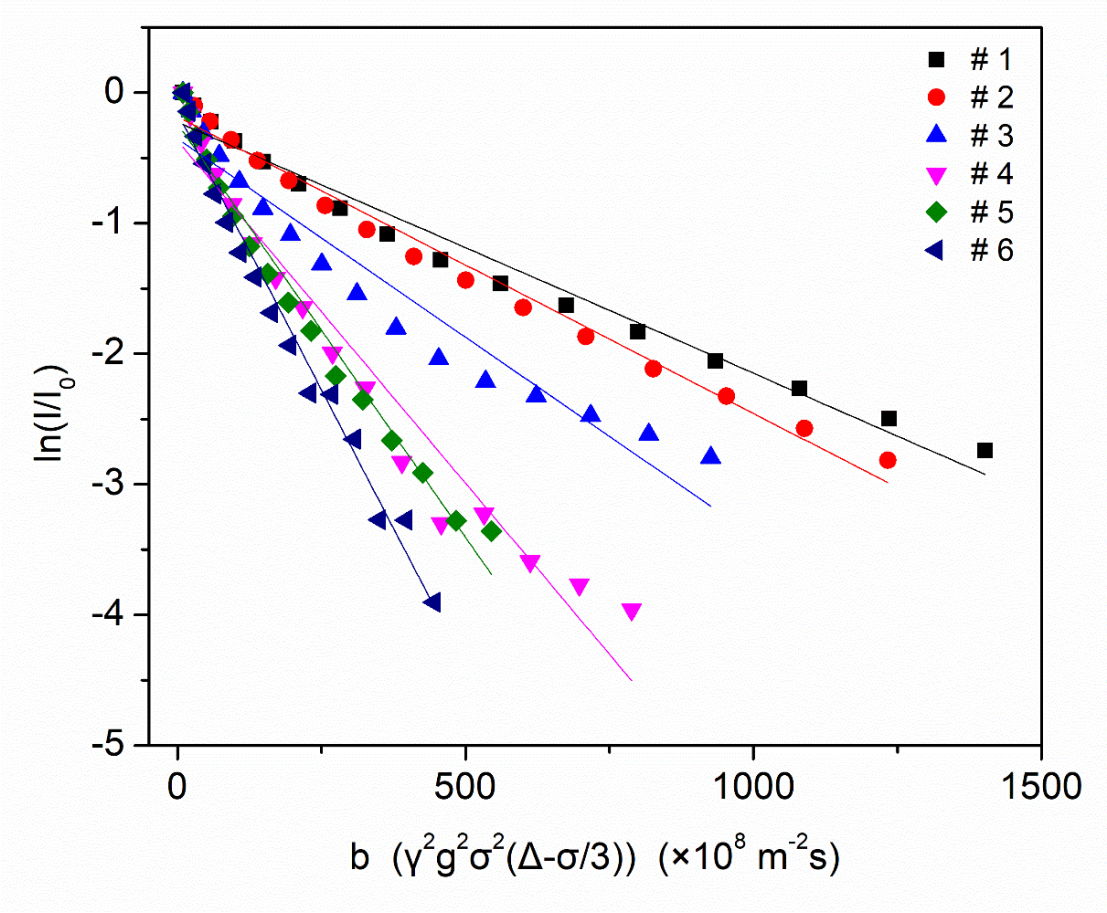

Figure 7.6. Stejskal-Tanner signal attenuation in ^{1}H NMR diffusometry from CsPAMS aqueous solutions. The concentrations for #1 to 6 are 0.05, 0.035, 0.025, 0.01, 0.008, 0.005 M, respectively.

In **Figure 7.7**, we have showed the determination of the number-averaged molecular weights (M_n) for a single polyelectrolyte in water using our method and compare with the other three methods. Molecular weights for CsPSS and CsPAMS are expected to be ~1.5 $\times 10^6$ g/mol and 3 $\times 10^6$ g/mol (labeled as dashed lines in graph) from the manufacturer. In Figure 7.7 (a), all the methods seem to deviate from the standard M_n of CsPSS to some extent. Our NMR method demonstrates a slightly higher molecular weights than expected, especially at higher polymer concentrations. As we switch to another polyelectrolyte CsPAMS in Figure 7.7 (b), four methods show less deviations compared to the standard M_n and the method that incorporates η_s, τ and ξ suggests the closest value. We will need to determine prefactors for the remaining methods for a specific polyelectrolyte type in future studies. More discussion of modifications will not be done here. Our NMR method still has higher predicted molecular weights at higher concentrations, which is probably affected by the entanglement weighting effects. In the future, we would like to reconsider the impacts from the molecular weight polydispersity in our measurement and predicted outcome. We are working on the incorporation of these features (molecular weight distributions of polymers) into our data analysis in the semidilute unentangled regime using NMR.

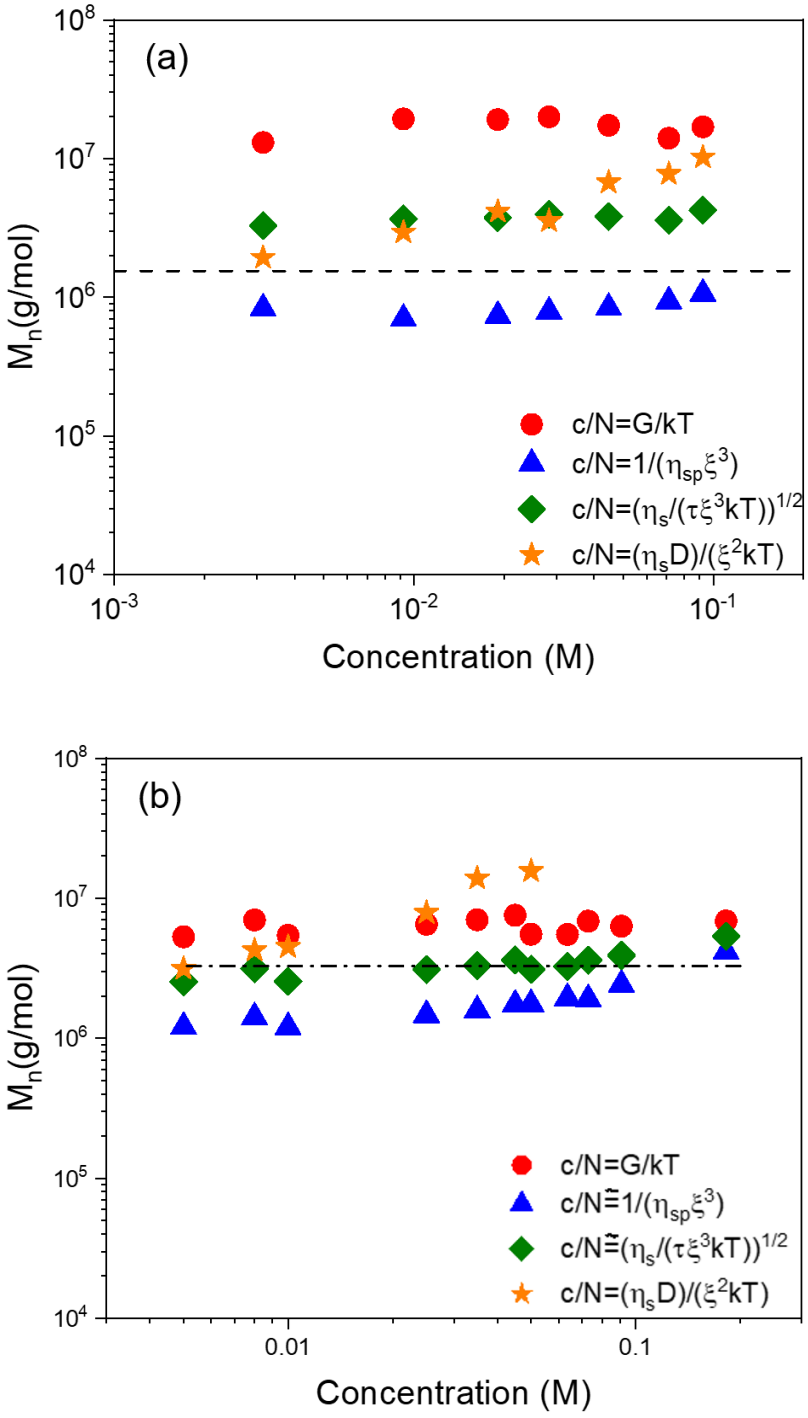

Figure 7.7. Number-averaged molecular weights (M_n) of (a) CsPSS and (b) CsPAMS using four proposed methods. Molecular weight for a single CsPSS and CsPAMS is ~ 1.5 $\times 10^6$ g/mol and 3 $\times 10^6$ g/mol (dashed lines in graph), respectively. Data courtesy to Aijie Han and Dr. Ralph Colby at Department of Materials Science and Engineering, Pennsylvania State University.

Above are our preliminary outcome of this project to explore new methods to determine molecular weights of ionic polymers in a reliable and precise way. We can also perform NMR measurements for other appropriate polar solvents such as ethylene glycol, which is > 10 times more viscous than water. Its D (> 10^{-13} m^2/s) is still accessible for NMR and provides more robust results in rheology. Moreover, we can do variable temperature NMR diffusion measurements. Increasing temperature can increase spin-spin relaxation (T_2) substantially, thus narrowing NMR linewidths and reducing experiment time to measure D.

7.2.4 Conclusions

In this section, we use our strength in NMR spectrometry and diffusometry, as well as other tools that involve rheology and X-ray scattering experiments to determine number-averaged molecular weights for ionic polymers. We successfully assessed a wide range of concentration of CsPSS and CsPAMS polyelectrolytes and compared the four proposed methods. NMR diffusometry suggests the existence of polydispersity and further investigations will be done to understand how it impacts our M_n determination. In all, we would like to provide knowledge to develop guidelines to measure M_n accurately with our current resources and expertise. After we have greater understandings of these methods, we can guide more precise measurements of M_n in dilute regime and quantitatively understand the distinction between chain diffusion in the dilute vs. semidilute regimes.

References

1. Yuan, J.; Antonietti, M., Poly(ionic liquid)s: Polymers expanding classical property profiles. *Polymer* **2011,** *52* (7), 1469-1482.
2. Yuan, J.; Mecerreyes, D.; Antonietti, M., Poly(ionic liquid)s: An update. *Prog. Polym. Sci.* **2013,** *38* (7), 1009-1036.
3. Vygodskii, Y. S.; Mel'nik, O. A.; Lozinskaya, E. I.; Shaplov, A. S.; Malyshkina, I. A.; Gavrilova, N. D.; Lyssenko, K. A.; Antipin, M. Y.; Golovanov, D. G.; Korlyukov, A. A.; Ignat'ev, N.; Welz-Biermann, U., The influence of ionic liquid's nature on free radical polymerization of

vinyl monomers and ionic conductivity of the obtained polymeric materials. *Polym. Adv. Technol* **2007,** *18* (1), 50-63.

4. Li, X.; Ni, X.; Liang, Z.; Shen, Z., Preparation of main-chain imidazolium-functionalized amphiphilic block copolymers through combination of condensation polymerization and nitroxide-mediated free radical polymerization and their micelle study. *J. Polym. Sci. A* **2012,** *50* (10), 2037-2044.

5. Steinkoenig, J.; Bloesser, F. R.; Huber, B.; Welle, A.; Trouillet, V.; Weidner, S. M.; Barner, L.; Roesky, P. W.; Yuan, J.; Goldmann, A. S.; Barner-Kowollik, C., Controlled radical polymerization and in-depth mass-spectrometric characterization of poly(ionic liquid)s and their photopatterning on surfaces. *Polym. Chem.* **2016,** *7* (2), 451-461.

6. Li, J.; Wilmsmeyer, K. G.; Hou, J.; Madsen, L. A., The role of water in transport of ionic liquids in polymeric artificial muscle actuators. *Soft Matter* **2009,** *5* (13), 2596-2602.

7. Hou, J.; Li, J.; Madsen, L. A., Anisotropy and Transport in Poly(arylene ether sulfone) Hydrophilic−Hydrophobic Block Copolymers. *Macromolecules* **2010,** *43* (1), 347-353.

8. Hou, J.; Zhang, Z.; Madsen, L. A., Cation/anion associations in ionic liquids modulated by hydration and ionic medium. *J. Phys. Chem. B.* **2011,** *115* (16), 4576-82.

9. Stejskal, E.; Tanner, J., Spin diffusion measurements: spin echoes in the presence of a time-dependent field gradient. *J. Chem. Phys.* **1965,** *42* (1), 288-292.

10. Zwanzig, R., Dielectric Friction on a Moving Ion. *J. Chem. Phys.* **1963,** *38* (7), 1603-1605.

11. Zwanzig, R., Dielectric Friction on a Moving Ion. II. Revised Theory. *J. Chem. Phys.* **1970,** *52* (7), 3625-3628.

12. Hubbard, J. B., Friction on a rotating dipole. *J. Chem. Phys.* **1978,** *69* (3), 1007-1009.

13. Kim, H. J.; Friedman, H. L.; Raineri, F. O., Smoluchowski fluctuation theory of dielectric relaxation. *J. Chem. Phys.* **1991,** *94* (2), 1442-1453.

14. Dobrynin, A. V.; Rubinstein, M., Theory of polyelectrolytes in solutions and at surfaces. *Progress in Polymer Science* **2005,** *30* (11), 1049-1118.

15. Dou, S.; Zhang, S.; Klein, R. J.; Runt, J.; Colby, R. H., Synthesis and Characterization of Poly(Ethylene Glycol)-Based Single-Ion Conductors. *Chem. Mater.* **2006,** *18* (18), 4288-4295.

16. Dou, S.; Colby, R. H., Solution Rheology of a Strongly Charged Polyelectrolyte in Good Solvent. *Macromolecules* **2008,** *41* (17), 6505-6510.

17. Kötz, J.; Kosmella, S., *Polyelectrolytes and nanoparticles*. Springer-Verlag: Heidelberg, 2007.

18. Wang, J.-H. H.; Yang, C. H.-C.; Masser, H.; Shiau, H.-S.; O'Reilly, M. V.; Winey, K. I.; Runt, J.; Painter, P. C.; Colby, R. H., Ion States and Transport in Styrenesulfonate Methacrylic PEO9 Random Copolymer Ionomers. *Macromolecules* **2015,** *48* (19), 7273-7285.

19. Schaefer, D. W., A unified model for the structure of polymers in semidilute solution. *Polymer* **1984,** *25* (3), 387-394.

20. Wang, L.; Bloomfield, V. A., Osmotic pressure of polyelectrolytes without added salt. *Macromolecules* **1990,** *23* (3), 804-809.
21. Rubinstein, M.; Colby, R. H.; Dobrynin, A. V., Dynamics of Semidilute Polyelectrolyte Solutions. *Phys. Rev. Lett.* **1994,** *73* (20), 2776-2779.
22. Okuda, J.; Rushkin, I. L., Mono(cyclopentadienyl)titanium complexes as initiators for the living ring-opening polymerization of .epsilon.-caprolactone. *Macromolecules* **1993,** *26* (20), 5530-5532.
23. Hansen, E. H.; Schnitzer, M., Molecular weight measurements of polycarboxylic acids in water by vapor pressure osmometry. *Analytica Chimica Acta* **1969,** *46* (2), 247-254.
24. Debye, P., Molecular-weight Determination by Light Scattering. *The Journal of Physical and Colloid Chemistry* **1947,** *51* (1), 18-32.
25. Evans, R.; Wallis, A. F. A., Cellulose molecular weights determined by viscometry. *J. Appl. Polym. Sci* **1989,** *37* (8), 2331-2340.
26. Yau, W. W.; Rementer, S. W., Polymer Characterization by SEC-Viscometry: Molecular Weight (MW), Size (Rg) and Intrinsic Viscosity (IV) Distribution. *J. Liq. Chromatogr.* **1990,** *13* (4), 627-675.
27. Holdcroft, S., Determination of molecular weights and Mark–Houwink constants for soluble electronically conducting polymers. *J. Polym. Sci. Poly. Phys* **1991,** *29* (13), 1585-1588.
28. Ying, Q.; Chu, B., Overlap concentration of macromolecules in solution. *Macromolecules* **1987,** *20* (2), 362-366.
29. De Gennes, P. G.; Pincus, P.; Velasco, R. M.; Brochard, F., Remarks on polyelectrolyte conformation. *Journal de Physique* **1976,** *37* (12), 1461-1473.
30. De Gennes, P. G., Dynamics of Entangled Polymer Solutions. I. The Rouse Model. *Macromolecules* **1976,** *9* (4), 587-593.
31. Baigl, D.; Ober, R.; Qu, D.; Fery, A.; Williams, C. E., Correlation length of hydrophobic polyelectrolyte solutions. *Europhysics Letters (EPL)* **2003,** *62* (4), 588-594.
32. Dobrynin, A. V.; Colby, R. H.; Rubinstein, M., Scaling Theory of Polyelectrolyte Solutions. *Macromolecules* **1995,** *28* (6), 1859-1871.
33. Callaghan, P. T.; Lelievre, J., The size and shape of amylopectin: A study using pulsed-field gradient nuclear magnetic resonance. *Biopolymers* **1985,** *24* (3), 441-460.
34. Chen, M.; Dugger, J. W.; Li, X.; Wang, Y.; Kumar, R.; Meek, K. M.; Uhrig, D. W.; Browning, J. F.; Madsen, L. A.; Long, T. E.; Lokitz, B. S., Polymerized ionic liquids: Effects of counter-anions on ion conduction and polymerization kinetics. *J. Polym. Sci. A* **2018,** *56* (13), 1346-1357.
35. Kidd, B. E.; Li, X.; Piemonte, R. C.; Cooksey, T. J.; Singh, A.; Robertson, M. L.; Madsen, L. A., Tuning Biocompatible Block Copolymer Micelles by Varying Solvent Composition: Dynamics and Populations of Micelles and Unimers. *Macromolecules* **2017,** *50* (11), 4335-4343.

36. Kidd, B. E.; Lingwood, M. D.; Lee, M.; Gibson, H. W.; Madsen, L. A., Cation and anion transport in a dicationic imidazolium-based plastic crystal ion conductor. *J. Phys. Chem. B.* **2014,** *118* (8), 2176-85.
37. Wilmsmeyer, K. G.; Li, X.; Madsen, L. A., Anisotropic viscoelasticity and molecular diffusion in nematic wormlike micelles. *Liq. Cryst.* **2018,** *45* (6), 844-856.
38. Li, X.; Cooksey, T. J.; Kidd, B. E.; Robertson, M. L.; Madsen, L. A., Mapping Coexistence Phase Diagrams of Block Copolymer Micelles and Free Unimer Chains. *Macromolecules* **2018,** *51* (20), 8127-8135.
39. Oostwal, M. G.; Blees, M. H.; De Bleijser, J.; Leyte, J. C., Chain self-diffusion in aqueous salt-free solutions of sodium poly(styrenesulfonate). *Macromolecules* **1993,** *26* (26), 7300-7308.
40. Fleischer, G., The effect of polydispersity on measuring polymer self-diffusion with the n.m.r. pulsed field gradient technique. *Polymer* **1985,** *26* (11), 1677-1682.
41. Viéville, J.; Tanty, M.; Delsuc, M.-A., Polydispersity index of polymers revealed by DOSY NMR. *J. Magn. Reson.* **2011,** *212* (1), 169-173.

Chapter 8: Summary and Future Work

8.1 Summary

This dissertation describes the design and characterization of block copolymer self-assemblies for nanoscale molecular cargo carriers for potential applications in targeted drug and signaling agent (e.g., H_2S) delivery, nanoreactors and catalysis and advanced coatings. It presents multiple works that highlight NMR spectroscopy, relaxation, and diffusometry, and includes other complementary methods (e.g. SANS, DLS, DSC, GPC, SAXS and rheology measurements). This dissertation also introduces preliminary investigations on ionic polymers, which aims to inform us how to use those combined methods to expand current understandings in more complicated polymeric systems.

Chapter 1 introduces the significance to design and develop efficient nanoscale delivery carriers in a wealth of applications, especially drug delivery in cancer therapeutics. In recent years, only a few targeted nanocarriers have been approved for clinical use. Therefore, it is crucial to understand the principles/mechanisms behind cargo delivery and develop successful strategies. Chapter 1 in general reviews the design and performance studies of various nanoscale delivery carriers, including self-assembled micelles, gels, stimuli-responsive nanocarriers, and dynamic and kinetic processes in micelles, which enhances our current understandings of such systems for potential drug delivery.

Chapter 2 briefly presents the basic theories of translational motion and NMR diffusometry. Among multiple techniques to study soft materials, the NMR method serves as a potent tool due to its non-destructive nature, and its chemically specific and isotopically selective merits, thereby providing valuable molecular information, such as chemical structure, intermolecular interactions, molecular dynamics, binding affinity, exchange kinetics, and mobility. By using NMR

diffusometry, which is also known as pulsed-field-gradient (PFG) NMR, we have performed a detailed qualitative and quantitative study of block copolymer micelles, and other polymeric systems to reveal their dynamic properties in the following chapters.

Chapter 3 used NMR spectroscopy and diffusometry to investigate spherical micelles formed from poly(ethylene oxide)-b-(ε-caprolactone) (PEO-PCL) at 1% wt/vol in D_2O-THF-d_8 mixed solvents. We are interested in the tunable properties of block copolymer micelles via polymer structure in combination with cargo and/or solution properties. For two series of micelles with different block masses, we quantified diffusion coefficients and populations of micelles and unimers over a range of temperature and solvent composition. Micelles and unimers coexist over areas of these micelle-unimer phase diagrams, which provides new understandings on how inter- and intramolecular interactions impact the tuning of micelle structure and dynamics.

Chapter 4 further studies the exchange kinetics of unimer chains in PEO-PCL micelles using time-resolved NMR spin-relaxation time (T_1). By monitoring the T_1 change in ^{1}H cores for mixed micelles solutions labeled with ^{1}H- and ^{2}H-cores, we were able to determine the unimer chain exchange time constants between micelles. The gyromagnetic ratio (γ) of ^{2}H is about 1/7 of ^{1}H, therefore ^{2}H is less effective to influence nearby ^{1}H and the T_1 for ^{1}H is enhanced due to intermolecular dipole-dipole interactions. Our TR-NMR showed no change over hours at 25 ℃ and 40 ℃, which indicates extremely slow chain exchange kinetics in micelles. As the temperature is increased to 55 ℃ and 62 ℃, the average time constants for unimer exchange are 130 min and 60 min, respectively. They are also in agreement with time-resolved small-angle neutron scattering (TR-SANS) results, which presents NMR as a simpler, more practical, less expensive method to understand polymeric micelles.

In Chapter 5 we proceed to study micelles self-assembled from a Pluronic® F127 (PEO_{99}-PPO_{69}-PEO_{99}) triblock copolymer in water. We successfully trapped 3 hydrophobic drugs, including hydrochlorothiazide (HCT), indomethacin (IND) and paclitaxel (PTX) in F127 micelles. We then quantified diffusion coefficients of different species (drug and polymer) in aqueous solution and calculated the partition percentages of the drug in micelles. The partition percentages of HCT and IND both increased with the increase of F127 concentration (from 1 to 5% w/v). This facile and non-invasive NMR method allows a direct measurement of drug distribution in a micellar system and opens opportunities to understand the dynamic process of cargo partitioning in micellar structures.

Chapter 6 expands our studies on polymeric micelles and their molecular as well as macroscopic behavior using the NMR technique. Here we proposed to design and synthesize a series of amphiphilic block copolymers, containing the hydrophilic block PEO and the hydrophobic block poly- (*tert*-butyl acrylate-*ran*-*n*-butyl acrylate). Based on the difference on the chemical structure between *n*-butyl acrylate (*n*BA) and *tert*-butyl acrylate (*t*BA), they exhibited glass transition temperatures (T_g) of - 46 °C and 25 °C, respectively. By fine-tuning the chemical moieties of those two blocks in the polymers, we realized the desired T_g of core-forming blocks in micelles. Further NMR diffusometry measurements supported that the variance in unimer concentration in solution as for the controlled chain mobility/dynamics in micelles.

Chapter 7 further applies NMR as a sophisticated and powerful tool to investigate block copolymer systems, such as ionic polymers in the applications of batteries, water purification and functionalized membrane. We introduced the influence of counter-anions diffusive properties on ion conduction as well as polymerization kinetics. Also, we used NMR diffusometry, rheology and small-angle X-ray scattering to innovatively explore the general number-average molecular

weight for ionic polymers via terminal modulus, relaxation time, diffusion rate, correlation length, and viscosity measurements.

8.2 Future Work

We have mainly discussed the development and characterization of block copolymer micelle (BCM) systems in this dissertation. Our next objective is to understand how the polymer, temperature, solvent, and cargo characteristics influence the cargo (e.g. hydrophobic drug) release processes. Especially, we will focus on the delivery and release of cargos in stimuli-responsive BCMs. As mentioned previously, poly(N-isopropyl acrylamide) (PNIPAM) is a thermoresponsive water-soluble polymer and exhibits "smart" behavior (phase transition) in aqueous solution. Xia et al.[1] reported the low critical solution temperatures (LCST) of PNIPAM with linear structures are dependent on their molecular weight and end groups, with a range of 32 ℃ to 45 ℃. In Chapter 3 we have investigated the structural changes of BCMs upon temperatures. Using NMR diffusometry, we are able to scrutinize phase transitions (which can be determined from chemical shifts and the diffusion coefficients of polymers) of thermo-responsive carriers, and these measurements may promote applications such as controlled drug or gene delivery, tissue engineering, and surface biocompatibilization. Moreover, we can extend this method to other stimuli-responsive polymer systems. For example, Miao et al.[2] reported that weak polyelectrolytes can experience transformation between the soluble ionized form and insoluble neutral form, as a function of pH. Similarly, we expect we can probe the transition within such polymer systems by new analyses with NMR spectroscopy and diffusometry.

We are working toward measurements of the release profile of drugs and we will correlate these results with the structure and dynamics of BCMs, as well as with the size and hydrophobicity of drug cargos. Building these relationships among polymer structure and drug structure, polymer

and drug dynamics and exchange, and diffusion of all these species can all help feed into rational design of micelle-based systems for tailored drug release.

Furthermore, we can achieve more desirable properties of block copolymer micelles (or other nanocarriers) by the sophisticated design of polymer structures. New directions of BCMs involve multifunctionality and compatibility. Firstly, the chemical versatility of block copolymers provides a wide availability to realize the multifunctionalities of nanocarriers, for example, dual-response or modified release of cargos. Li and Lodge et al.[3-4] created a new polymer chain architecture that combined multiple building blocks (polyfluorinated polyether, poly(ethylene oxide), polymeric hydrocarbon) to form a mixed-arm star BCM. Micelle structures can be tuned by relative lengths of the polymeric components, which broadens their potential applications as nanocarriers for more than one cargo release in a controlled manner in drug delivery or catalysis.

Similarly, Wang et al.[5] proposed a polymeric multicompartment gel that realized separate encapsulation and release of hydrophobic anticancer drugs (Doxorubicin and Paclitaxel). Both *in vitro* and *in vivo* antitumor activity demonstrated a better treatment of the combined platform compared to a single drug formulation. **Figure 8.1** has shown the schematic of this temperature-responsive multicompartment hydrogel formation.

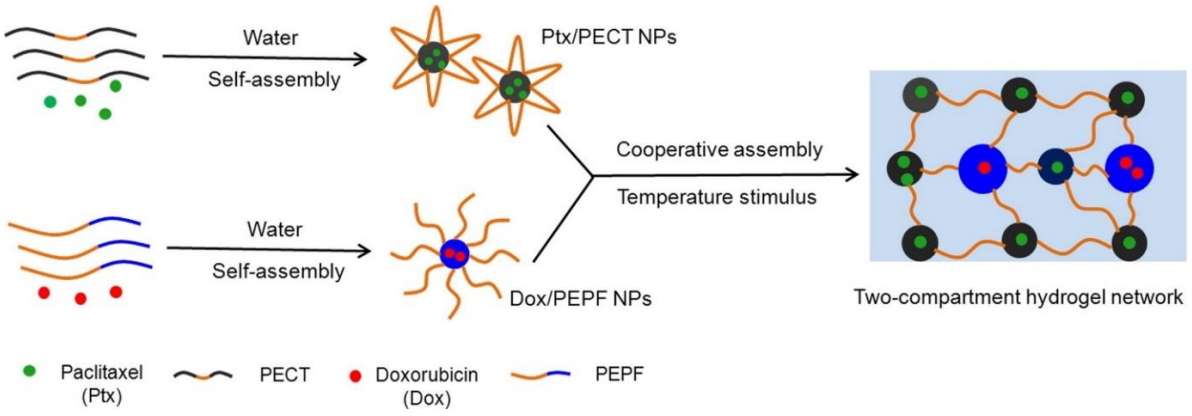

Figure 8.1. The diagram of temperature-induced hydrogel formation with two compartments. Reproduced from Reference 5.

Future studies of polymeric nanocarrier stability and cargo release can be made using NMR, as polymers and trapped drugs in compartments or different nm-scale phases would demonstrate distinctive chemical shifts in spectra and we can possibly investigate their dynamic behaviors with less cost of experimental time.

Secondly, biocompatibility and toxicity of delivery carriers must be addressed prior to any clinical application. Degradation and excretion of drug delivery systems *in vivo* is another issue that is poorly understood. Detailed toxicity studies and future data from clinical trials are required to apply those promising delivery systems to commercial medical practice.

In particular, researchers are using NMR spectroscopy, relaxometry, and diffusometry extensively to determine characteristics of BCMs such as diameter and structure, ion-binding, and solubilization. The development of novel NMR techniques will be of great interest in our future work. The time-resolved spin-lattice relaxation NMR method described in Chapter 4 that we have developed is a breakthrough for study of chain exchange kinetics in micellar systems. We also plan to extend this method to study cargo exchange kinetics by TR-NMR with e.g., isotope-labeled cargo molecules.

In summary, this dissertation provides new measurements and new ideas to guide research on block copolymers used in multiple applications. We aim to offer more insights into fundamental properties such as molecular transport, quantification of molecules in different phases or chemical environments, and chain or cargo exchange in polymers, with each of these observations covering a range of time and length scales.

References

1. Xia, Y.; Burke, N. A. D.; Stöver, H. D. H., End Group Effect on the Thermal Response of Narrow-Disperse Poly(N-isopropylacrylamide) Prepared by Atom Transfer Radical Polymerization. *Macromolecules* **2006,** *39* (6), 2275-2283.

2. Miao, Z.; Kubo, T.; Pal, D.; Sumerlin, B. S.; Veige, A. S., pH-Responsive Water-Soluble Cyclic Polymer. *Macromolecules* **2019,** *52* (16), 6260-6265.
3. Li, Z.; Hillmyer, M. A.; Lodge, T. P., Control of Structure in Multicompartment Micelles by Blending μ-ABC Star Terpolymers with AB Diblock Copolymers. *Macromolecules* **2006,** *39* (2), 765-771.
4. Li, Z.; Kesselman, E.; Talmon, Y.; Hillmyer, M. A.; Lodge, T. P., Multicompartment Micelles from ABC Miktoarm Stars in Water. *Science* **2004,** *306* (5693), 98-101.
5. Wang, W.; Song, H.; Zhang, J.; Li, P.; Li, C.; Wang, C.; Kong, D.; Zhao, Q., An injectable, thermosensitive and multicompartment hydrogel for simultaneous encapsulation and independent release of a drug cocktail as an effective combination therapy platform. *J. Control. Release* **2015,** *203*, 57-66.